Adaptive Predictive Feedback Techniques for Vibration Control

Kenneth W. Eure

Dissertation submitted to the Faculty of the Virginia Polytechnic Institute and State University in partial fulfillment of the requirements for the degree of

Doctor of Philosophy
in
Electrical Engineering

William Baumann, Chair
Jer-Nan Juang
Richard Silcox
Chris Fuller
Hugh VanLandingham

February 3, 1998
Blacksburg, Virginia

Keywords: Feedback, Adaptive, Real Time, Broadband
Copyright 1998, Kenneth W. Eure

Adaptive Predictive Feedback Techniques for Vibration Control

Kenneth W. Eure

(ABSTRACT)

In this dissertation, adaptive predictive feedback control is used to suppress plate vibrations. The adaptive predictive controller consists of an on-line identification technique coupled with a control scheme. Various system identification techniques are investigated and implemented including batch least squares, projection algorithm, and recursive least squares. The control algorithms used include Generalized Predictive Control and Deadbeat Predictive Control. This dissertation combines system identification and control to regulate broadband disturbances in modally-dense structures. As it is assumed that the system to be regulated is unknown or time varying, the control schemes presented in this work have the ability to identify and regulate a plant with only an initial estimate of the system order. In addition, theoretical development and experimental results presented in this work confirm the fact that an adaptive controller operating in the presence of disturbances will automatically incorporate an internal noise model of the disturbance perturbing the plant if the system model order is chosen sufficiently large. It is also shown that the adaptive controller has the ability to track changes in the disturbance spectrum as well as track a time varying plant under certain conditions. This work presents a broadband multi-input multi-output control scheme which utilizes both the DSP processor and the PC processor in order to handle the computational demand of broadband regulation of a modally-dense plant. Also, the system identification technique and the control algorithm may be combined to produce a direct adaptive control scheme which estimates the control parameters directly from input and output data. Experimental results for various control techniques are presented using an acoustic plant, a rectangular plate with clamped boundary conditions, and a time varying plate.

This work was supported by the NASA Langley Research Center.

(CONTRIBUTIONS OF THESIS)

The major contribution of this thesis is the development and implementation of adaptive feedback control algorithms which are able to regulate structural vibrations over a large bandwidth, i.e., several kHz. The main problems overcome in this work were (1) feedback control applied to an unknown nonminimum-phase plant, (2) real-time implementation of a broadband adaptive control system, and (3) multi-input multi-output (MIMO) control implementation using current microprocessor technology to regulate a high-order plant in the acoustic frequency range. Other contributions of this thesis include the development and implementation of an adaptive feedback regulator which is guaranteed stable for regulating the system model, the development and implementation of a direct adaptive feedback controller, the inclusion of an internal disturbance model to enhance regulation, and the development and implementation of feedforward control within the feedback control schemes given that a coherent disturbance reference is available for feedforward.

Acknowledgments

I want to thank Dr. Jer-nan Juang for the major contributions he has made to this thesis. His technical support and insight have been of great value, without which I humbly admit this work would have never been possible. I would like to also thank Ran Cabell and Donald Drown for supplying the software support which made the real-time implementations possible. Thanks also to Dr. Richard Silcox for providing the test facilities and supervision necessary to complete the experiments and for provided insight concerning the physics of vibration and acoustics. I would also like to thank Dr. William Baumann for overseeing the development and direction of this thesis. His insight into feedback control theory is appreciated. Also, I would like to thank Dr. Chris Fuller for his helpful comments and supervision. Thanks to my parents, John and Clementine Eure for their love and support.

Oro, deus, cognoscam te, amem te, ut gaudeam de te.

Contents

Chapter 1

Introduction 1

1.1 Background 1

1.2 Thesis Organization 2

Chapter 2

Literature Review 4

2.1 System Identification 4

2.2 Predictive Control Theory 5

2.3 Adaptive Predictive Control 6

Chapter 3

Fundamentals of Predictive Control 8

3.1 Introduction 8

3.2 System Identification Using MATLAB 11

3.2 Predictive Control Algorithms 12

3.2.1 Generalized Predictive Control, Basic Formulation 12

3.2.2 Deadbeat Predictive Control, Basic Formulation 15

3.3 Experimental Setup and Results 17

3.3.1 Experimental Setup 17

3.3.2 Experimental Results 23

3.3.3 Effect of Dampening on Feedback Control 28

3.4 Summary 31

Chapter 4

Feedforward and Internal Noise Models for Predictive Control 34

4.1 Introduction 34

4.2 System Identification for Feedback/Feedforward Control 35

4.3 Feedback/Feedforward Generalized Predictive Control 36

4.4 Feedback/Feedforward Deadbeat Predictive Control 43

4.5 Approximation of an Internal Noise Model 47

4.6 Exact Solution for the Internal Noise Model 48

4.7 Experimental Results 50
Chapter 5
Adaptive Predictive Feedback Control 63
5.1 Introduction 63
5.2 Real-time System Identification 65
5.3 Indirect Adaptive Predictive Control 67
5.4 Direct Adaptive Deadbeat Predictive Control 70
5.5 Adaptive Implementations 71
5.6 Summary 76
Chapter 6
Block Adaptive Feedback Control 78
6.1 Introduction 78
6.2 System Identification for Block Adaptive Control 80
6.3 Block Adaptive Control 83
6.4 Experimental Results Using Block Adaptive Control 85
6.4.1 Non-Adaptive MIMO Control 89
6.4.2 Adaptive Feedback Control 95
6.4.3 Feedback/Feedforward Adaptive Control 105
6.4.4 Non-Collocated Adaptive Control 115
6.5 Experimental Results Using Time Varying Plate 119
6.6 Conclusions 127
6.6.1 Summary 128
6.6.2 Suggested Applications 129
Appendix A
Application of Predictive Control Using Active Foam 131
Appendix B
Fast Computation of the Information Matrix 139
Appendix C
Frequency Shaped Predictive Control 143
C.1 Control Derivation 143

C.2 Experimental Results 144
References 151
Vita 155

List of Figures

Figure 3.1 Test Box 18
Figure 3.2 Block Diagram of Control System 19
Figure 3.3 Pole Zero Plot of Transfer Function 21
Figure 3.4 GPC Simulation Results 22
Figure 3.5 Plot of Time History 23
Figure 3.6 Plot of Autocorrelation of Accelerometer Signal 24
Figure 3.7 Generalized Predictive Control 25
Figure 3.8 Deadbeat Predictive Control 26
Figure 3.9 DPC With Large Bandwidth 27
Figure 3.10 Sand Weighted Plate Experiment 28
Figure 3.11 Plate Experiment With Rubber 30

Figure 4.1 Block Diagram of Control System 48
Figure 4.2 GPC Performance with Feedback/Feedforward Control 51
Figure 4.3 Feedback/Feedforward Tone Rejection Using Internal Noise Model 52
Figure 4.4 Plot of Control Using Internal Noise Model 53
Figure 4.5 Pole-Zero Plot of OMP Without (left) & With (right) Disturbance 54
Figure 4.6 Cancellation of Tone With Feedback Only 55
Figure 4.7 Plot of Resonance Tone Rejection 56
Figure 4.8 Plot of Off Resonance Tone Rejection 57
Figure 4.9 GPC with Internal Noise Model vs. Feedback/Feedforward 58
Figure 4.10 Reduced Order Feedback/Feedforward Controller 59
Figure 4.11 Feedback with Internal Noise Model of 800 Hz Tone 60
Figure 4.12 High-order Feedback with Internal Noise Model 61
Figure 4.13 Feedback/Feedforward with AR Noise Model 61
Figure 4.14 Feedback/Feedforward Performance Gain for Higher Order 62

Figure 5.1 Block Diagram of Adaptive Control System. 68
Figure 5.2 Block Diagram of Multirate Adaptive Control 69

Figure 5.3 Plot of Multirate Adaptive Controller Using GPC 72
Figure 5.4 Plot of Direct Adaptive Controller Performance 73
Figure 5.5 Increased Bandwidth DPC Multirate Controller..... 74
Figure 5.6 Multirate Adaptive Controller Using Projection Algorithm..... 75

Figure 6.1 Diagram of Block Adaptive Controller..... 84
Figure 6.2 Diagram of Adaptive Controller Test Facility 85
Figure 6.3 Test Plate with Sensors and Actuators..... 86
Figure 6.4 Plate Acceleration at Point #1 in dB..... 90
Figure 6.5 Plate Acceleration at Point #2 in dB..... 90
Figure 6.6 Plate Acceleration at Point #3 in dB..... 91
Figure 6.7 Plate Acceleration at Point #4 in dB..... 91
Figure 6.8 Plot of Vibration Energy..... 93
Figure 6.9 Plot of Radiated Sound Power..... 94
Figure 6.10 Plate Acceleration at Point #1 in dB..... 96
Figure 6.11 Plate Acceleration at Point #2 in dB..... 96
Figure 6.12 Plate Acceleration at Point #3 in dB..... 97
Figure 6.13 Plate Acceleration at Point #4 in dB..... 97
Figure 6.14 Bode Plot of Channel #1 Performance..... 99
Figure 6.15 Bode Plot of Channel #2 Performance..... 99
Figure 6.16 Bode Plot of Channel #3 Performance..... 100
Figure 6.17 Bode Plot of Channel #4 Performance..... 100
Figure 6.18 Acceleration at Point #1 in dB, Channel #1 Regulated..... 101
Figure 6.19 Acceleration at Point #2 in dB. Channel #1 Regulated..... 102
Figure 6.20 Acceleration at Point #3 in dB. Channel #1 Regulated..... 102
Figure 6.21 Acceleration at Point #4 in dB. Channel #1 Regulated..... 103
Figure 6.22 Bode Plot of Channel #1 Adaptive Controller Performance..... 104
Figure 6.23 Broadband Acceleration at Point #1 in dB..... 105
Figure 6.24 Feedback/feedforward SISO Controller Performance 106
Figure 6.25 Improvement Using Noise Predictor..... 107

Figure 6.26 Single Tone Feedback/Feedforward With AR Noise Predictor 108
Figure 6.27 Feedback/Feedforward with Anti-resonance Tonal Disturbance 109
Figure 6.28 Feedback/Feedforward With Off Resonance Tonal Disturbance 110
Figure 6.29 Feedback/Feedforward With Off Resonance Tone and AR Model 111
Figure 6.30 Channel #1 MIMO With Tonal Disturbance 112
Figure 6.31 Channel #2 MIMO With Tonal Disturbance 113
Figure 6.32 Channel #3 MIMO With Tonal Disturbance 113
Figure 6.33 Channel #4 MIMO With Tonal Disturbance 114
Figure 6.34 Diagram of Non-Collocated Sensors and Actuators 116
Figure 6.35 Channel #1 Feedback for Non-Collocated Sensors and Actuators 117
Figure 6.36 Channel #2 Feedback for Non-Collocated Sensors and Actuators 117
Figure 6.37 Channel #3 Feedback for Non-Collocated Sensors and Actuators 118
Figure 6.38 Channel #4 Feedback for Non-Collocated Sensors and Actuators 118
Figure 6.39 Test Plate With Time Varying Pressure Differential 119
Figure 6.40 Controller With Large Pressure Differential (Starting) 121
Figure 6.41 Controller With No Pressure Differential (Finishing) 121
Figure 6.42 Plot # 1 Gray Open-loop, Black Closed-Loop 123
Figure 6.43 Plot # 2 Gray Open-loop, Black Closed-Loop 123
Figure 6.44 Plot # 3 Gray Open-loop, Black Closed-Loop 124
Figure 6.45 Plot # 4 Gray Open-loop, Black Closed-Loop 124
Figure 6.46 Plot # 5 Gray Open-loop, Black Closed-Loop 125

Figure A.1 Diagram of Plant to be Regulated by Active Foam 131
Figure A.2 Diagram of Active Foam #1 132
Figure A.3 Diagram of Active Foam #2 133
Figure A.4 GPC Feedback Using Foam #1 134
Figure A.5 GPC Feedback Using Foam #2 135
Figure A.6 Feedback/Feedforward Control Using Foam #1 136
Figure A.7 Feedback/Feedforward Using an External Reference 137

Figure C.1 Plot of acceleration with no control weighting filter..... 145
Figure C.2 Plot of acceleration when filter #1 was applied 146
Figure C.3 Control effort when filter #1 was applied 147
Figure C.4 Frequency magnitude response of control filter #1..... 147
Figure C.5 Plot of acceleration when filter #2 was used..... 148
Figure C.6 Plot of control effort when filter #2 was used..... 149
Figure C.7 Frequency magnitude response of control filter #2..... 149

List of Tables

Table 3.1 Integrated Spectra for Sand Experiment 29
Table 3.2 Integrated Spectra for Rubber Experiment..... 30
Table 3.3 Natural Frequencies and Dampening of Dominant Modes 31

Table 6.1 Natural Frequencies of Test Plate 87
Table 6.2 Experimental Natural Frequencies and Dampening..... 88
Table 6.3 Total Reductions, 4 Channel Non-adaptive Controller..... 92
Table 6.4 Total Reductions, 4 Channel Adaptive Controller..... 98
Table 6.5 Total Reductions, Channel 1 Feedback Only..... 103
Table 6.6 Total Reductions, Feedback and Feedforward/Feedback Control 115
Table 6.7 Total Reduction Using Non-Collocated Sensors and Actuators 119
Table 6.8 Total Reductions Using Block Adaptive Controller and Dither 127

Chapter 1

Introduction

In this chapter, a brief discussion of the background of this problem will be given, followed by an outline of the chapters.

1.1 Background

The central problem addressed in this dissertation is regulating structural vibrations within the acoustic frequency range using current microprocessor technology. It is assumed that no coherent reference is available for feedforward, although if a reference is available, the control scheme should be able to incorporate it to provide enhanced regulation. Since the regulation is broadband, the control schemes must have the ability to regulate a given structure over a several KHz frequency range. In addition, the response of structures to broadband disturbances is modally dense. Modal density implies that the controller must be of high order so as to capture the dynamics of the plant. Given the high-order plant model and the need for a fast sampling rate due to the large bandwidth, the control schemes developed must be computationally efficient. Another problem to be addressed when regulating structural vibrations is that of nonminimum-phase. Even if sensors and actuators are collocated, the plant may appear as a nonminimum-phase system due to the fact that the plant model and controller are discrete time. This demands that the control scheme be able to regulate a nonminimum-phase system. It is also preferred, although not required, that the regulator be multi-input multi-output. This is done to improve regulation since a single-input single-output controller may not be able to observe and/or control all vibration modes of interest. A final problem which needs to be addressed is that of regulating a time varying plant in the presence of a disturbance which has a time varying spectral content. This demands that the control scheme be adaptive and able to incorporate an adaptive internal noise model.

1.2 Thesis Organization

This thesis consists of six chapters and three appendices. Chapter 1 is an introduction to the work completed and a brief description of the problems addressed. Chapter 2 is a literature review. In this chapter, several relevant works are cited which aided in the development of this thesis. Included are references to system identification techniques, predictive control theory, and adaptive predictive control theory. Chapter 3 presents the fundamentals of predictive control. The goal of Chapter 3 is to show the basics of Single-Input-Single-Output (SISO) system identifications, control, and real-time implementation. Here, MATLAB programs are used to perform the system identification and the fundamentals of non-adaptive Generalized Predictive Control (GPC) and Deadbeat Predictive Control (DPC) are developed and implemented on a SISO plant. In Chapter 4, a more rigorous development of both GPC and DPC is undertaken. Both predictive control techniques are extended to include a feedforward path. In addition, it is shown that if the system identification is performed in the presence of any disturbance acting on the plant, an internal noise model of the disturbance will be included in the system identification if the model order is sufficiently large. Experimental results are presented using SISO non-adaptive feedback and feedback/feedforward controllers. In these results, the improvement gained by incorporating a feedforward path into the controller is demonstrated. Also, it is shown that exact cancellation of a periodic disturbance is possible under certain conditions using feedback control only. In Chapter 5 the theory and implementation of adaptive predictive control is presented. In this chapter, the multirate adaptive controller is described which utilizes both the DSP hardware and the host PC. The multirate adaptive controller consists of a system identification technique which runs in real time plus a control parameter computation technique which periodically updates the controller. Also, a direct adaptive version of DPC is presented which runs on DSP hardware only. In this chapter adaptive SISO experimental results are presented showing the performance of the various techniques.

Adaptive controllers are further explored in Chapter 6. Here, the block adaptive controller is presented. The block adaptive controller differs from the multirate adaptive

controller in that the system identification is not performed in real time but rather updated based on blocks of input and output data. This scheme allows for MIMO implementation of large-order controllers. In Section 6.4.1 non-adaptive MIMO GPC is shown to provide vibration regulation of a four-input four-output plant. The effect on the acoustic far field is also shown. In Section 6.4.2 the controller is allowed to adapt and the improvement in performance is observed. Also, the bandwidth is greatly increased for the SISO adaptive case and the results are presented. The performance of the block adaptive feedback/feedforward controller is analyzed in Section 6.4.3 for the case of broadband disturbance and tonal disturbance. Here, the effect of the tonal disturbance is considered both at resonance and anti-resonance of the plate. Both SISO and MIMO implementations are investigated. In Section 6.4.4 the effect of non-collocated sensors and actuators is explored. It is shown that the adaptive block controller retains its ability to regulate without the need for collocation. In Section 6.5 the block adaptive controller is applied to a time varying plate. In this implementation it is shown that the controller loses its ability to provide stable regulation. Reasons for the inability of the controller to track changes in the plant and produce stable control are suggested. A modification of the block adaptive controller is later presented and regulation is obtained.

Appendix A of this thesis presents the application of adaptive predictive control using acoustic foam. In this appendix, it is shown that both passive and active attenuation of acoustic radiation may be obtained by using foam with a built-in actuator. In Appendix B, the algorithm for system identification using the Information Matrix[8] is presented along with a computation comparison with batch least squares. Finally, Appendix C presents a method for frequency shaping the GPC regulation performance. Here, it is shown that by redefining the cost function the level of regulation may be specified as a function of frequency across the regulation bandwidth. A non-adaptive SISO implementation is used to demonstrate the performance of the frequency-shaped controller.

Chapter 2

Literature Review

This chapter contains a brief review of the literature on system identification, control theory, and adaptive control theory in relation to real-time regulation of plants using discrete-time feedback controllers applied to nonminimum-phase systems.

2.1 System Identification

System Identification (SI), plays a crucial role in any adaptive control system. A classic study of various techniques for SI may be found in Ref. [1]. Here, Ljung presents the theoretical development of various techniques for SI as well as convergence analyses with advantages and disadvantages of several model types. Ref. [2-6] are text books which treat SI from the standpoint of control and filtering. These references present the theory and application of SI. An excellent study of SI for the purpose of feedback control may be found in Ref. [6] while SI for adaptive filtering may be found in Ref. [4-5]. References [2-3] present SI from the stand point of control. When SI is performed for control purposes, the system model may be in the form of state space or a finite difference equation. For adaptive control, the form chosen is typically polynomial when there is only a small number of input and output channels. The coefficients of the polynomial representations are referred to as Observer Markov Parameters (OMP), as in Ref. [6] or Auto-Regressive model with eXogenous input (ARX) parameters, as in Ref. [1]. It is the goal of the SI algorithm to identify the numerical values of the parameters. The simplest and most intuitive method for parameter identification is batch least squares as described in Ref. [1,6]. This method uses blocks of input and output data to perform the identification. When performing real-time identification, an algorithm is needed to update the OMP at every time step. As described in Ref. [2], various gradient descent methods may be employed. The stochastic gradient method is the simplest computationally, yet has the slowest convergence rate. An algorithm which converges faster at the cost of being more computationally expensive is the projection algorithm as described in Ref. [1]. The Recursive Least Squares (RLS) algorithm as described in Ref. [6] has a very fast

convergence rate, yet is the most computationally expensive of the real- time SI techniques. Other variations of RLS such as Extended Least Squares as in Ref. [2], Fast Transversal Filter as in Ref. [4-6], and Least-Squares Lattice Filter as in Ref. [6] offer both advantages and disadvantages in comparison to RLS. In Ref. [7], the similarity between several SI algorithms is shown in both state space and polynomial form. Reference [8] shows that several SI techniques can be derived from a common source known as the information matrix while Ref. [9] presents an improved technique for Kalman Filter identification.

In order to perform SI in a computationally efficient manner, an algorithm is needed which is capable of performing SI based on a block of input and output data rather than at every time step. A modification of the SI algorithm presented in Ref. [10] which uses the information matrix is ideal for such a task due to the efficient recursive method used to compute the correlation matrix. Since current microprocessor technology is too limited in bandwidth to perform adaptive control updates every time step while regulating a reasonable portion of the acoustic bandwidth, the algorithm presented in Ref. [10] may be modified to accomplish block SI updates based on batches of input and output data.

2.2 Predictive Control Theory

Classical papers which present Generalized Predictive Control (GPC), are Ref. [11-12]. In Ref. [11], the basic theory and algorithm of GPC is presented along with some interpretations. In Ref. [12], the interpretations are expanded and additional filters are introduced into the GPC algorithm and their use explained. In Ref.[13], a GPC algorithm is presented with guaranteed theoretical stability, although this algorithm is rather computationally intensive for adaptive control. In Ref. [47], the state space derivation of deadbeat predictive control is presented. In Ref. [15] the deadbeat predictive controller is further developed to include an extended control horizon and presented in both state space and polynomial form.

While DPC and GPC are the basic control algorithms used in this study, many other control techniques exist which are suitable for vibration regulation. References [2,16] present some alternative control methods, although many of the simpler algorithms are unsuitable for the control of nonminimum-phase plants. The Linear Quadratic Regulator (LQR), as presented in Ref. [17] is known to offer optimal control of a nonminimum-phase plant. This control technique has been applied to structures Ref. [18], however, the LQR is computationally expensive. An excellent theoretical development of finite-horizon predictive controllers may be found in Ref. [19] and a review of several predictive controllers in Ref. [20]. The use of Neural Networks for control purposes may be found in Ref. [21]. In the application of control techniques to structures, Ref. [22] describes the physics of a controlled structure and Ref. [23-24] relate the use of control theory to acoustics.

2.3 Adaptive Predictive Control

The combination of a system identification technique plus a control algorithm produces an adaptive controller. Traditionally, the SI is performed every time step with the controller being updated every time step as in Ref. [2-3]. A review of self-tuning predictive controllers which adapt every time step for nonminimum-phase system may be found in Ref. [25], while Ref. [26] uses the LQR solution as an adaptive controller. The behavior of adaptive controllers has also been studied as in Ref. [27-29] for the adaptive GPC algorithm. An algorithm for adaptive pole placement may be found in Ref. [30] which can also handle nonminimum-phase systems. In addition to the indirect adaptive control algorithms mentioned so far, direct adaptive controllers may also be used for the regulation task. References [31-32] describe a direct adaptive GPC algorithm and Ref. [33] describes a direct adaptive DPC algorithm. Also direct adaptive predictive controllers are described in Ref. [2].

Both direct and indirect adaptive controllers have been developed and implemented for several decades, Ref. [2,3]. However, in order to regulate disturbances over a large bandwidth, a control scheme which does not need to perform updates every

time step is advantageous. This thesis fills this need by investigating control schemes which reduce the computational burden of the adaptive regulator in comparison to traditional adaptive techniques, Ref. [34,35], and which remove the need to perform updates every time step, Ref. [36]. Instead, updates are performed on blocks of data which greatly increases the bandwidth of the regulator while still offering the possibility of tracking both changes in the disturbance spectral content as well as the plant.

Chapter 3

Fundamentals of Predictive Control

3.1 Introduction

Predictive controllers have found application in a wide range of industrial processes[2]. Two examples of such controllers are generalized predictive control and deadbeat control. Generalized predictive control is presented in Ref. [11] as a technical paper and deadbeat control is presented in Ref. [16] which is a text book. Recently, deadbeat control has been augmented to include an extended horizon[15]. This modification, named deadbeat predictive control, retains the advantage of guaranteed stability if an exact system model is known and offers a simple way of control weighting. This chapter presents an application of both predictive control techniques to vibration suppression of plate modes. Several system identification routines are presented. Both algorithms are shown to be useful in the suppression of plate vibrations. Experimental results are given and the algorithms are shown to be applicable to nonminimum-phase systems.

The goal of the control techniques described is to reduce the level of unwanted structural vibrations. In general, the structure is excited by broad-band noise and the response is multi-modal. Traditional methods of achieving vibration control are primarily focused on feed-forward techniques[37] and rate feedback control is the dominate method used for feedback implementations. In the literature, there is a large amount of information on such techniques along with impressive results[38].

To achieve feed-forward control, it is required that a coherent reference be available. It is also required that processing be done on this reference signal before it reaches the controlled location. Recent advances in microprocessors have increased the processing speed to the point where if a coherent reference is available, vibration reduction can be achieved[38]. However, it is not possible to use feed-forward when no such reference is available.

The feedback control approach does not need a reference to achieve vibration control, as the control signal is derived from the error sensor. The advances in microprocessor speed have made it possible to compute the control effort and apply it to the actuator within one sampling period[35]. In designing control systems for this purpose, the algorithms must be fast enough to be implemented in real time. The control methods presented here are computationally efficient.

In order to design the controller, an input/output model of the plant must be identified. This model is the transfer function from the actuator to the error sensor. Typical methods of system identification are used to determine the parameters of this model. These methods include batch least squares and recursive least squares[6]. If faster computation is desired, the projection algorithm[2] may be used at the expense of convergence speed. In general, any system identification technique may be used which will return an Auto-Regressive with eXogenous input (ARX) model of the plant[1].

Based on the ARX model obtained using a system ID technique, a controller can be designed. Since the system identification can only return an approximation of the true plant under test, the controller must be robust against parameter uncertainties[19]. This implies that the control method chosen must have the ability to tolerate uncertainties to a certain degree without going unstable or suffering a large performance degradation. The LQR solution offers the robustness needed to provide regulation. However, the LQR solution is computationally intensive since the prediction horizon goes to infinity. Many of the LQR properties may still be realized in finite horizon controllers such as Generalized Predictive Control.

Generalized Predictive Control (GPC) may be used to regulate a plant based on an identified model. This control technique may be tuned to the desired balance between performance and robustness. If an increased level of performance is desired, the control penalty may be decreased as long as stability is maintained. On the other hand if a more

robust controller is desired, the control penalty may be increased at the expense of performance[35]. Increasing the control penalty will decrease the control effort because the control effort will be penalized more in the cost function. GPC also has the ability to regulate a nonminimum-phase plant. However, the GPC algorithm suffers from the fact that there are many parameters to adjust and it is not known ahead of time the best settings for these parameters[11].

Another technique for achieving vibration control is Deadbeat Predictive Control (DPC)[15]. In DPC there are only two integer parameters to adjust and stability is guaranteed if the plant model is exact. The DPC algorithm is similar to GPC in that it is a receding horizon controller, but differs from GPC in that the current control output is designed to the drive the sensor error to zero after a number of time steps equal to or greater than the system order[15]. By doing so, the problem of instability resulting from regulating a nonminimum-phase plant is always avoided if the plant model is exact. The GPC solution will seek to drive the sensor error to zero starting at the next time step and ending at the control horizon. The performance of DPC is shown in this work to be comparable to that of GPC for low order systems.

While DPC and GPC are presented here, in general any feedback technique may be a good candidate for vibration suppression. By extending the control and prediction horizons to very large values, the GPC solution approaches the Linear Quadratic Regulator (LQR)[12]. The limitation on LQR for adaptive control is the computational burden. Various methods of minimum-variance control offer solutions to minimum-phase plants[2]. It is well known that collocation of sensors and actuators produces a minimum-phase transfer function in continuous time[22]. However, when in discrete time, this is not always the case. Various forms of Proportional-Integral-Differential (PID) controllers have also been applied to achieve regulation[22]. These controllers have a drawback in that they do not always approximate an optimal controller and collocation is necessary for reasonable robustness.

This chapter presents the experimental results obtained by applying GPC and DPC to vibration suppression of an aluminum plate. Section 3.2 outlines the system identification technique and the model structure. Section 3.3 presents the GPC algorithm and the DPC algorithm. Section 3.4 describes the experimental setup and presents an off-line simulation based on the identified plant. Also presented are experimental results for both GPC and DPC with a discussion following in section 3.5.

3.2 System Identification Using MATLAB

For small displacements the input/output model of a structure can be reasonably represented by a linear finite-difference model[6]. If the plate displacement is large or the control effort becomes too great, the input/output map may become nonlinear. Even for nonlinear systems, the linear finite-difference model can be shown to be a reasonable approximation over a small spectral region of interest[1]. For both GPC and DPC a finite-difference model is used. The form of this model, commonly called the Auto-Regressive with eXogenous input model (ARX), is shown in Eq. (3.1)[6].

$$y(k) = \alpha_1 y(k-1) + \alpha_2 y(k-2) + \ldots + \alpha_p y(k-p) + \beta_0 u(k) + \beta_1 u(k-1) + \ldots + \beta_p u(k-p) + d(k) \qquad (3.1)$$

It is the task of the system identification technique to produce estimates of β_j and α_j where $j = 1,2,\ldots p$ and p is the ARX model order. The batch least squares solution may be used to find the desired parameters. If it is desired to obtain a solution on-line, then recursive least squares or any one of the numerous recursive techniques may be used[6]. In general, any system identification technique can be used which will produce estimates of the α's and β's. For the implementations described in this section, the system identification was achieved using MATLAB's system ID toolbox. This was accomplished by exciting the actual plant with band-limited white noise, and observing the output. Both the input and output data sets were then used by MATLAB using the command *arx( )* to compute the ARX parameters. The ARX parameters were then used to determined the control parameters.

3.2 Predictive Control Algorithms

Once the system model of the plant to be regulated is determined, some sort of control algorithm must be used to compute the control parameters based on the ARX parameters. Two such algorithms are presented. The first is Generalized Predictive Control and the second is Deadbeat Predictive Control.

3.2.1 Generalized Predictive Control, Basic Formulation

The basic GPC algorithm was formulated by D. W. Clarke[11], a modification of it is presented here for SISO systems. An ARX model is used to represent the input/output relationship for the system to be regulated. In this discrete-time model, y is the plant output and u is the control input. The disturbance is $d(t)$ and z^{-1} is the backwards shift operator. The ARX model shown in Eq. (3.1) may be written in compact notation to become

$$A(z^{-1})y(k) = B(z^{-1})u(k-1) + d(k) \tag{3.2}$$

where

$$A(z^{-1}) = 1 - \alpha_1(z^{-1}) - \alpha_2(z^{-2}) - \ldots - \alpha_p(z^{-p})$$

$$B(z^{-1}) = \beta_0 + \beta_1(z^{-1}) + \beta_2(z^{-2}) + \ldots + \beta_p(z^{-p})$$

In order to reduce the effects of the disturbance on the system, a way of predicting the future plant outputs must be devised. It is desirable to express the future outputs as a linear combination of past plant outputs, past control efforts, and future control efforts. Once this is done, the future plant outputs and controls may be minimized for a given cost function. The Diophantine equation is used to estimate the future plant outputs in an open-loop fashion[11]. The Diophantine equation shown in Eq. (3.3) uses the ARX model to mathematically predict future system outputs.

$$1 = A(z^{-1})E_j(z^{-1}) + z^{-j}F_j(z^{-1}) \tag{3.3}$$

The integer N is the prediction horizon and $j = 1,2,3,\ldots N$. In the above equation, we have that

$$E_j(z^{-1}) = 1 + e_1z^{-1} + e_2z^{-2} + \ldots + e_{N-1}z^{-N+1}$$

$$F_j(z^{-1}) = f_0 + f_1z^{-1} + f_2z^{-2} + \ldots + f_{N-1}z^{-N+1}$$

For any given $A(z^{-1})$ and prediction horizon N, a unique set of j polynomials $E_j(z^{-1})$ and $F_j(z^{-1})$ can be found. A fast recursive technique for finding these parameters is presented in Ref.[11]. If Eq. (3.2) is multiplied by $E_j(z^{-1})z^j$, one obtains

$$E_j(z^{-1})A(z^{-1})y(k+j) = E_j(z^{-1})B(z^{-1})u(k+j-1) + E_j(z^{-1})d(k+j)$$

Combining this with Eq. (3.3) yields

$$y(k+j) = E_j(z^{-1})B(z^{-1})u(k+j-1) + F_j(z^{-1})y(k) + E_j(z^{-1})d(k+j)$$

Since we are assuming that future noises can not be predicted, the best approximation is given by

$$y(k+j) = G_j(z^{-1})u(k+j-1) + F_j(z^{-1})y(k) \tag{3.4}$$

Here we have that $G_j(z^{-1}) = E_j(z^{-1})B(z^{-1})$. The above relationship gives the predicted output j steps ahead without requiring any knowledge of future plant outputs. We do, however, need to know future control efforts. Such future controls are determined by defining and minimizing a cost function.

Since Eq. (3.4) consists of future control efforts, past control efforts, and past system outputs it is advantageous to express it in a matrix form containing all j step ahead relationships. It is also desirable to separate what is known at the present time step k from what is unknown, as this will aid in the cost function minimization. Consider the following matrix relationship

$$y = Gu + f$$

where the $N \times 1$ vectors are

$$y = [y(t+1), y(t+2), \ldots, y(t+N)]^T$$
$$u = [u(t), u(t+1), \ldots, u(t+N-1)]^T$$
$$f = [f(t+1), f(t+2), \ldots, f(t+N)]^T$$

The vector y contains the predicted plant responses, the vector u contains the future control efforts yet to be determined, and the vector f contains the combined known past controls and past plant outputs. The vector f may be filled by the following relationship.

$$f(t+1) = [G_1(z^{-1}) - g_0]u(t) + F_1 y(t)$$
$$f(t+2) = z[G_2(z^{-1}) - z^{-1}g_1 - g_0]u(t) + F_2 y(t)$$
$$f(t+3) = z^2[G_3(z^{-1}) - z^{-2}g_2 - z^{-1}g_1 - g_0]u(t) + F_3 y(t)$$
etc

The matrix *G* is of dimension *N x N* and consists of the plant pulse response. This differs from Ref. [11] where the matrix G consists of the plant step response. This difference is due to the inherent integration of Ref. [11].

$$G = \begin{bmatrix} G_1 \\ G_2 \\ \vdots \\ G_N \end{bmatrix} = \begin{bmatrix} g_0 & 0 & \cdots & 0 \\ g_1 & g_0 & \cdots & 0 \\ \vdots & & \ddots & \vdots \\ g_{N-1} & g_{N-2} & \cdots & g_0 \end{bmatrix}$$

It is desired to find a vector *u* which will minimize the vector *y*. Consider the following cost function for a single-input single-output system.

$$J = \sum_{j=1}^{N} (y(k+j))^2 + \sum_{j=1}^{NU} \lambda (u(k+j-1))^2$$

Where the scalar λ is the control cost. Minimization of the cost function with respect to the vector *u* results in

$$u = -(G^T G + \lambda I)^{-1} G^T f \qquad (3.5)$$

The above equation returns a vector of future controls. In practice, the first control value is applied for the current time step and the rest are discarded. The above computations are repeated for each time step resulting in a new control value.

As can be found in the literature, the above algorithm has many variations[19]. One way to achieve control of a nonminimum-phase plant is to chose a value of *NU*, the control horizon, smaller than the prediction horizon *N*, i.e. $NU < N$ where *NU* is the control horizon. This may be achieved by simply deleting the last *NU* to *N* columns of the *G* matrix. Doing this will also result in faster computations. The control effort may be suppressed by increasing λ. It has been found that setting the control horizon smaller than the prediction horizon results in a controller which can regulate nonminimum-phase plants[12]. This is due to the fact that if the control horizon is set small enough in comparison to the prediction horizon, the controller will not seek to place closed-loop

poles at all of the plant zeros. Generally, one should set the prediction horizon *N* at least equal to or greater than the system order *p*. The GPC algorithm has four parameters to adjust. The system order *p*, the prediction horizon *N*, the control horizon *NU*, and the control weight λ all must be chosen. As in most control systems, one has to balance performance with system stability and actuator authority. More information on GPC may be found in Section 4.3 of this thesis.

3.2.2 Deadbeat Predictive Control, Basic Formulation

The Deadbeat Predictive Controller (DPC) offers comparable performance without the need to tune as many parameters as GPC[15]. The basic algorithm is presented below and is based on the observable canonical state space form. Given the estimated values of the α*'s* and β*'s* in Eq. (3.1), the system may be represented in observable canonical form shown in Eq.(3.6). *Z(k)* is the state at time step *k*. We assume a zero direct transmission term, i.e., $\beta_0 = 0$.

$$Z(k+1) = A_p(k) + B_p u(k) \tag{3.6}$$
$$y(k) = C_p Z(k)$$

where

$$Z(k) = \begin{bmatrix} y(k) \\ z_1(k) \\ z_2(k) \\ \vdots \\ z_{p-1}(k) \end{bmatrix}, \qquad A_p = \begin{bmatrix} \alpha_1 & I & 0 & \cdots & 0 \\ \alpha_2 & 0 & I & \ddots & \vdots \\ \alpha_3 & 0 & 0 & \ddots & 0 \\ \vdots & \vdots & \vdots & \vdots & I \\ \alpha_p & 0 & 0 & \cdots & 0 \end{bmatrix}, \qquad B_p = \begin{bmatrix} \beta_1 \\ \beta_2 \\ \beta_3 \\ \vdots \\ \beta_p \end{bmatrix}, \qquad C_p = \begin{bmatrix} I & 0 & \cdots & 0 \end{bmatrix}$$

If the controller is to be implemented in state space a state observer is needed. Once the observer is determined, the control effort for the present time step is given by

$$u(k) = GZ(k) \tag{3.7}$$

where *G* is the first *r* rows of

$$-[A_p^{q-1}B_p, \ldots A_pB_p, \ B_p]^+ A_p^q$$

r is the number of inputs, *q* is the prediction horizon, and $^+$ means the pseudo inverse. The prediction horizon is chosen to be greater than or equal to the system order *p*. If *q* is

set equal to *p*, then one obtains deadbeat control. Typically, *q* is set greater than *p* in order to limit the control effort so as not to saturate the actuator.

The DPC controller may also be implemented in polynomial form thereby eliminating the need for a state observer. The technique is shown below. The derivation can be found in Ref. [14]. The matrix *G* of Eq. (3.7) may be partitioned as shown in Eq. (3.8).

$$G = \begin{bmatrix} g_1 & g_2 & g_3 & \cdots & g_p \end{bmatrix} \tag{3.8}$$

Combining Eq. (3.6), Eq. (3.7) and Eq. (3.8), the feedback control may be found as shown in Eq. (3.9) based on past input and output data.

$$u(k) = F_1 y(k-1) + F_2 y(k-2) + \ldots + F_p y(k-p) + H_1 u(k-1) + H_2 u(k-2) + \ldots + H_p u(k-p) \tag{3.9}$$

Where the controller parameters are given by

$$F_1 = [g_1 \;\; g_2 \;\; \ldots \;\; g_p] \begin{bmatrix} \alpha_1 \\ \alpha_2 \\ \vdots \\ \alpha_p \end{bmatrix}, \qquad F_2 = [g_1 \;\; g_2 \;\; \ldots \;\; g_{p-1}] \begin{bmatrix} \alpha_2 \\ \alpha_3 \\ \vdots \\ \alpha_p \end{bmatrix}, \quad \ldots \quad F_p = g_1 \alpha_p$$

$$H_1 = [g_1 \;\; g_2 \;\; \ldots \;\; g_p] \begin{bmatrix} \beta_1 \\ \beta_2 \\ \vdots \\ \beta_p \end{bmatrix} \qquad H_2 = [g_1 \;\; g_2 \;\; \ldots \;\; g_{p-1}] \begin{bmatrix} \beta_2 \\ \beta_3 \\ \vdots \\ \beta_p \end{bmatrix}, \quad \ldots \quad H_p = g_1 \beta_p$$

where $[g_1 \;\; g_2 \;\; g_3 \;\; \ldots]$ consist of the appropriate number of columns of the *G* matrix defined above and the values of the α*'s* and β*'s* are those found by the system ID technique. The formulation above eliminates the need for a state observer as it can compute the control effort based only on input and output measurements. The DPC will always be stable as long as $q \geq p$ and the plant model exactly matches the physical plant. This stability property will hold true for nonminimum-phase system as well.

The DPC algorithm requires only two parameters to be adjusted, *p* the system order and *q* the prediction horizon. Both *p* and *q* are integers, so the tuning process is

simplified in comparison to GPC. The tuning of DPC is a balance between performance and actuator saturation. If the control effort exceeds the limits of the actuator, then q may be increased to reduce the control signal. If q is decreased then the control effort will increase. This increase in the control effort for a reduced q is due to the fact that the controller is trying to bring the plant to zero state in a smaller number of time steps. The value of p is typically chosen to be five or six times the number of significant modes of the structure. A large value of p allows for more complete modeling of the plant dynamics and allows for computational poles and zeros to improve the system identification results, i.e., if there is a sufficient number of parameters to adjust in the system identification a Kalman filter will be approximated[6]. This is to say that the state observer embedded within the polynomial model will closely approximate the Kalman filter for the state space model. If the polynomial model order is sufficiently large, then the properties of the Kalmann filter may be assumed to be embedded within the controller designed from the polynomial model. The state space Kalman filter and plant model may be determined from input and output data using a technique such as OKID as in Ref. [6]. More information on DPC may be found in Section 4.4 of this thesis.

3.3 Experimental Setup and Results

This section presents the experimental setup and results obtained using both the Generalized Predictive Controller and the Deadbeat Predictive Controller. The system identification was performed using the MATLAB *arx( )* command and input and output data blocks. The system ID results were then used to compute the controller parameters in polynomial form. The control parameters were downloaded to the digital signal processor for real-time control.

3.3.1 Experimental Setup

Figure 3.1 below shows the structure to be controlled by GPC or DPC.

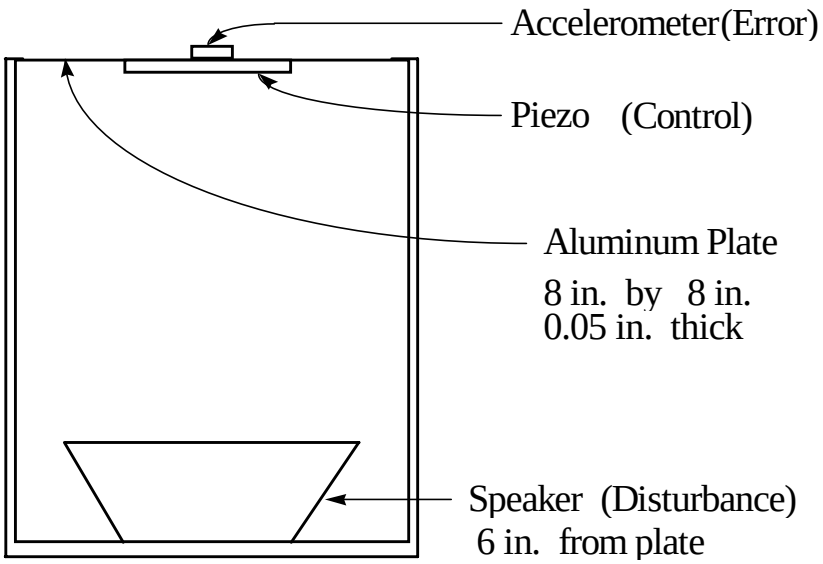

Figure 3.1 Test Box

The test box consists of an aluminum plate with clamped boundaries mounted on the top of a plexi-glass box. The disturbance enters the plant through the loud speaker at the bottom of the box and causes the plate to vibrate, thereby radiating noise to the exterior space. A piezo-electric transducer is mounted under the plate as the control actuator. The error, or plant output, is the signal read from the accelerometer. It is desired to reduce the amount of noise radiated from the plate. This is accomplished by reducing the vibration amplitude of the odd plate modes. Since the accelerometer is placed at the center of the plate, those modes with a node at the accelerometer are not observable. Even though even modes are poor radiators[39], if it is desired to exercise control over them an additional piezo and accelerometer pair may be added. This addition may also improve the control authority over all modes. Since the control techniques presented can easily be extended to multi-input multi-output (MIMO) systems, the addition of additional sensors and actuators poses no problem.

It is well known that collocation of sensors and actuators may result in a minimum-phase system in continuous time[22]. Even though both DPC and GPC can

handle nonminimum-phase systems, collocation results in improved performance. From a controls standpoint, this comes from the fact that the more minimum-phase like a system is, the easier it is to control[2]. From a physical standpoint, this amounts to saying that the controller has a direct influence over the sensor output. Direct in this context means that the actuator's efforts do not have to propagate through any of the structure to reach the sensor.

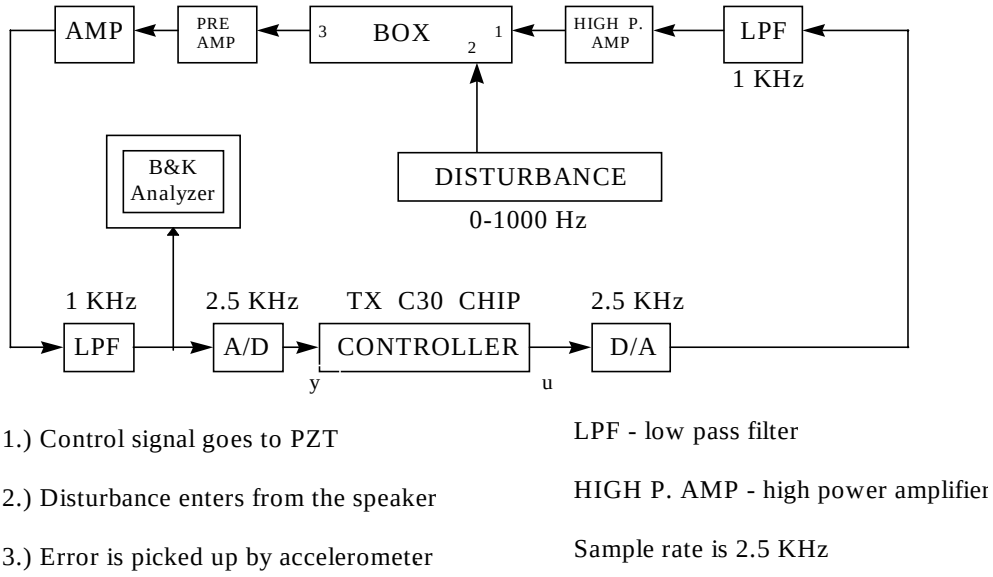

Figure 3.2 Block Diagram of Control System

Figure 3.2 shows the block diagram of the closed-loop system. This experimental setup was used to test the performance of both GPC and DPC. Band-limited (0-1KHz) white noise was used as a disturbance input to excite the plate. The noise was generated by a white noise generator and then filtered through a four pole filter which had a three dB cut off of 1KHz. The four pole filters were found to provide a reasonable balance between the need for high frequency attenuation and small phase lag. If filters with a sharper cut-off were chosen, the resulting closed-loop system would have better high frequency suppression at the expense of greater phase lag. The increased phase lag within the feedback controller will degrade regulation. The aluminum plate had two odd modes

in the bandwidth of interest. The fundamental mode is around 300 Hz and the other around 1 KHz. The control output and the accelerometer signal were also filtered with four pole Butterworth low pass filters set to 1 KHz. Because of the filters gradual roll off, the 1KHz mode was not greatly attenuated by the filters. The filters did, however, greatly suppress the higher modes.

When sampling any continuous time system, one must chose a sampling rate carefully[6]. If a continuous-time system is sampled too fast, a poor discrete-time system identification results from the loss of frequency resolution for a fixed order system model. In addition to this, sampling too fast results in the placement of more zeros outside the unit circle which degrades the control performance. If sampling is performed too slow, then the higher frequencies alias[40]. Typically, experience has shown that a sampling rate between two to three times the highest frequency to be controlled results in the best performance. After trying several different sampling rates, 2.5 KHz was found to yield reasonable performance for the experimental setup shown.

With a sample rate of 2.5 KHz, the input and output data were gathered for system identification. It is desired to find the transfer function between the points labeled u and y in Fig. 3.2. This was accomplished by inputting band limited white noise into the system at location u and measuring the resulting system response at location y. In performing the system identification in this manner, all system components, even the A/D and D/A, were modeled. Ten thousand input and output points were collected and a fit was made to a 12^{th} order ARX model, i.e. $p = 12$, using the MATLAB program *arx()*. The model order was chosen based on the number of modes and the fact that computational poles and zeros are needed for a good fit in the presence of disturbances. Several different orders were tried and 12 provided a good fit. A pole zero plot of the resulting system model is shown in Fig. 3.3.

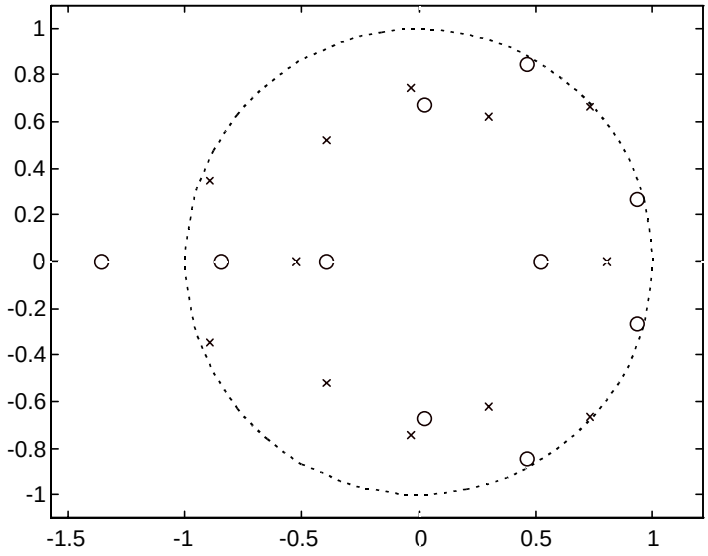

Figure 3.3 Pole Zero Plot of Transfer Function

In Fig. 3.3 the dashed line represents the unit circle, the symbol x represents the poles, and the symbol o the zeros. There are four x's just inside the unit circle which result from the two lightly damped plate modes. Also note that there is a zero outside the unit circle. This nonminimum-phase characteristic resulted from discretizing the minimum-phase continuous time system.

After the system identification was complete, the GPC algorithm was used for controller design. Before implementing the controller, it is instructive to run a simulation and test the controller performance. The simulation results are shown in Fig. 3.4.

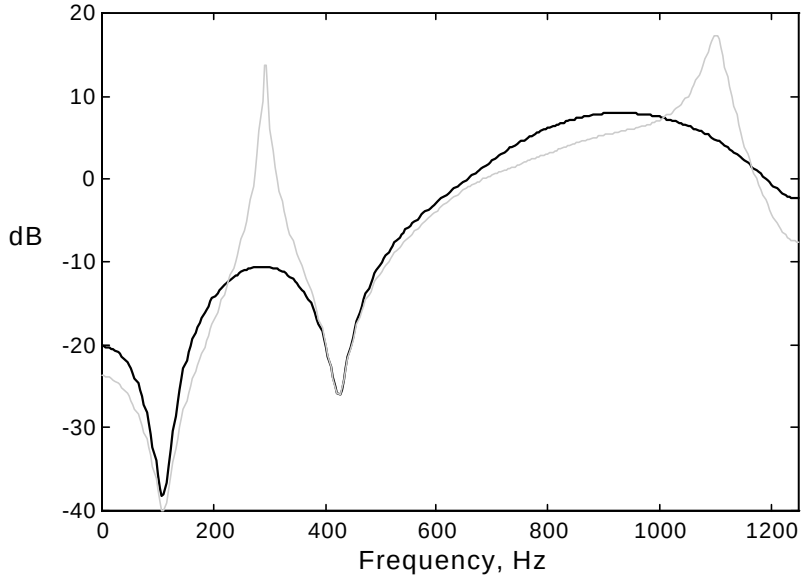

Figure 3.4 GPC Simulation Results

In Fig. 3.4, the black line is the bode plot magnitude of the closed-loop (controlled) system with the GPC controller and the gray line is the magnitude of the bode plot for the open-loop system. In both plots the identified model was used as the plant. As can be seen from Fig. 3.4, the two modes are present. When the loop is closed, we get about 22 dB reduction on the first mode and about 12 dB reduction on the second. There are some regions of the spectrum where the GPC controller is actually causing amplification. This results from the fact that the cost function was designed to minimize the overall system output for a random disturbance with the control effort in mind. Minimizing the plant output does not necessarily imply that the closed-loop response will be reduced for all frequencies. It does, however, mean that the variance of the error sensor will be minimized.

In designing the GPC controller, both control and prediction horizons were set to 20 and the control weight, λ, was set to 0.01. The horizon length was chosen to have a sufficient number of time steps beyond the system order (12^{th} order) and the control weight, λ, was adjusted to yield a stable closed-loop system. This adjusting of the

horizons and control penalty was done both in the simulations and in the actual implementation. It was found that greater control could be exercised in the simulations which resulted in better disturbance rejection. This is not surprising since the plant model from which the controller was designed was used in the simulations so the plant model is exact and the actual plant was used in the experiment. Also, in the experiment noise is present whereas the simulations are noise free. For both the experiment and simulation, performance may be increased by increasing the prediction horizon and decreasing the control penalty as long as stability is maintained.

3.3.2 Experimental Results

Figure 3.5 shows the time history of the experimental output data. The plot includes the open- and closed-loop accelerometer signal. The accelerometer signal was measured by the B&K analyzer as shown in Fig 3.2. As in the simulations, the horizons were set to 20 and the control penalty to 0.01.

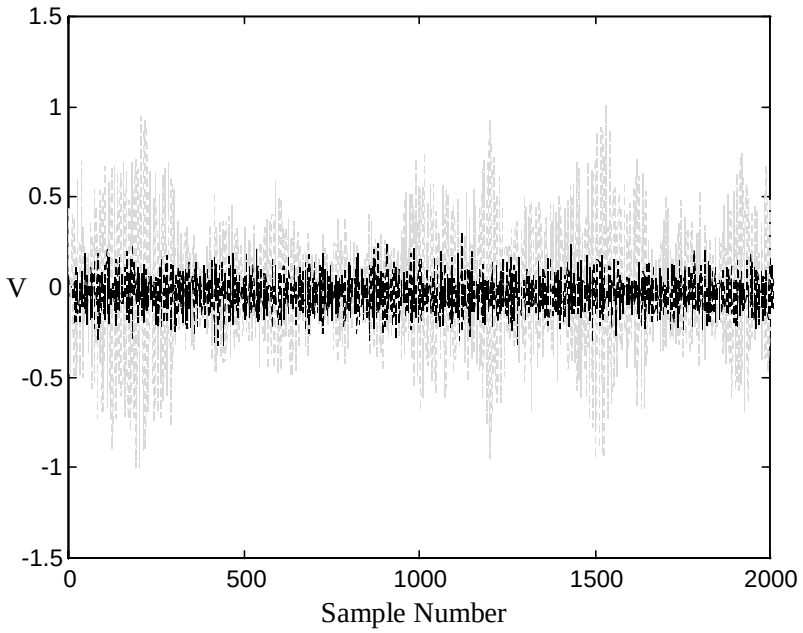

Figure 3.5 Plot of Time History

In Fig. 3.5, the gray line is the open-loop accelerometer voltage and the black line is the closed-loop accelerometer voltage. Since the sample rate was set to 2.5 KHz, 0.80 second

of data is shown. It is obvious that some disturbance rejection is being obtained by closing the loop.

One way to judge how well a controller is performing is to examine the auto-correlation of the system output[16]. The autocorrelation of the controlled and uncontrolled accelerometer output are plotted in Fig. 3.6.

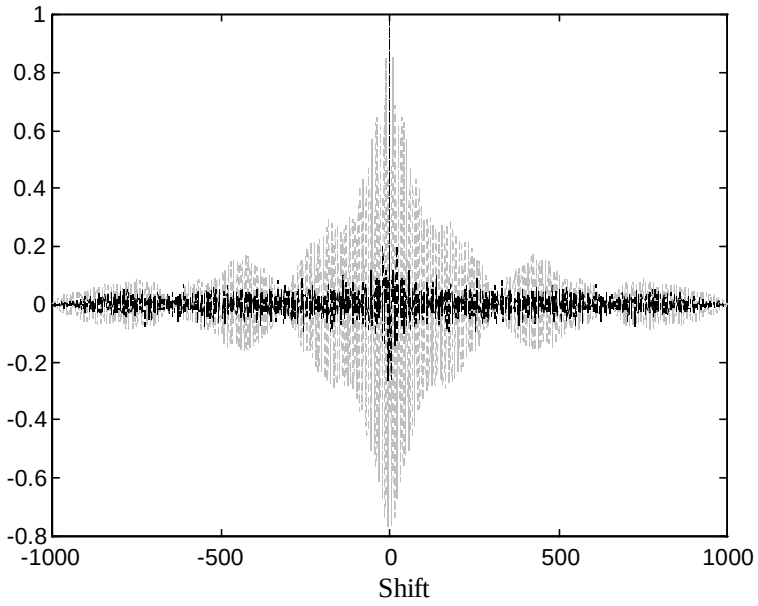

Figure 3.6 Plot of Autocorrelation of Accelerometer Signal

The open-loop autocorrelation is gray and the closed-loop is black. As can be seen in Fig. 3.6, the open-loop output has correlation in it. This correlation is due to the presence of the two modes at 300 Hz and 1 KHz. In theory, it is known that applying feedback control to the plant will remove the correlation from the output[16]. Feedback control can only remove correlation from the plant response. Correlation here means the autocorrelation of the plant output. The feedback controller cannot reduce the level of uncorrelated noise at the sensor output. As can be seen from Fig. 3.6, the correlation has been mostly removed.

The Fourier transform of the autocorrelation will give the spectrum. The spectra of the open- and closed-loop systems are shown in Fig. 3.7. Once again GPC was used

with the horizons set to 20 and the control penalty to 0.01. The sampling rate was 2.5 KHz.

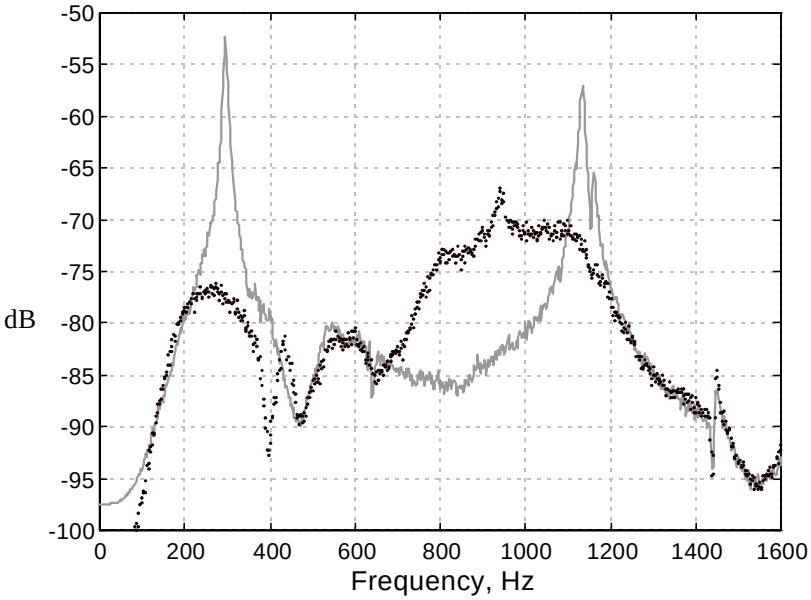

Figure 3.7 Generalized Predictive Control

In Fig. 3.7, the gray line is the spectrum of the accelerometer output without control and the dotted black line is the output with control. The result is similar to that shown in Fig. 3.4. In Fig. 3.7, the vertical axis is not calibrated and is used only to show the closed-loop result relative to the open-loop result. At the first mode, around 300 Hz, we see an approximate reduction of around 22 dB while at the second mode we see a reduction of around 13 dB. This is in close agreement with the simulation results. Some of the differences between Figs. 3.4 and 3.7 can be accounted for by uncertainties in the identified ARX model parameters and noise in the experiment. However, in comparing the open-loop plot of Fig. 3.4 with the open-loop plot of Fig. 3.7 we see that the responses differ greatly between the frequencies 400 Hz to 1100 Hz. One contributing factor to this difference is that in the simulation of Fig. 3.4 the disturbance was white noise applied directly to the plant output. The model response seen in Fig. 3.4 is due to the autoregressive nature of the ARX model. This is to say that the signal *d(k)* in Eq. (3.2) is simply white noise. In contrast, the disturbance acting on the actual plant does not

manifest itself in the form of white noise added to the plant output. Instead, the white noise is filtered by the dynamics of the plate and the effects of the white noise are observed at the sensor. A closer match between Fig. 3.4 and Fig. 3.7 would be obtained if the disturbance was modeled as $C(z^{-1})d(k)$ rather than just $d(k)$ in Eq. (3.2). Here, $d(k)$ is white noise and $C(z^{-1})$ is a polynomial describing the effects of the white noise on the plant as seen by the accelerometer.

Deadbeat Predictive Control was also tested in the same setup. The spectrum results of the open- and closed-loop accelerometer responses are shown in Fig. 3.8.

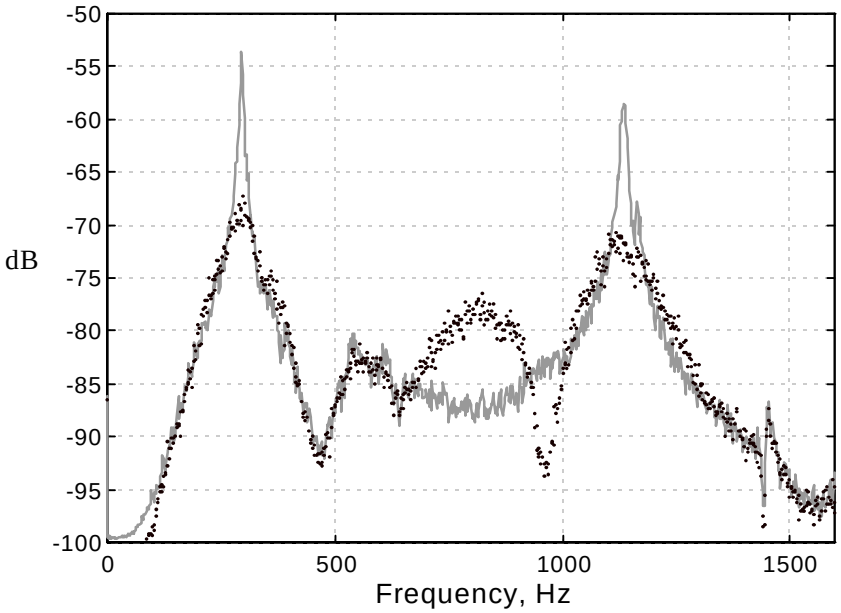

Figure 3.8 Deadbeat Predictive Control

The gray line is the open-loop accelerometer output and the black dotted line is the closed-loop. From Fig. 3.8 both modes are lowered to around the same level. The mode at 300 Hz has an approximate reduction of 15 dB while the 1 KHz mode is reduced by around 13 dB. As in the GPC spectrum, the vertical scale is used only for comparison purposes. The fact that DPC lowers the peaks in the spectrum to an approximately equal level is a result of not having a control weight. In tuning the DPC controller, one has to adjust only one integer parameter after the order of the system has been determined[15].

This integer parameter, the control horizon, was adjusted to give the best reduction without saturating the actuator. For the system order of $p = 10$ which was used, the control horizon was set to $q = 12$. Since the control horizon is always chosen to be greater than or equal to the system order, the tuning of DPC was found to be a simple task. The performance of the controller could be increased by decreasing the control horizon q as long as the actuator was not saturated. Alternatively, by increasing q a smaller control effort could be obtained resulting in reduced regulation.

The performance of the DPC algorithm was further tested by increasing the bandwidth. The results are shown in Fig. 3.9.

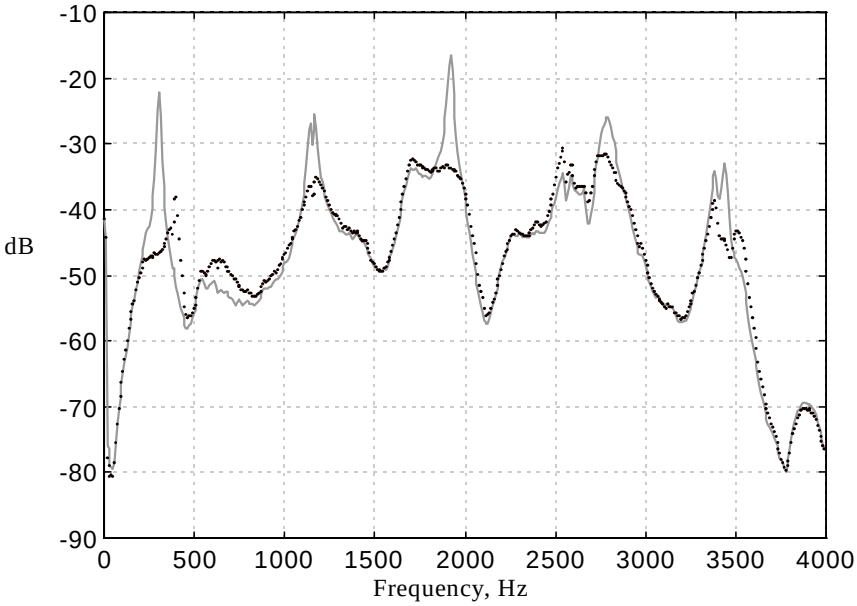

Figure 3.9 DPC With Large Bandwidth

Fig. 3.9 shows that deadbeat predictive control can be used to suppress the vibrations of a plate over a wide bandwidth. The total reduction is 5.00 dB. As can be seen in the figure, five modes are attenuated. This was accomplished by increasing the filter bandwidths to 3150 Hz, the sampling rate to 12 kHz, and the system order to 18. In this case, the control horizon was also set to 18.

3.3.3 Effect of Dampening on Feedback Control

The test box shown in Fig. 3.1 has lightly damped poles which make feedback control of resonant responses an easy task. This section investigates the relationship between the performance of feedback control an dampening. Intuitively, one would expect that the amount of regulation feedback control can offer is dependent on the amount of correlation in the plant output, i.e., the less damped the plant poles are the better the performance. The following experiments show that the level of regulation achievable using feedback control is dependent on plant dampening.

The box shown in Fig 3.1 may be modified by placing sand on top of the aluminum plate. In this experiment, 256 grams of sand is evenly distributed across the top of the aluminum plate. A system ID is performed for the sand weighted plate and GPC is used to regulate the plate vibrations.

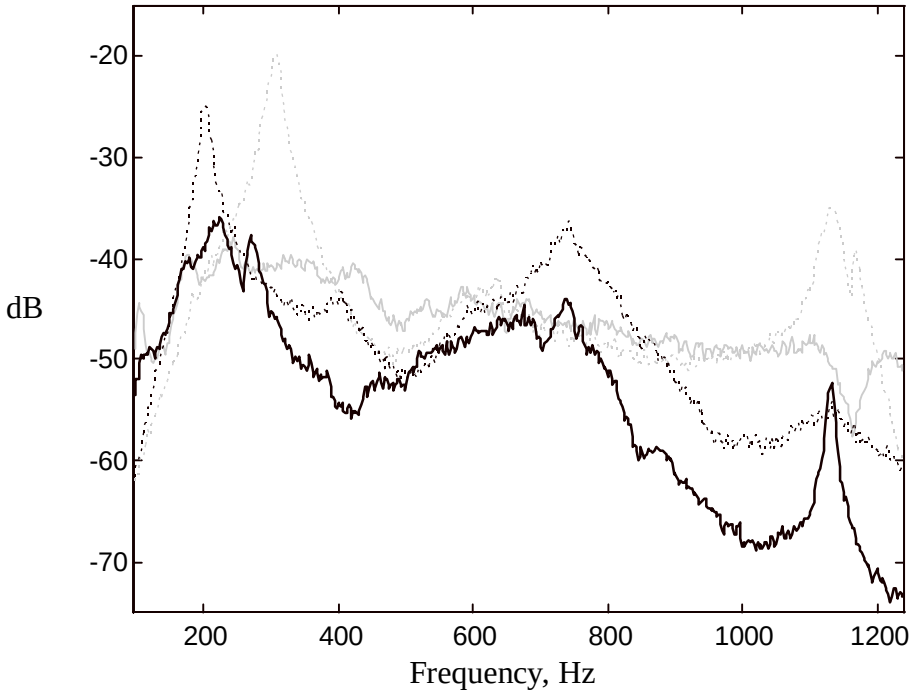

Figure 3.10 Sand Weighted Plate Experiment

Figure 3.10 shows the autospectrum of the accelerometer signal for the open-loop plate response without sand, gray dotted line, closed-loop without sand, gray line, open-loop with sand, dotted line, and closed-loop with sand, black line. In this experiment, seven pole filters with 1 kHz 3db cutoffs were used to low-pass filter both the accelerometer and piezo signals. The sample rate was 4 kHz and the GPC control penalty was 0.0003. The system model order was 50 and both prediction and control horizons were set to 100. By comparing the plots in Fig. 3.10, we see that placing sand on top of the plate did dampen the resonant response of the plate and also mass loaded the plate. Table 3.1 summarizes the results.

Table 3.1 Integrated Spectra for Sand Experiment

	No Sand dB	Sand dB	Difference dB
Open Loop	-10.2	-14.6	4.4
Closed Loop	-18.7	-19.6	0.9
Difference dB	8.5	5.0	

In order to dampen the plate response without mass loading, the clamped boundary conditions used in Fig. 3.1 may be altered by placing rubber between the aluminum plate and the mounting support. This was done for the bottom side of the plate. The rubber was only applied to the boundaries and did not interfere with the plate excitation or radiation.

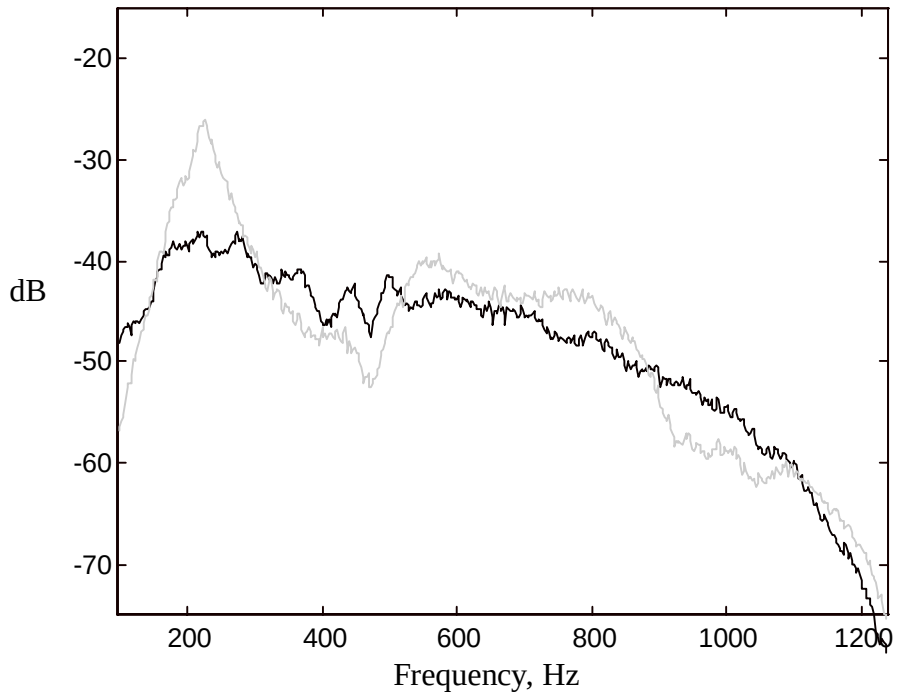

Figure 3.11 Plate Experiment With Rubber

Figure 3.11 is a plot of the accelerometer signal with the box altered by the addition of rubber in the plate boundary conditions. The gray line is the open-loop response and the black line is the closed-loop response. The control settings remained the same as in Fig. 3.10. By comparing the open-loop responses of Figs. 3.10 and 3.11, we see that the plants resonant response have been reduced without significantly shifting the resonant frequency. Also, the amount of vibration reduction gained by using feedback control has diminished. A summary of the totals for Fig. 3.11 is shown in Table 3.2.

Table 3.2 Integrated Spectra for Rubber Experiment

	No Rubber dB	Rubber dB	Difference dB
Open Loop	-10.2	-13.6	3.4
Closed Loop	-18.7	-18.4	0.3
Difference dB	8.5	4.8	

Table 3.3 Natural Frequencies and Dampening of Dominant Modes

Free Plate		Sand Plate		Rubber Plate	
Freq. Hz	%Damp	Freq. Hz	%Damp	Freq. Hz	%Dampen
289.551	6.750	200.945	2.174	187.529	6.090
311.129	2.797	582.836	6.468	226.874	3.814
1131.903	1.114	707.923	4.957	565.876	16.469
1170.137	0.944	781.368	4.392	1083.938	5.503

Table 3.3 list the natural frequencies and dampening of the dominate modes for the open-loop experiments. The first two columns are for the plate with no rubber applied to the boundaries and no sand. The next two are for the sand loaded plate and the final two are the plate with rubber applied to the boundaries.

3.4 Summary

The LQR controller has been proven to be the optimal solution for the regulation of a linear plant[17]. If one extends both control and prediction horizons to infinity, the GPC becomes the LQR solution. As can be seen from Fig. 3.6, the finite-horizon solution has removed all noticeable correlation, so there is very little room for improvement regardless of the feedback technique chosen.

By using a finite-horizon technique, we have a solution which offers the possibility of being derived on-line in an adaptive controller. In this chapter, both the system identification and the controller design were done off line. Because of the computational speed of GPC or DPC, it is believed that the system identification can be updated, a new controller computed, and a new control effort applied every time step. This will create a controller which can regulate a time varying plant.

Regulating the vibration of a structure often means the control of a nonminimum-phase system, as can be seen in Fig. 3.3. The GPC solution may be tuned to produce an

acceptable solution without going unstable. However, in order to provide guaranteed stability for an exact plant model, computational speed is sacrificed[13]. Because all system identifications will have some uncertainty[1], both algorithms require tuning. In tuning DPC, two integer values are adjusted and GPC requires the adjustment of two integer values and one real positive value. These are the horizons and control weighting, respectively.

In addition to instability, actuator saturation must be avoided. In the experimental results, the actuator limit was the 3 volt limit of the D/A card. For the GPC algorithm the control effort can be limited by increasing the control penalty. For the DPC solution the control effort is limited by increasing the control horizon. If the DPC control horizon is set to the system order, a deadbeat controller is realized. If the control horizon is greater than the system order then a smaller control effort will be generated.

Predictive control techniques have been shown to offer a solution for suppressing the vibrations of a structure. Often researchers in active noise control have relied on a coherent reference and employed feedforward control techniques. While feedforward techniques are in general the most effective, they assume that a reference is available and that it can be processed fast enough to cancel the disturbance at the area of interest. When such requirements cannot be met, feedback control may be used to offer some regulation.

In summary, it was the purpose of this chapter to demonstrate the possibilities of using feedback control as a method of vibration regulation. By canceling out the odd vibration modes, the amount of acoustic energy radiated will be significantly reduced[39]. Improvements may be made in noise reduction by optimal sensor and actuator locations on the structure along with incorporating a knowledge of which modes are most efficient at producing acoustic energy at the area of interest.

This chapter demonstrated the use of two receding finite-horizon controllers, generalized predictive control and deadbeat predictive control. These techniques were

chosen because of their fast computational speed which offers extendibility to adaptive control. While generalized predictive control and deadbeat predictive control are not the optimal solution, i.e. Linear Quadratic Regulator (LQR), they may come very close to the optimal solution without the computational burden of solving a Riccati equation. Also, since these finite-horizon controllers have many of the properties of LQR, it may be assumed that both the stability and robustness properties of these controllers closely follow that of LQR. This will become especially true for large prediction horizons.

Chapter 4

Feedforward and Internal Noise Models for Predictive Control

4.1 Introduction

As shown in Chapter 3, predictive feedback control has been successfully used in the regulation of plate vibrations when no reference signal is available for feedforward control. However, if a reference signal is available it may be used to enhance regulation by incorporating a feedforward path in the feedback controller[41]. Such a controller is known as a feedback/feedforward controller. This chapter presents the theory and implementation of the feedback/feedforward controller to achieve vibration regulation. Generalized Predictive Control (GPC) and Deadbeat Predictive Control (DPC) are both extended to include a feedforward path in the Multi-Input Multi-Output (MIMO) case and both are implemented on a Single-Input Single-Output (SISO) plant to demonstrate plate vibration regulation.

There are cases in vibration control where the disturbance signal is not available to be used by the controller, but a disturbance model is available. In this case the disturbance model may be used in the feedback controller to enhance performance, i.e., the internal model principle. This chapter presents the theory of incorporating the noise model into the feedback controller for the MIMO case. Implementations are done on a SISO plant and regulation improvements over the case where no noise model was used is demonstrated.

The internal noise model has been shown to enhance the performance of the Linear Quadratic Regulator (LQR) if the disturbance states can be estimated[17]. Predictive control may likewise be extended to take advantage of disturbance information. The disturbance information may be in the form of a noise model or the input disturbance

signal may be available. Using the present and past values of the disturbance signal, an Auto-Regressive model, (AR), may be determined to model the correlation in the disturbance signal[1]. With this AR model, future disturbance values may be estimated and incorporated into the feedback/feedforward controller to enhance performance. In the case of single frequency disturbances, plant regulation may be dramatically improved if there is sufficient actuator authority. As the disturbance bandwidth increases, the regulation enhancement obtained by the AR disturbance predictions diminishes due to lack of correlation. So then for highly correlated disturbances, one can expect an improvement by using the AR noise model. For disturbances with little correlation, i.e., disturbances with energy spread over a large bandwidth, the advantage gained by using the AR noise predictor is small.

If the disturbance signal is not available for feedforward, enhanced feedback performance may be obtained by performing the system identification in the presence of the disturbance[1]. In order to include disturbance information within the plant model, the order of the plant model is increased. The additional coefficients of the plant model will give the extra degrees of freedom to incorporate disturbance model information[41]. Experimental results demonstrate the improvement in plant regulation gained by applying this technique.

4.2 System Identification for Feedback/Feedforward Control

The plant to be regulated may be represented by the following Auto-Regressive Moving Average model with eXogenous input (ARMAX)[2].

$$y(k) = \alpha_1 y(k-1) + \alpha_2 y(k-2) + \ldots + \alpha_p y(k-p) + \beta_0 u(k) + \beta_1 u(k-1) + \beta_2 u(k-2) + \ldots + \beta_p u(k-p) + \delta_0 d(k) + \delta_1 d(k-1) + \delta_2 d(k-2) + \ldots + \delta_p d(k-p) \quad (4.1)$$

In Eq. (4.1), k is the time step number, $y(k)$ is the m by one system output vector at time step k, $u(k)$ is the r by one control input vector, and $d(k)$ is the s by one disturbance input vector. The integer p is the system order. Here it is assumed that the order of both the α and β polynomials is p. The number of plant outputs is m, the number of plant control inputs is r, and the number of disturbance inputs is s. If $m = 1$ and $r = 1$, then a single-

input single-output system model is obtained. The coefficient matrices, α_j *(j = 1,2, …,p)* of *mxm,* β_j *(j = 0,1,2,…,p)* of, *mxr,* and δ_j *(j = 0,1,2,…,p)* of *mxs* are commonly referred to as Observer Markov Parameters (OMP)[6] or ARMAX parameters. Equation (4.1) differs from Eq. (3.1) in that a model of the disturbance is included. Based on the input and output data, the ARMAX parameters may be estimated using batch least squares, recursive least squares, or any other appropriate system ID technique. The identification of the ARMAX parameters is accomplished by simultaneously applying independent band-limited white noise to each control input and to each disturbance input and observing each output. Based on this input and output data, the ARMAX parameters are estimated. The resulting estimate is an identification of both the control and the disturbance paths.

4.3 Feedback/Feedforward Generalized Predictive Control

Given the ARMAX parameters of a plant, a control scheme must be devised to perform regulation of a MIMO system. Generalized Predictive Control (GPC), is one such scheme[11]. In order to predict the future plant outputs, some assumptions need to be made about the future control inputs and the future disturbance inputs. In determining the future control inputs, it is assumed that control is applied only over a finite horizon known as the control horizon. Beyond the control horizon, the control input is assumed to be zero. In addition to the horizons, a control penalty is introduced to limit the control effort and stabilize the closed-loop system. Eq. (4.2) is the cost function to be minimized in the GPC algorithm.

$$J(k) = \sum_{j=N_1}^{N_2} [y(k+j)]^T [y(k+j)] + \sum_{j=M_1}^{M_2} [u(k+j)]^T \lambda [u(k+j)] \qquad (4.2)$$

In Eq. (4.2), *y(k+j)* is the *mx1* plant output vector, *u(k+j)* is the *rx1* control input vector, and λ is the control penalty matrix. The prediction horizon is from N_1 to N_2 and the control horizon is from M_1 to M_2 where $M_2 \leq N_2$. Typically, N_1 and M_1 are set to zero. Minimizing Eq. (4.2) with respect to $u(k+j)$ $j = M_1,\ldots,M_2$ will give the control sequence to be applied to the plant. The first *rx1* control vector is applied, the remainder is discarded, and a new control sequence is calculated the next time step. In order to carry

out the above process, the future plant outputs $y(k), y(k+1), \ldots, y(k+N_2)$ must be predicted based only on past and present input and output data.

If the ARMAX model of the plant is known, the future plant outputs may be predicted based on the ARMAX coefficients using a recursive relationship[15]. If Eq. (3.1) is time shifted by one step, we obtain,

$$y(k+1)=\alpha_1 y(k)+\alpha_2 y(k-1)+\ldots+\alpha_p y(k-p+1)+\beta_0 u(k+1)+\beta_1 u(k)+\ldots+\beta_p u(k-p+1) \tag{4.3}$$

Define the following quantities

$$\begin{aligned}
\alpha_1^{(1)} &= \alpha_1\alpha_1+\alpha_2 & \beta_1^{(1)} &= \alpha_1\beta_1+\beta_2\\
\alpha_1^{(1)} &= \alpha_1\alpha_2+\alpha_3 & \beta_1^{(1)} &= \alpha_1\beta_2+\beta_3\\
\vdots \quad &\vdots \quad \vdots & \vdots \quad &\vdots \quad \vdots\\
\alpha_{p-1}^{(1)} &= \alpha_1\alpha_{p-1}+\alpha_p & \beta_{p-1}^{(1)} &= \alpha_1\beta_{p-1}+\beta_p\\
\alpha_p^{(1)} &= \alpha_1\alpha_p & \beta_p^{(1)} &= \alpha_1\beta_p
\end{aligned}$$

and

$$\beta_0^{(1)}=\alpha_1\beta_0+\beta_1$$

Substituting $y(k)$ from Eq. (3.1) into Eq. (4.3) results in Eq. (4.4).

$$\begin{aligned}
y(k+1)=&\alpha_1^{(1)}y(k-1)+\alpha_2^{(1)}y(k-2)+\ldots+\alpha_p^{(1)}y(k-p)\\
&+\beta_0 u(k+1)+\beta_0^{(1)}u(k)\\
&+\beta_1^{(1)}u(k-1)+\beta_2^{(1)}u(k-2)+\ldots+\beta_p^{(1)}u(k-p)
\end{aligned} \tag{4.4}$$

Eq. (4.4) shows that the output at time step $k+1$ may be estimated based on only the current input and past input and output data without the need of knowing the system output at time k. By induction, the system output at time step $k+j$ may be estimated as shown in Eq. (4.5)

$$\begin{aligned}
y(k+j)=&\alpha_1^{(j)}y(k-1)+\alpha_2^{(j)}y(k-2)+\ldots+\alpha_p^{(j)}y(k-p)\\
&+\beta_0 u(k+j)+\beta_0^{(1)}u(k+j-1)+\ldots+\beta_0^{(j)}u(k)\\
&+\beta_1^{(j)}u(k-1)+\beta_2^{(j)}u(k-2)+\ldots+\beta_p^{(j)}u(k-p)
\end{aligned} \tag{4.5}$$

where

$$\begin{aligned}
\alpha_1^{(j)} &= \alpha_1^{(j-1)}\alpha_1 + \alpha_2^{(j-1)} & \beta_1^{(j)} &= \alpha_1^{(j-1)}\beta_1 + \beta_2^{(j-1)} \\
\alpha_1^{(j)} &= \alpha_1^{(j-1)}\alpha_2 + \alpha_3^{(j-1)} & \beta_1^{(j)} &= \alpha_1^{(j-1)}\beta_2 + \beta_3^{(j-1)} \\
&\vdots \quad \vdots \quad \vdots & &\vdots \quad \vdots \quad \vdots \\
\alpha_{p-1}^{(j)} &= \alpha_1^{(j-1)}\alpha_{p-1} + \alpha_p^{(j-1)} & \beta_{p-1}^{(j)} &= \alpha_1^{(j-1)}\beta_{p-1} + \beta_p^{(j-1)} \\
\alpha_p^{(j)} &= \alpha_1^{(j-1)}\alpha_p & \beta_p^{(j)} &= \alpha_1^{(j-1)}\beta_p
\end{aligned}$$

and

$$\beta_0^{(j)} = \alpha_1^{(j-1)}\beta_0 + \beta_1^{(j-1)}$$

In Eq. (4.5), $\alpha_i^{(0)} = \alpha_i$ and $\beta_i^{(0)} = \beta_i$ for all *i* including *0* if applicable. Note that the future system outputs may be predicted based only on the past system outputs and the past and future system inputs. It is also of interest to note that the quantities $\beta_0^{(i)}(i = 0,1,\ldots)$ are the pulse response sequence i.e., system Markov parameters[15].

If the index *j* runs from *0* to *p+q-1*, then the matrix equation shown in Eq. (4.6) is produced by iterating Eq. (4.5).

$$y_{p+q}(k) = T_c u_{p+q}(k) + \beta\ u_p(k-p) + A\ y_p(k-p) \tag{4.6}$$

Equation (4.6) predicts the future plant responses without the effect of the disturbance inputs. The disturbance inputs may be included in the plant output predictions in the same way that the control inputs were accounted for. If it is assumed that past disturbance inputs are available and that future disturbance inputs can be predicted, the future plant responses may be obtained as shown in Eq. (4.7).

$$y_{p+q}(k) = T_c u_{p+q}(k) + \beta u_p(k\text{-}p) + A y_p(k\text{-}p) + T_d d_{p+q}(k) + D d_p(k\text{-}p) \tag{4.7}$$

where

$$y_{p+q}(k) = \begin{bmatrix} y(k) \\ y(k+1) \\ \vdots \\ y(k+q) \\ y(k+q+1) \\ \vdots \\ y(k+p+q-1) \end{bmatrix} \qquad u_{p+q}(k) = \begin{bmatrix} u(k) \\ u(k+1) \\ \vdots \\ u(k+q) \\ u(k+q+1) \\ \vdots \\ u(k+p+q-1) \end{bmatrix} \qquad d_{p+q}(k) = \begin{bmatrix} d(k) \\ d(k+1) \\ \vdots \\ d(k+q) \\ d(k+q+1) \\ \vdots \\ d(k+p+q-1) \end{bmatrix}$$

$$y_p(k-p)=\begin{bmatrix} y(k-p) \\ y(k-p+1) \\ \vdots \\ y(k-1) \end{bmatrix} \qquad u_p(k-p)=\begin{bmatrix} u(k-p) \\ u(k-p+1) \\ \vdots \\ u(k-1) \end{bmatrix} \qquad d_p(k-p)=\begin{bmatrix} d(k-p) \\ d(k-p+1) \\ \vdots \\ d(k-1) \end{bmatrix}$$

$$A=\begin{bmatrix} \alpha_p & \alpha_{p-1} & \cdots & \alpha_1 \\ \alpha_p^{(1)} & \alpha_{p-1}^{(1)} & \cdots & \alpha_1^{(1)} \\ \vdots & \vdots & \ddots & \vdots \\ \alpha_p^{(q)} & \alpha_{p-1}^{(q)} & \cdots & \alpha_1^{(q)} \\ \alpha_p^{(q+1)} & \alpha_{p-1}^{(q+1)} & \cdots & \alpha_1^{(q+1)} \\ \vdots & \vdots & \ddots & \vdots \\ \alpha_p^{(p+q-1)} & \alpha_{p-1}^{(p+q-1)} & \cdots & \alpha_1^{(p+q-1)} \end{bmatrix} \qquad \beta=\begin{bmatrix} \beta_p & \beta_{p-1} & \cdots & \beta_1 \\ \beta_p^{(1)} & \beta_{p-1}^{(1)} & \cdots & \beta_1^{(1)} \\ \vdots & \vdots & \ddots & \vdots \\ \beta_p^{(q)} & \beta_{p-1}^{(q)} & \cdots & \beta_1^{(q)} \\ \beta_p^{(q+1)} & \beta_{p-1}^{(q+1)} & \cdots & \beta_1^{(q+1)} \\ \vdots & \vdots & \ddots & \vdots \\ \beta_p^{(p+q-1)} & \beta_{p-1}^{(p+q-1)} & \cdots & \beta_1^{(p+q-1)} \end{bmatrix}$$

$$D=\begin{bmatrix} \delta_p & \delta_{p-1} & \cdots & \delta_1 \\ \delta_p^{(1)} & \delta_{p-1}^{(1)} & \cdots & \delta_1^{(1)} \\ \vdots & \vdots & \ddots & \vdots \\ \delta_p^{(q)} & \delta_{p-1}^{(q)} & \cdots & \delta_1^{(q)} \\ \delta_p^{(q+1)} & \delta_{p-1}^{(q+1)} & \cdots & \delta_1^{(q+1)} \\ \vdots & \vdots & \ddots & \vdots \\ \delta_p^{(p+q-1)} & \delta_{p-1}^{(p+q-1)} & \cdots & \delta_1^{(p+q-1)} \end{bmatrix} \qquad T_c=\begin{bmatrix} \beta_0 & & & & & & \\ \beta_0^{(1)} & \beta_0 & & & & & \\ \vdots & \vdots & \ddots & & & & \\ \beta_0^{(q)} & \beta_0^{(q-1)} & \cdots & \beta_0 & & & \\ \beta_0^{(q+1)} & \beta_0^{(q)} & \cdots & \beta_0^{(1)} & \beta_0 & & \\ \vdots & \vdots & \cdots & \vdots & \vdots & \ddots & \\ \beta_0^{(p+q-1)} & \beta_0^{(p+q-2)} & \cdots & \beta_0^{(p-1)} & \beta_0^{(p-2)} & \cdots & \beta_0 \end{bmatrix}$$

$$T_d=\begin{bmatrix} \delta_0 & & & & & & \\ \delta_0^{(1)} & \delta_0 & & & & & \\ \vdots & \vdots & \ddots & & & & \\ \delta_0^{(q)} & \delta_0^{(q-1)} & \cdots & \delta_0 & & & \\ \delta_0^{(q+1)} & \delta_0^{(q)} & \cdots & \delta_0^{(1)} & \delta_0 & & \\ \vdots & \vdots & \cdots & \vdots & \vdots & \ddots & \\ \delta_0^{(p+q-1)} & \delta_0^{(p+q-2)} & \cdots & \delta_0^{(p-1)} & \delta_0^{(p-2)} & \cdots & \delta_0 \end{bmatrix}$$

In Eq. (4.7), p is the system order, q is an intermediate time step, and the prediction horizon is $N_2 = p+q-1$. $y_{p+q}(k)$ is a length $m(p+q)$ vector containing the predicted future plant outputs, $u_{p+q}(k)$ is a $r(p+q)$ vector containing the future control inputs yet to be determined, and $d_{p+q}(k)$ is the vector containing the future disturbance inputs yet to be predicted. Also $y_p(k-p)$ is a mp, (m multiplied by p), vector containing the past plant outputs, $u_p(k-p)$ is the rp vector containing the past control inputs, and $d_p(k-p)$ is the

vector containing the past disturbance inputs. A is a $m(p+q)xmp$ matrix and β is a $m(p+q)xrp$ matrix. T_c is a $m(p+q)xr(p+q)$ Toeplitz matrix which consist of the system pulse response sequence[15].

In the regulation problem, the desired plant output is zero. The cost function of Eq. (4.2) may be written in terms of Eq. (4.7) to produce the cost function of Eq. (4.8).

$$J(k) = y'_{p+q}(k)y_{p+q}(k) + u'_{p+q}(k)\lambda\, u_{p+q}(k) \tag{4.8}$$

Inserting Eq. (4.7) into Eq. (4.8) and minimizing with respect to $u_{p+q}(k)$ will produce Eq. (4.9).

$$u_{p+q}(k) = -(T_c^{'}T_c + \lambda)^{+}T_c^{'}(\beta u_p(k-p) + Ay_p(k-p) + T_d d_{p+q}(k) + Dd_p(k-p)) \tag{4.9}$$

In Eq.(4.9), the prime means the matrix transpose, λ is the control penalty, and I is a $m(p+q)xr(p+q)$ identity matrix. The super-script $^{+}$ is the matrix pseudo-inverse. The first r rows of the resulting vector $u_{p+q}(k)$ are applied to the plant as control inputs and the remainder of $u_{p+q}(k)$ is discarded. The prediction horizon in the formulation of Eq. (4.9) is $p+q-1$. The value of q may be chosen to meet performance and stability requirements. If q is chosen to be zero, then the control will predict ahead p steps, which is the order of the system. A larger value of q will increase the stability of the closed-loop system at the expense of a greater computational burden. As q goes to infinity the Linear Quadratic Regulator (LQR) is approached[12]. If q is set to a negative number greater than $-p$, the prediction horizon will be less than the system order. In practice, however, choosing a negative q is not done as it may lead to stability problems for nonminimum-phase systems[35].

The control penalty λ in Eq. (5.7) is critical to the performance of GPC. A large value of λ will decrease regulation and increase stability while a smaller value of λ will increase regulation at the loss of robustness[12]. In applying GPC to regulate plate vibrations, a non-zero value of λ must be selected to meet performance and robustness requirements.

The formulation given in Eq. (4.9) assumes that the control horizon is equal to the prediction horizon. However, in general, this need not be. The control horizon may be chosen to be less than the prediction horizon resulting in a more stable and sluggish regulator[12]. This is achieved by truncating the matrix T_c in Eq. (4.7) as shown in Eq. (4.10).

$$\tilde{T}_c = \begin{bmatrix} \beta_0 & & & \\ \beta_0^{(1)} & \beta_0 & & \\ \vdots & \vdots & \ddots & \\ \beta_0^{(q)} & \beta_0^{(q-1)} & \cdots & \beta_0 \\ \beta_0^{(q+1)} & \beta_0^{(q)} & \cdots & \beta_0^{(1)} \\ \vdots & \vdots & \vdots & \vdots \\ \beta_0^{(p+q-1)} & \beta_0^{(p+q-2)} & \cdots & \beta_0^{(M_2)} \end{bmatrix} \tag{4.10}$$

The tilde over-bar in Eq. (4.10) represents truncation. The control sequence determined by using Eq. (4.10) in Eq. (4.9) is for a shorter control horizon, i.e. $M_2 \leq p+q-1$. Beyond the control horizon the control input is assumed to be zero. The resulting controller is shown in Eq. (4.11).

$$u_{M_2}(k) = -(\tilde{T}_c'\tilde{T}_c + \lambda)^{+}\tilde{T}_c'(\beta\, u_p(k-p) + A\, y_p(k-p) + T_d d_{p+q}(k) + D d_p(k-p)) \tag{4.11}$$

The formulation given in Eq. (4.11) differs from that given in Ref. [12] in that it assumes the current control will be applied at the next time step rather than at the present time step. This is important in implementation because the present formulation allows time to perform computations. The above formulation also differs from that of Ref. [12] in the manner in which the controller coefficients are calculated. Rather than solving the Diophantine equation for future predictions, the above formulation uses a different recursive relationship. By adjusting the control horizon M_2, the prediction horizon $N_2 = p+q-1$, and the control cost λ, Eq. (4.11) may be tuned to yield the best results for a given regulation problem. Also, in the formulation of Eq. (4.11) it is possible to set λ equal to zero even for nonminimum-phase systems. This may be achieved by decreasing the control horizon until a stable solution is reached. In general, as the value of the control horizon approaches the prediction horizon, better regulation is achieved at the expense of

robustness. To gain stability in this case, the value of λ is increased. As the value of the control horizon is made smaller than the prediction horizon, a more robust controller results at the expense of regulation. Also, a shorter control horizon makes the GPC algorithm more computationally efficient in that the matrix pseudo-inverse of Eq. (4.11) is smaller.

The plant model order, prediction horizon, control horizon, and control penalty are all design parameters determined by the user. However, certain rules of thumb may be followed in tuning the controller. In general, the plant model order is chosen to be around five or ten times the number of significant modes of the plant. This is done in order to closely model the dynamics of the system to be regulated. A good fit in the plant model will aid in stability and enhance regulation of the actual plant. The prediction horizon should have a minimum value of the rise-time of the plant[11]. As described in Ref. [11], this will aid in regulation by giving the controller sufficient information about where the plant output is heading. The prediction horizon has no maximum value, although setting the prediction horizon beyond the settling-time of the plant will yield little beniefit[11]. The value of the control horizon should be set to at least the number of lightly damped plant poles[11]. This will allow the control sequence to account for the significant degrees of freedom of the plant. At most the control horizon may be set to the prediction horizon which will result in a more active controller. The control penalty should be adjusted to balance performance demands, robustness, and actuator authority. Although a simulation may yield an approximate range, the control penalty is adjusted by trial and error.

Equation (4.11) also includes a feedforward path if the disturbance signals are measurable. If it is not possible to measure the disturbance signal, then the last two terms in Eq. (4.11) are simply dropped. If the disturbance signal is measurable, then the measurements are placed in the $d_p(k\text{-}p)$ vector. This vector contains the last p disturbance measurements. If there is correlation in the disturbance measurements, then this correlation may be used to estimate future disturbance values based on past disturbance values and fill the $d_{p+q}(k)$ vector. If there is no correlation in the disturbance signal, then

the second to last term in Eq. (4.11) is dropped. Given that correlation does exist, an AR model may be used together with past disturbance measurements to predict future disturbance values[1]. The AR model is shown in Eq. (4.12).

$$d(k) + \xi_1 d(k-1) + \xi_2 d(k-2) + \ldots + \xi_v d(k-v) = 0 \tag{4.12}$$

In Eq. (4.12), v is the disturbance model order and ξ_j $(j = 1,2,\ldots,v)$ are the AR disturbance model coefficients. In order to include the second to last term in Eq. (4.11), we need the future disturbance signal. This signal may be estimated by recursively solving for future values of the disturbance signal based on past disturbance measurements and Eq. (4.12). This recursive relationship is the same as that of Ref. [15]. Shown below in Eq. (4.13) is the j^{th} prediction of the disturbance signal.

$$d(k + j) = \xi_1^{(j)} d(k-1) + \xi_2^{(j)} d(k-2) + \ldots + \xi_v^{(j)} d(k-v) \tag{4.13}$$

In Eq. (4.8) j will go from 0 to the prediction horizon $p+q-1$. In this manner the future disturbance signals will be estimated and the second to last term of Eq. (4.11) may be used to enhance performance.

4.4 Feedback/Feedforward Deadbeat Predictive Control

Deadbeat Predictive Control (DPC) may also be extended to incorporate a feedforward path and disturbance predictor. With extensions, enhanced regulation may be achieved. The DPC algorithm is developed in Ref. [14,15] and is extended here to include a feedforward path and AR noise predictor. To formulate DPC Eq. (4.7) is modified to obtain Eq. (4.14) shown below[15].

$$y_p(k+q) = \bar{T}_c u_q(k) + \bar{\beta}\, u_p(k-p) + \bar{A}\, y_p(k-p) + \bar{T}_d d_{p+q}(k) + \bar{D} d_p(k-p) \tag{4.14}$$

where

$$y_p(k+q) = \begin{bmatrix} y(k+q) \\ y(k+q+1) \\ \vdots \\ y(k+q+p-1) \end{bmatrix} \qquad u_q(k) = \begin{bmatrix} u(k) \\ u(k+1) \\ \vdots \\ u(k+q-1) \end{bmatrix}$$

$$\overline{T}_c = T_c(qm+1:pm+qm,1:qr) = \begin{bmatrix} \beta_0^{(q)} & \beta_0^{(q-1)} & \cdots & \beta_0^{(1)} \\ \beta_0^{(q+1)} & \beta_0^{(q)} & \cdots & \beta_0^{(2)} \\ \vdots & \vdots & \ddots & \vdots \\ \beta_0^{(q+p-1)} & \beta_0^{(q+p-2)} & \cdots & \beta_0^{(p)} \end{bmatrix}$$

$$\overline{T}_d = \begin{bmatrix} \delta_0^{(q)} & \delta_0^{(q-1)} & \cdots & \delta_0 & & & \\ \delta_0^{(q+1)} & \delta_0^{(q)} & \cdots & \delta_0^1 & \delta_0 & & \\ \vdots & \vdots & \ddots & \vdots & \vdots & \ddots & \\ \delta_0^{(q+p-1)} & \delta_0^{(q+p-2)} & \cdots & \delta_0^{(p-1)} & \delta_0^{(p-2)} & \cdots & \delta_0 \end{bmatrix}$$

$$\overline{\beta} = \beta(qm+1:pm+qm,:) = \begin{bmatrix} \beta_p^{(q)} & \beta_{p-1}^{(q)} & \cdots & \beta_1^{(q)} \\ \beta_p^{(q+1)} & \beta_{p-1}^{(q+1)} & \cdots & \beta_1^{(q+1)} \\ \vdots & \vdots & \ddots & \vdots \\ \beta_p^{(q+p-1)} & \beta_{p-1}^{(q+p-1)} & \cdots & \beta_1^{(q+p-1)} \end{bmatrix}$$

$$\overline{D} = \begin{bmatrix} \delta_p^{(q)} & \delta_{p-1}^{(q)} & \cdots & \delta_1^{(q)} \\ \delta_p^{(q+1)} & \delta_{p-1}^{(q+1)} & \cdots & \delta_1^{(q+1)} \\ \vdots & \vdots & \ddots & \vdots \\ \delta_p^{(q+p-1)} & \delta_{p-1}^{(q+p-1)} & \cdots & \delta_1^{(q+p-1)} \end{bmatrix}$$

$$\overline{A} = A(qm+1:pm+qm,:) = \begin{bmatrix} \alpha_p^{(q)} & \alpha_{p-1}^{(q)} & \cdots & \alpha_1^{(q)} \\ \alpha_p^{(q+1)} & \alpha_{p-1}^{(q+1)} & \cdots & \alpha_1^{(q+1)} \\ \vdots & \vdots & \ddots & \vdots \\ \alpha_p^{(q+p-1)} & \alpha_{p-1}^{(q+p-1)} & \cdots & \alpha_1^{(q+p-1)} \end{bmatrix}$$

The vectors $u_p(k\text{-}p)$, $y_p(k\text{-}p)$, $d_{p+q}(k)$, and $d_p(k\text{-}p)$ are as defined in Eq. (4.7). In Eq. (4.14) the system order is p, the control horizon is q, m is the number of system outputs, and r is the number of system inputs. To formulate the deadbeat control solution, it is assumed that the control vector $u_q(k)$ will drive the plant output to zero in q time steps and that q is always chosen to be greater than or equal to p. This implies that all control values after time step $k+q\text{-}1$ will be zero and that the vector of future plant outputs $y_p(k+q)$ will be a zero vector if no further disturbances enter the plant. In reality, however, disturbances are entering the plant every time step k so the controller is continually trying to drive the future plant output to zero. In the DPC formulation, the plant output from time step k to

time step *k+q-1* is allowed to be free, i.e., is not penalized. With these assumptions, the deadbeat control solution is then given by[15]

$$u_q(k) = -(\bar{T}_c^T \bar{T}_c + \lambda)^+ \bar{T}_c^T (\bar{\beta}\, u_p(k-p) + \bar{A} y_p(k-p) + \bar{T}_d d_{p+q}(k) + \bar{D} d_p(k-p)) \tag{4.15}$$

The super-script symbol $^+$ is the pseudo inverse and λ is of the appropriate dimensions. The first *r* rows of Eq. (4.15) are used for feedback control as shown in Eq. (4.16).

$$u(k) = \textit{first r rows of } \{u_q(k)\}$$

$$u(k) = \alpha_1^c y(k-1) + \alpha_2^c y(k-2) + \cdots + \alpha_p^c y(k-p) + \beta_1^c u(k-1) + \beta_2^c u(k-2) + \cdots + \beta_p^c u(k-p) \tag{4.16}$$

The superscript *c* signifies the control parameters. *u(k)* is the *rx1* control vector, α_j^c, *(j = 1,2,…,p)* is a *rxm* matrix, and β_j^c is a *rxr* matrix. The control generated by Eq. (4.16) is guaranteed stable for an exact model, even for nonminimum-phase systems[15]. However, it must be kept in mind that the guarantee of stability is only for the plant model closed-loop system. The actual plant will differ somewhat from the model, so the promise of guaranteed stability is not realized in practice. The control effort may be adjusted by varying the integer parameters *p* (system order) and *q* (control horizon). If *q* is chosen equal to *p* a larger control effort results which tends toward the best regulation if the actuators are not saturated. This large control effort is due to the fact that the controller is only given a small amount of time, (*p* time steps), to drive the output to zero. A larger value of *q*, (*q* > *p*), will allow more time to drive the plant output to zero which means a smaller control effort may be used. As the value of *q* is increased a smaller control effort results which generally means a decrease in regulation for plants with lightly damped poles.

GPC has been proven to be stable under certain conditions[13]. However, the conditions require a great deal of computations. The DPC algorithm avoids this stability problem and is easier to tune because it only has two integer values to adjust, *p* and *q*. The DCP algorithm may, however, require more computations to determine the controller parameters than does GPC. This is due to the fact that the DPC prediction horizon must go up to *p+q-1* and the GPC prediction horizon may only require a few time steps. The inclusion of the control penalty λ in the DPC formulation, although not necessary, is to help promote closed-loop stability in the presence of disturbances and unmodeled

dynamics. The fundamental difference between the DPC and GPC algorithms is that the GPC algorithm calculates a control sequence to reduce the plant output starting at the next time step while the control sequence returned by the DPC algorithm is design to drive the plant output to zero after p (system order), time steps[14]. This can be seen by comparing Eq. (4.17) with the vector $y_{p+q}(k)$ in the GPC algorithm, Eq. (4.7).

$$y_q(k) = \begin{bmatrix} y(k+q) \\ y(k+q+1) \\ \vdots \\ y(k+q+p-1) \end{bmatrix} \tag{4.17}$$

In Eq. (4.8) of the GPC algorithm, the plant output is penalized from time step k to time step $k+p+q-1$. This is to say that minimizing Eq. (4.8) will penalize the plant output for being non-zero starting at the next time step all the way to the prediction horizon, $N_2 = p+q-1$. In the DPC algorithm, the plant output from time step k to time step $k+q-1$ is allowed to be free, i.e., not penalized. The DPC algorithm will return a sequence of control inputs from time step k to $k+q-1$ which will seek to drive the plant response to zero at time step $k+q$, i.e., deadbeat after q time steps. In summary, the GPC algorithm will try to drive the vector $y_{p+q}(k)$ to zero and the DPC algorithm will try to drive the vector $y_{q(}(k)$ of Eq. (4.17) to zero. The advantage gained by using the DPC algorithm is that in theory stability can be guaranteed without the large computational penalty incurred with guaranteed stable GPC. More details about the DPC algorithm and a proof of stability may be found in Ref. [15]. The AR disturbance model is used to predict the future disturbance values to fill the vector $d_{p+q}(k)$ in the same manner as was done for the GPC algorithm. As for the GPC algorithm, if the disturbance can not be measured then the last two terms in Eq. (4.9) are dropped. If the disturbance can be measured and has no correlation, then only the second to last term in Eq. (4.9) is dropped. If the disturbance can be measured and there is correlation, an AR model may be determined to model the correlation and construction of the vector $d_{p+q}(k)$ for the inclusion of the last term in Eq. (4.15) to enhance performance is possible.

4.5 Approximation of an Internal Noise Model

For both the DPC and GPC algorithms, the disturbance signal must be measurable in order to incorporate feedforward and the disturbance predictor. However, there are cases where the disturbance signal does contain correlation at the output sensor but can not be measured before entering the plant. In this case one possible approach is to ID the system in the presence of the disturbance. By doing this, some of the disturbance characteristics will be incorporated into the plant model and therefore the controller based on this model will contain some information about the disturbance[1]. Assume that Eq. (4.18) represents the actual physical plant to be controlled.

$$A_o(z^{-1})y(k) = B_o(z^{-1})u(k) + C_o(z^{-1})e(k) \tag{4.18}$$

In Eq. (4.18) we see that the plant response *y(k)* is due to the control input *u(k)* and the disturbance. The disturbance is modeled as a transfer function driven by white noise *e(k)*. The disturbance transfer function in the last term of Eq. (4.18) includes both correlation in the noise before entering the plant and the transfer function from where the disturbance enters the plant to the plant output. If the system ID is done with the disturbance off (e(k) = 0), then the ID technique will return the ARMAX parameters of the model shown in Eq. (4.19).

$$A(z^{-1})y(k) = B(z^{-1})u(k) \tag{4.19}$$

As the data length approaches infinity, it has been shown in Ref. [1] that A will approach A_o and B will approach B_o of Eq. (4.18). The ARX model of Eq. (4.19) represents the map from the system control input to the system output. If, however, the system ID is performed in the presence of the disturbance, then the following model may be obtained if the order of the ARX model is extended to infinity and the data length is infinite. The proof may be found in Ref. [1].

$$A_e(z^{-1})y(k) = B_e(z^{-1})u(k) \tag{4.20}$$

where $$A_e(z^{-1}) = \frac{C_o(z^{-1}) - A_o(z^{-1})}{C_o(z^{-1})} \qquad B_e(z^{-1}) = \frac{B_o(z^{-1})}{C_o(z^{-1})}$$

Equation (4.20) includes information about the disturbance which will be used to enhance performance in the controller design. Although neither the data length nor the system

order can actually approach infinity, Eq. (4.20) does indicate that increasing the number of coefficients will produce a more accurate prediction of future plant outputs.

Figure 4.1 is a block diagram of the overall implementation scheme for the feedback controller with an internal noise model. The model of the disturbance is imbedded in the controller parameters.

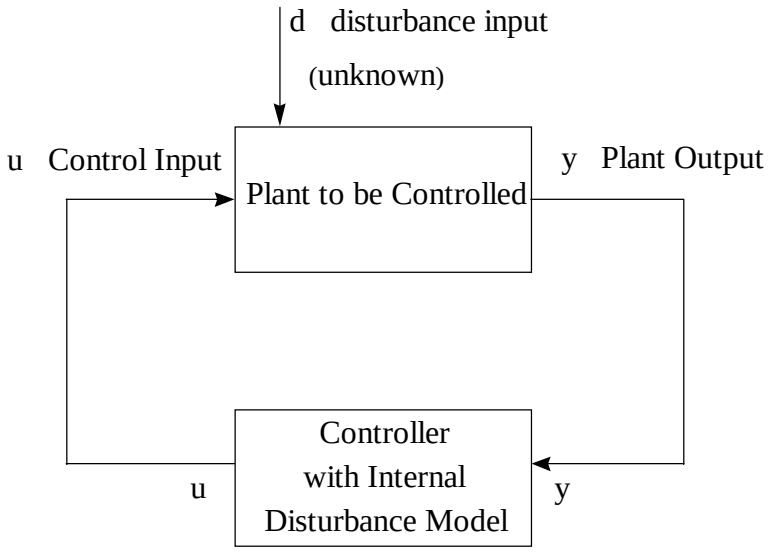

Figure 4.1 Block Diagram of Control System

4.6 Exact Solution for the Internal Noise Model

It is the purpose of this section to describe how a system model will incorporate an exact internal noise model given that the disturbance is periodic and the system model is of sufficient order. The input-output relationship of a linear system may be described by the finite-difference model of Eq. (4.1), which may also be written in the z-domain as shown in Eq. (4.21)[41].

$$\alpha(z)y(z) = \beta(z)u(z) + \delta(z)d(z) \tag{4.21}$$

where *u(z)*, *d(z)*, and *y(z)* are the z-transforms of *u(k)*, *d(k)*, and *y(k)* respectively, and

$$\alpha(z) = I_m - \alpha_1 z^{-1} - \alpha_2 z^{-2} - \ldots - \alpha_p z^{-p}$$

$$\beta(z) = \beta_0 + \beta_1 z^{-1} + \beta_2 z^{-2} + \ldots + \beta_p z^{-p}$$

$$\delta(z) = \delta_0 + \delta_1 z^{-1} + \delta_2 z^{-2} + \ldots + \delta_p z^{-p}$$

Disturbances which consist of only a single-input periodic signal may be represented by the finite-difference model shown in Eq. (4.22)[41].

$$d(k) = \eta_1 d(k-1) + \eta_2 d(k-2) + \ldots + \eta_{n_d} d(k-n_d) \tag{4.22}$$

In Eq.(4.22), n_d is the disturbance model order and is twice the number of commensurable frequencies in the disturbance signal. Taking the z transform of Eq.(4.22), results in Eq. (4.23).

$$\eta(z) d(z) = 0 \tag{4.23}$$

where

$$\eta(z) = 1 - \eta_1 z^{-1} - \eta_2 z^{-2} - \ldots - \eta_{n_d} z^{-n_d}$$

Premultiplying Eq. (4.21) by $\eta(z)$ and using Eq. (4.23) results in

$$\eta(z)\alpha(z)y(z) = \eta(z)\beta(z)u(z)$$

which may be written as

$$\tilde{\alpha}(z)y(z) = \tilde{\beta}(z)u(z) \tag{4.24}$$

where

$$\tilde{\alpha}(z) = \eta(z)\alpha(z) = I_m - \tilde{\alpha}_1 z^{-1} - \tilde{\alpha}_2 z^{-2} - \ldots - \tilde{\alpha}_p z^{-p-n_d}$$

$$\tilde{\beta}(z) = \eta(z)\beta(z) = \tilde{\beta}_0 - \tilde{\beta}_1 z^{-1} - \tilde{\beta}_2 z^{-2} - \ldots - \tilde{\beta}_p z^{-p-n_d}$$

In Eq. (4.24) the system order is $p + n_d$ rather than p. This is due to the fact that the model given by Eq. (4.24) has imbedded within the parameters an exact model of the disturbance[41]. The value of n_d is twice the number of periodic disturbances acting on the system. The resulting system model provides an exact input output map for the discrete-time system being identified given that the periodic disturbance is the only disturbance acting on the system. A similar proof for MIMO systems with periodic disturbances may be found in Ref. [41] were it is proven that an exact input-output map may be obtained for MIMO systems in the presence of periodic disturbances.

4.7 Experimental Results

The GPC algorithm with feedforward and a noise predictor was implemented on a Texas Instrument C-30 chip. The plant to be regulated is shown in Fig. 3.1. The accelerometer signal was measured by the B&K analyzer as shown in Fig 3.2. The control input enters the plant through the piezo mounted on the bottom center of the aluminum plate. The plant output to be regulated is the accelerometer signal taken at the top center of the aluminum plate. A block diagram of the plant and control system is shown in Fig. 3.2. The disturbance *d* is band limited to 1KHz and enters the plant at point 2 of Fig. 3.2. The plant output is the accelerometer signal taken at point 3. The control input is applied to the plant at point 1 of Fig. 3.2. Low pass filters and amplifiers were used where appropriate. The controller has a sample rate of 2.5 KHz and has input signals of *y*, the filtered and amplified accelerometer signal and *d*, the disturbance measurement. The controller outputs *u*, the control signal. The total reduction presented for some of the plots is give to demonstrate the overall performance of the controller. This value is obtain by integrating the spectrum of the open- and closed-loop accelerometer autospectrum. The closed-loop integrated spectrum is then divided by the open-loop integrated spectrum. The result is then expressed in dB. The total reductions presented throughout this thesis are obtained in this manner.

Since the implementation in this study is not adaptive, we must first estimate an ARMAX model of the plant in order to design a controller. This is accomplished by applying two independent white noise signals (band limited to 1Kz), to point 2 of Fig. 3.2 and at u. With both these random inputs applied, the system output y of Fig. 3.2 is measured. The two input data vectors and the one output vector are then used to approximate an ARMAX model of the system. It is important to note that the ARMAX model represents both the plexi- glass box and the filters and amplifiers used in the controller loop. The form of the model is that of Eq. (4.1). The ARMAX model was then used to find the GPC controller coefficients shown in Eq. (4.9).

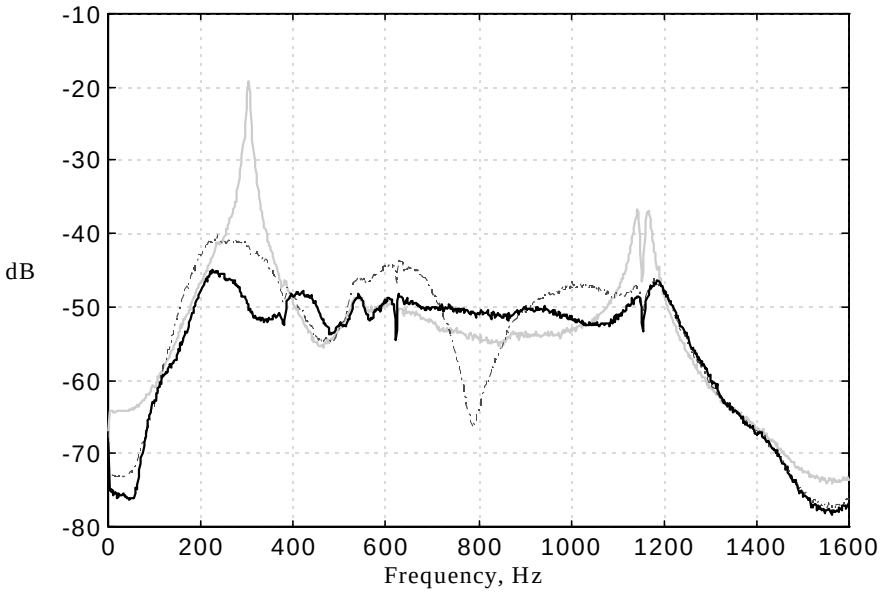

Figure 4.2 GPC Performance with Feedback/Feedforward Control

Figure 4.2 shows the autospectrum of plant output (accelerometer signal, *y*) without control (gray line), feedback only (dotted line), and with feedback/feedforward control (solid line). A 12^{th} order system model was used with a sample rate of 2.5 KHz. Both control and prediction horizons were set to 12. Since the disturbance applied to the plant was band-limited white noise, no AR model could be used to predict future disturbances before they enter the plant. Therefore the second to last term in Eq. (4.9) was dropped. It is also of interest to consider the controller performance around 800 Hz. Here we see that the feedback controller is performing better than the feedback/feedforward controller. This is probably due to the fact that the feedforward path is introducing additional noise into the system around this frequency which is not created by the disturbance. This additional noise comes from leveling the output spectrum. It is a small sacrifice made in order to regulate the modal responses of the plant. It must be kept in mind that both feedback and feedback/feedforward control only penalize the amplitude squared of the sensor signal as described by the cost function. This does not guarantee that the controllers will regulate across the entire bandwidth. It does, however, mean that the overall level of the plant output will be reduced for all stable control designs.

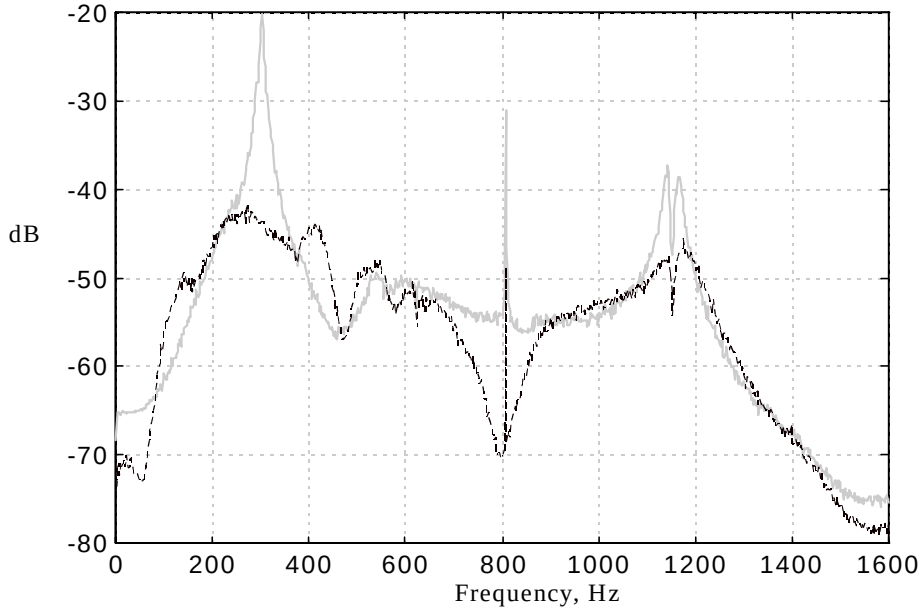

Figure 4.3 Feedback/Feedforward Tone Rejection Using Internal Noise Model

In Fig. 4.3, the plots are the autospectrum of the plant output without control (gray line), and with feedback/feedforward control plus a 2^{nd} order internal noise model (solid line). The total reduction was 9.67 dB. A 12^{th} order system model was used, 2^{nd} order AR tone model, and the sample rate was 2.5 KHz. The internal noise model was formed based on a 2^{nd} order AR model obtained by performing a system ID on the disturbance signal. The resulting AR model and the past disturbance measurements were then used to predict the future disturbance values and incorporate the last term of Eq. (4.9). Figure 4.3 shows the advantage gained by including the second to last term of Eq. (4.9) when possible. In this case, both band-limited white noise and a 800 Hz sine wave disturbance were applied to the plant through the speaker. Only the sine wave was used in the feedforward path. As seen in Fig. 4.3, this greatly attenuated the accelerometer signal due to the sine wave disturbance.

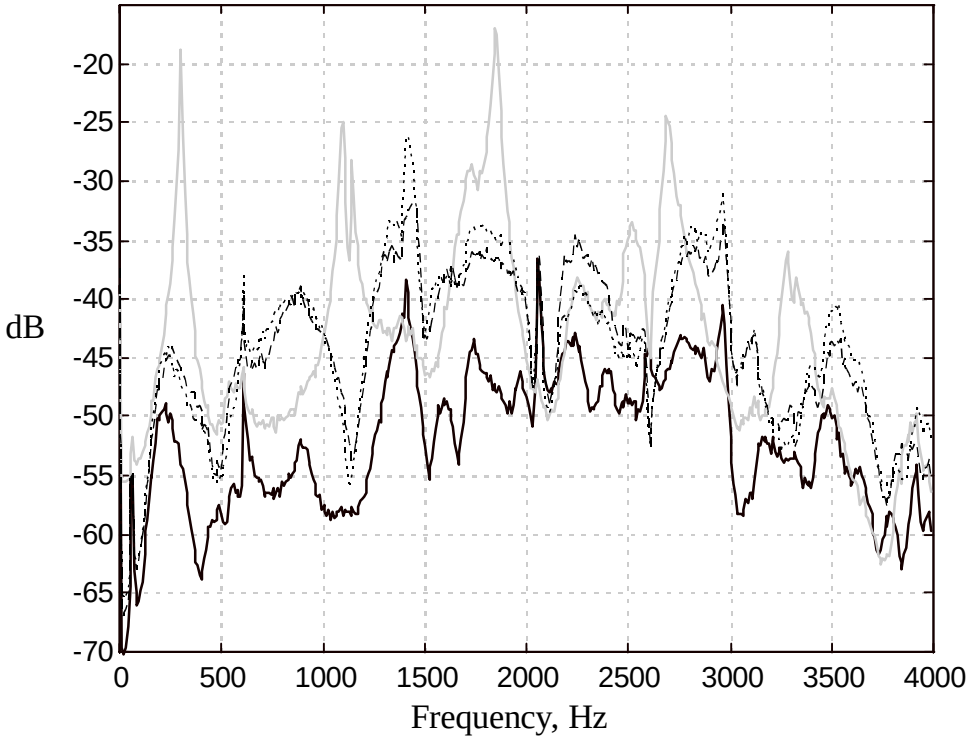

Figure 4.4 Plot of Control Using Internal Noise Model

Figure 4.4 is the autospectrum of the plant output without control (gray line), feedback (dotted line, 5.15 dB reduction), feedback with internal noise model (dashed line, 6.51 dB reduction), and feedback/feedforward control (solid line, 14.40 dB reduction). The system order was 38 and the sample rate was 10 KHz. Figure 4.4 shows broadband results using the GPC controller. Here band-limited white noise was applied as the disturbance so no AR disturbance model exists to enhance performance. The black line is the autospectrum of the accelerometer signal when the feedback/feedforward controller of Eq. (4.9) was used without the second to last term. It is of interest to compare the result obtained using feedback only, (dotted line), with that of feedback using an internal noise model, (dashed line). In both cases no feedforward was used. The system ID was performed with the disturbance on for the dashed line. For the dotted line, the system ID was done with the disturbance off. By having the disturbance on while gathering input and output data for the system ID, the resulting ID will incorporate some information about how the disturbance propagates through the plant and to the

accelerometer. The controller design will use this information to increase regulation as can be seen in when comparing the dashed line to the dotted line in Fig. 4.4.

The figures shown thus far used controllers with broadband internal noise models. Incorporating disturbance information into the feedback controller can be used to improve the regulation of periodic disturbances as well. For this case, a large increase in regulation may be obtained by performing the system ID in the presence of the disturbance. By doing this, an internal model of the disturbance is incorporated into the observer Markov parameters returned by the system ID[41] as shown in Fig. 4.5.

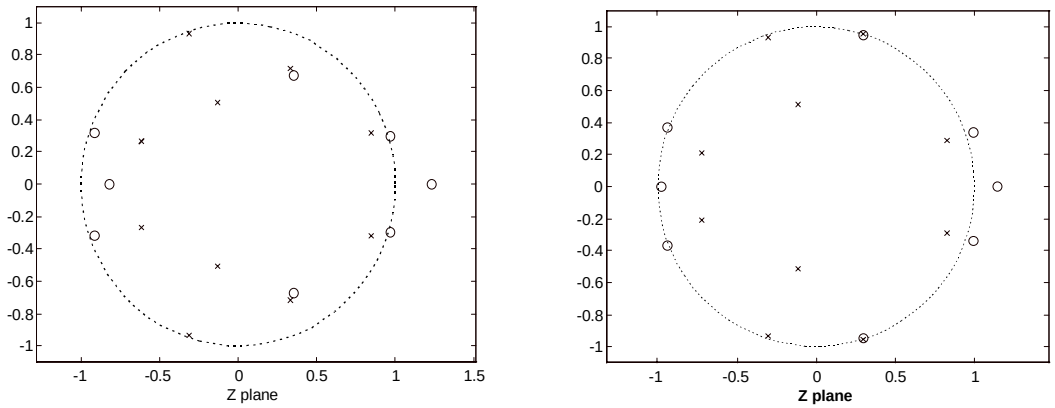

Figure 4.5 Pole-Zero Plot of OMP Without (left) & With (right) Disturbance

Figure 4.5 shows the pole zero plots of OMP obtained with disturbance off (left), and disturbance on (right). A 10th order system model and 1 KHz sampling rate were used. The disturbance was a 200 Hz sine wave. Figure 4.5 illustrates the internal disturbance model obtained by performing the system ID with the disturbance on. The figure is a pole- zero plot of the transfer function which describes the dynamics between the control input and accelerometer output. Both plots represent the same system (same system Markov parameters), however, the right plot contains the disturbance model. In this case, the disturbance was a 200 Hz sine wave. The plant has a mode at 300 Hz and was modeled as a 10th order system. Note the pole zero cancellation in the right plot. This plot has the same system Markov parameters as the left plot, but has different OMP[41,6].

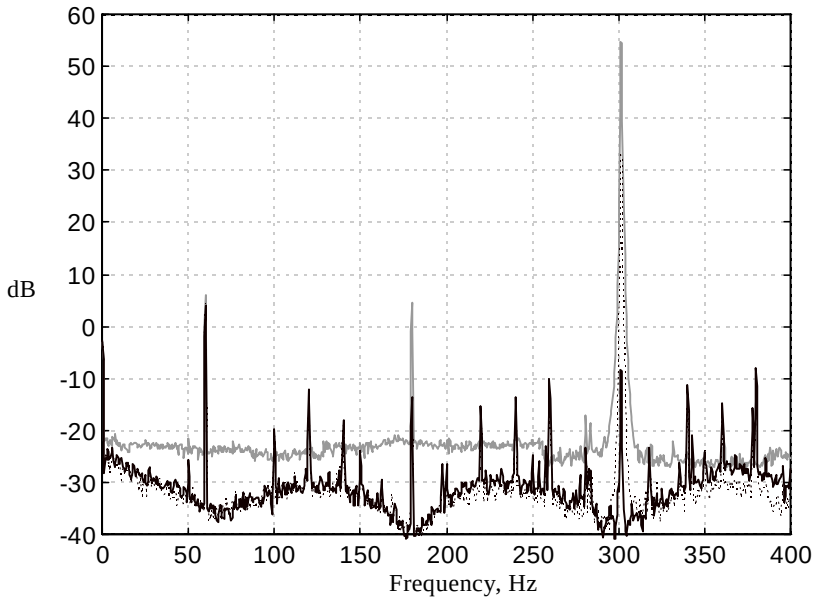

Figure 4.6 Cancellation of Tone With Feedback Only

Figure 4.6 shows the ability of a feedback controller with an internal noise model to cancel a sine wave disturbance. Here, the autospectrum of the plant output without control (gray line), feedback only (dotted line), and feedback with internal noise model (solid line), is shown. A 20^{th} order system model was used with a sample rate of 1 KHz. The disturbance in Fig. 4.6 was a 300 Hz tone. Since this is a resonant frequency of the plant, regulation may be performed with little control effort. The advantage of using the internal noise model may be seen by comparing the dotted line to the solid black line. Fig. 4.6 illustrates the ability of feedback control to greatly attenuate a periodic disturbance without the need of a reference source as in feedforward control.

Multiple sine waves may also be modeled in the observer Markov parameters (OMP), returned by the system ID. Figure 4.7 illustrates the performance of a broadband controller which was designed using the OMP containing the disturbance model.

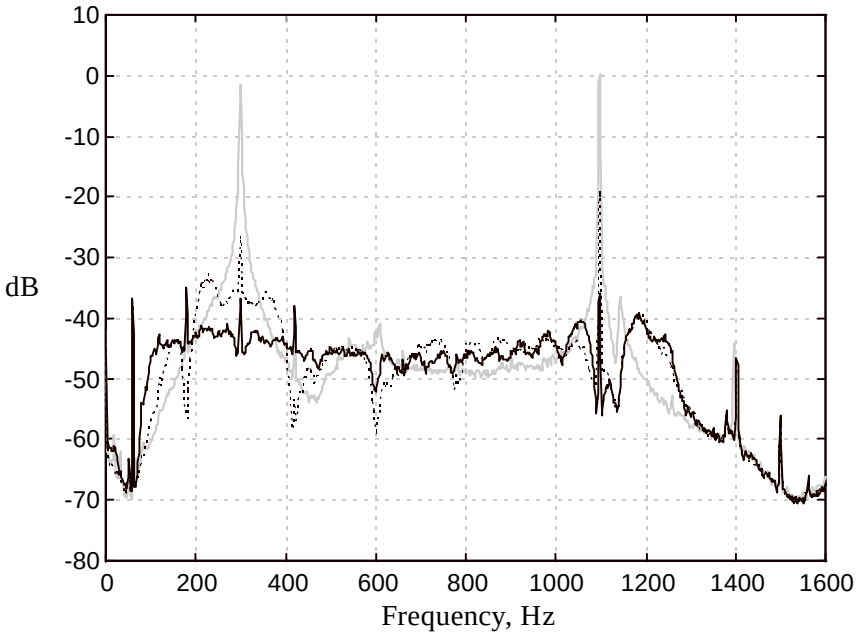

Figure 4.7 Plot of Resonance Tone Rejection

Figure 4.7 shows the autospectrum of the plant output without control (gray line), feedback (dotted line), and feedback with internal noise model (solid line). A 50^{th} order system model was used with a sample rate of 2.5 KHz. The disturbance signal entering the plant of Fig. 4.7 was the sum of a 300 Hz sine wave, a 1100 Hz sine wave and band limited white noise. When the system ID was performed with the disturbance on, the resulting OPM contained a model of both sine wave disturbances. As can be seen by comparing the solid line to the dotted line in Fig. 4.7, the internal noise model greatly improved regulation at the frequencies of both sine wave disturbances.

The periodic disturbances in both Fig. 4.6 and 4.7 were at resonant frequencies of the plant. If the disturbance is at an off resonant frequency, regulation may still be performed if the control actuator has sufficient authority. This may be seen in Fig. 4.8.

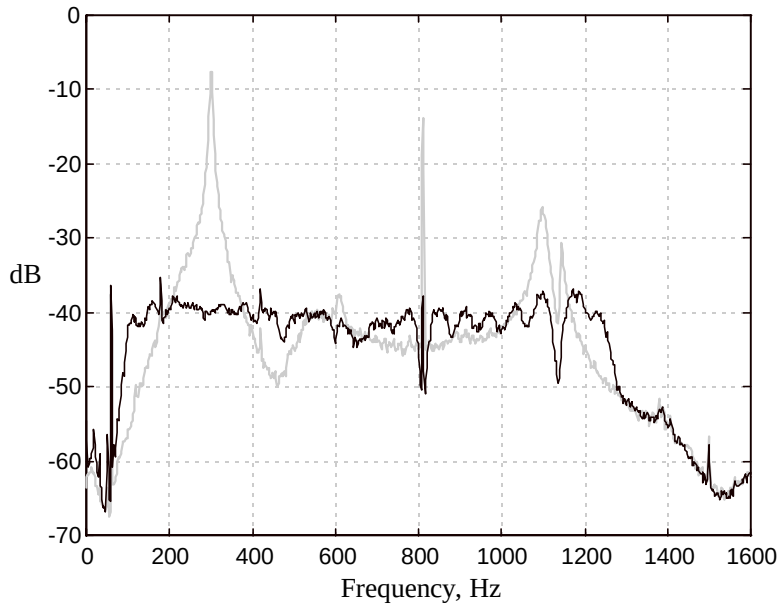

Figure 4.8 Plot of Off Resonance Tone Rejection

Figure 4.8 shows the autospectrum of the plant output without control (gray line), and feedback with internal noise model (solid line). A 50^{th} order system model was used with a sample rate of 2.5 KHz. The disturbance in Fig 4.8 was a 800 Hz tone plus band limited white noise. As can be seen in the figure, resonance response control is obtained along with cancellation of the off resonance tone. The frequency range shown in Fig. 4.8 goes up to 1.6 KHz. The spectrum analyzer in this experiment obtained the accelerometer signal after passing through the amplifiers and low pass filter as shown in Fig. 3.2. Since this is a continuous-time signal, the fact that the DSP system is running at 2.5 KHz is not related to the bandwidth shown in Fig. 4.8. The bandwidth of Fig. 4.8 is half the sample rate of the B&K analyzer, not half the DSP sample rate.

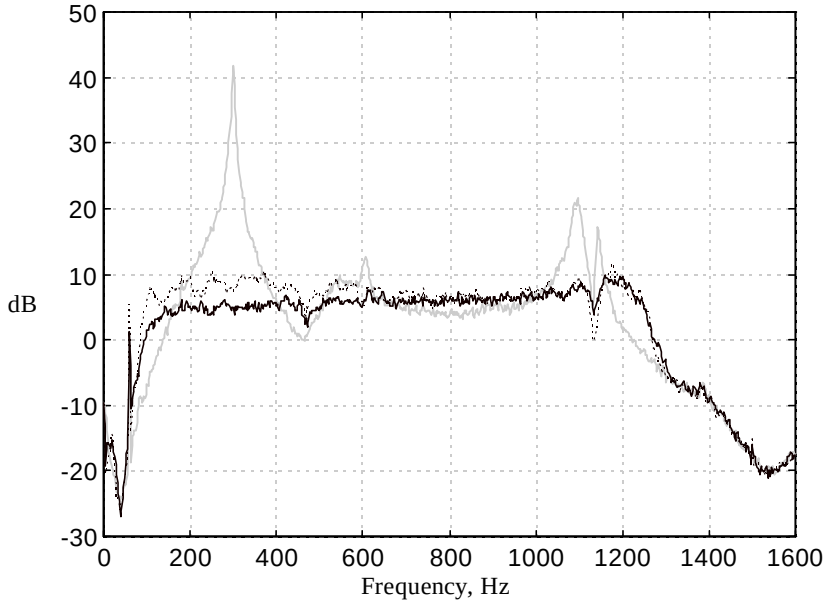

Figure 4.9 GPC with Internal Noise Model vs. Feedback/Feedforward

Figure 4.9 shows the autospectrum of the plant output without control (gray line), feedback with internal noise model (dotted line), and feedback/feedforward control (solid line). A 50^{th} order system model was used for all cases with a sample rate of 2.5 KHz. The disturbance was white noise band-limited to 1 KHz. The reason for the resonant response beyond 1 KHz is due to the fact that the filter used to band-limit the disturbance signal was a four-pole butterworth filter with a 3 dB cut-off of 1 KHz. This filter allowed enough noise beyond 1 KHz into the plant to excite the first and second resonance beyond 1 KHz. Alaising occurred due to the spectrum beyond 1.25 KHz shown in Fig. 4.9, but this is a small amount and is tolerable. Both prediction and control horizons were set to the system order. The control weighting was 0.001. Figure 4.9 compares the performance of the GPC feedback controller with an internal disturbance model to feedback/feedforward GPC control. As can be seen in the figure, the feedback/feedforward controller gave an additional 3 or 4 dB reduction around the first mode in comparison to the feedback controller.

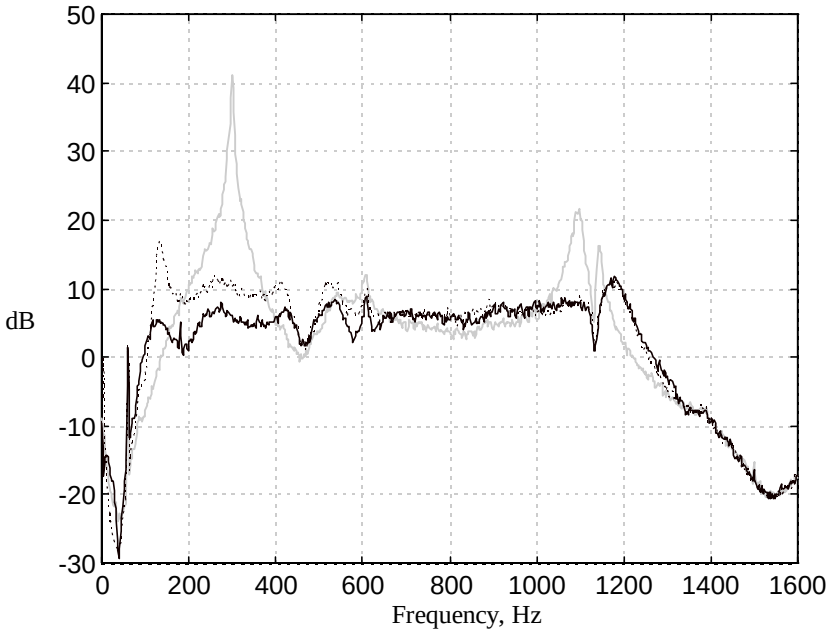

Figure 4.10 Reduced Order Feedback/Feedforward Controller

Figure 4.10 is similar to Fig. 4.9 except here the system order was decreased to 12 and all other settings were the same. As can be seen, the feedback controller with the internal disturbance model has lost some of its ability to regulate due to the reduced system order[41,1].

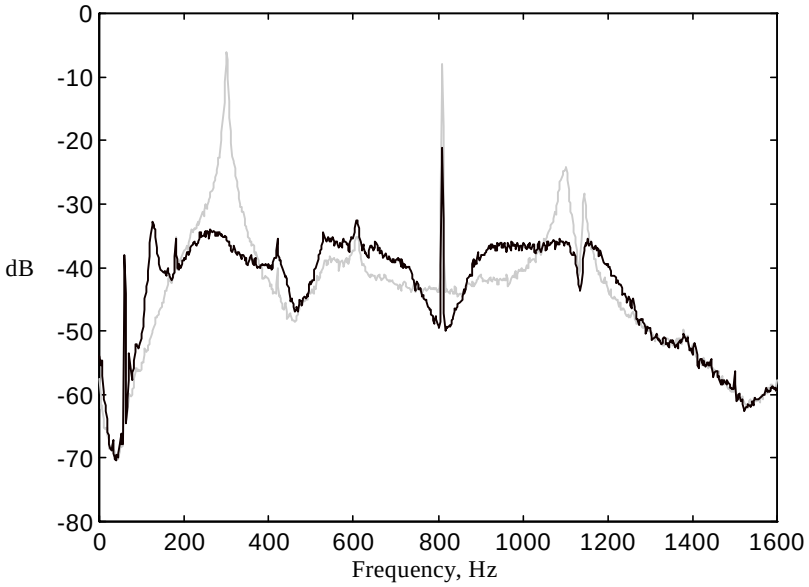

Figure 4.11 Feedback with Internal Noise Model of 800 Hz Tone

Figure 4.11 shows the autospectrum of the plant output without control (gray line), and with GPC feedback control with an internal noise model (solid line). Here a 14^{th} order system model was used with sample rate of 2.5 KHz. The reason for increasing the system order from 12 in Fig. 4.10 to 14 in Fig. 4.11 was based on the need to increase the plant model order by two to model the single tone as described in Section 4.6. The model was determined based on input and output data taken in the presence of white noise band-limited to 1 KHz plus an 800 Hz tone. As can be seen, the controller did not completely cancel the 800 Hz tone due to the low system order. This results from the fact that there are not enough OMP coefficients to model both the system and disturbance characteristics[41]. In theory, only two additional OMP coefficients are needed to model the single tone. However, since the plant is not adequately modeled, the addition of more OMP coefficients will go to model the plant dynamics more so than the disturbance. Once almost all of the plant dynamics are adequately modeled, then any additional OMP may be used to model the disturbance.

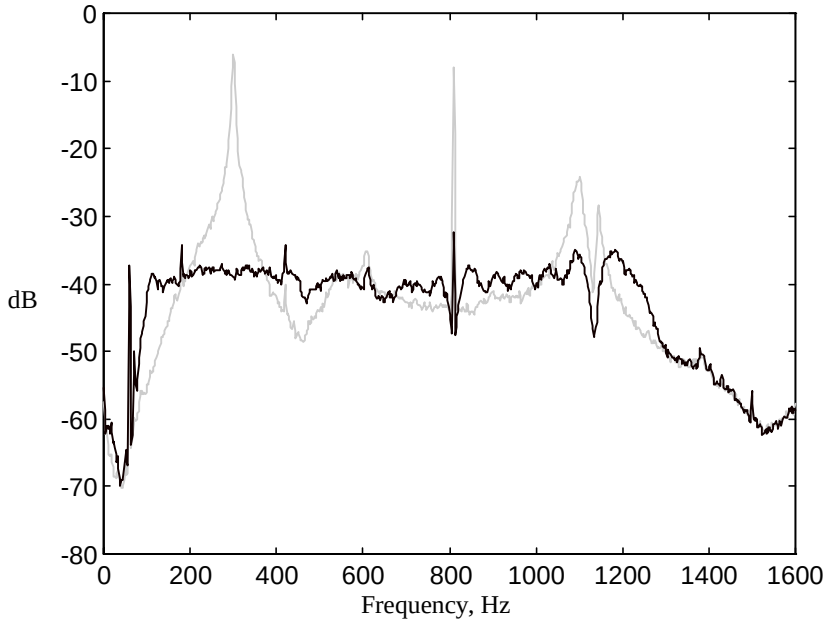

Figure 4.12 High-order Feedback with Internal Noise Model

Figure 4.12 shows the results of increasing the system order to 50. All other settings remained the same as in Fig. 4.11. As can be seen in Fig. 4.12, the 800 Hz wave was properly modeled, resulting in the tone being pushed down almost to the noise floor.

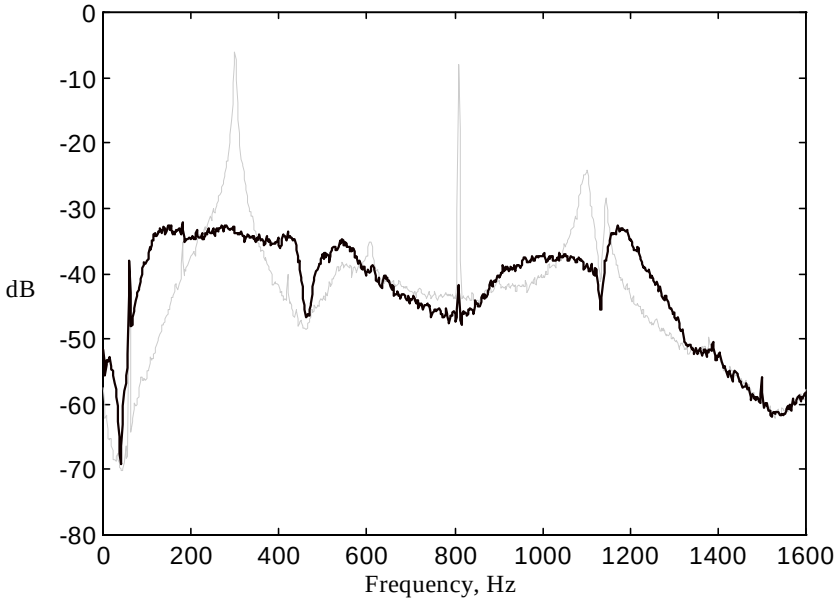

Figure 4.13 Feedback/Feedforward with AR Noise Model

Figure 4.13 illustrates the performance of the feedback/feedforward GPC controller in canceling white noise band-limited to 1 kHz plus an 800 Hz sine wave. A 12^{th} order system with sample rate of 2.5 kHz was used. The feedback/feedforward controller used in Fig. 4.13 incorporates a 2^{nd} order AR model of the 800 Hz sine wave to predict future disturbance values. Only the sine wave is used in the feedforward path. As can be seen, the 800 Hz tone is nearly canceled. The 1.6 KHz bandwidth shown reflects that the B&K analyzer was sampling at 3.2 KHz and should not be confused with the DSP system, sampling at 2.5 KHz.

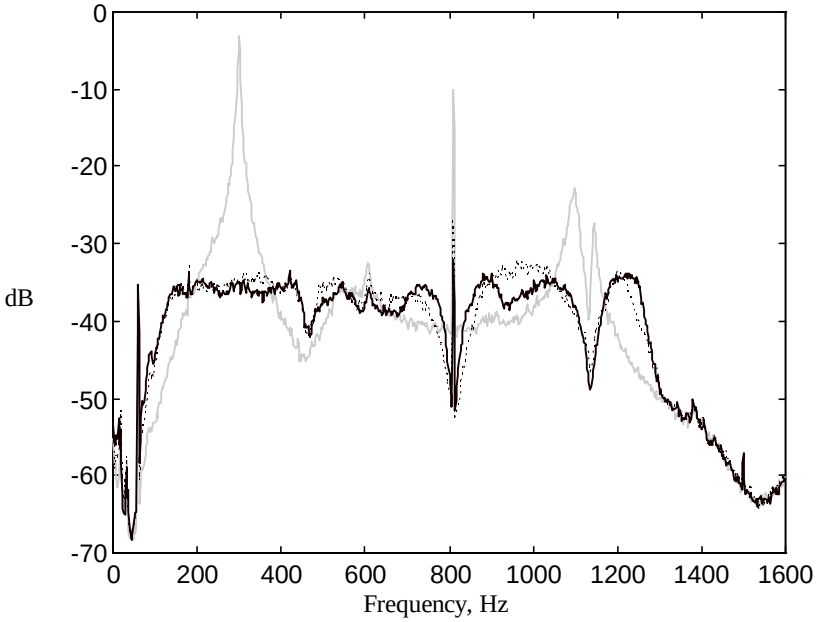

Figure 4.14 Feedback/Feedforward Performance Gain for Higher Order

Figure 4.14 compares the performance of a 20^{th} order controller, (dotted line), to that of a 30^{th} order controller, (solid line). All other parameters are the same as in Fig. 4.13. As can be seen, there is an increase in regulation with an increase in system order.

Chapter 5

Adaptive Predictive Feedback Control

5.1 Introduction

Adaptive predictive control theory may be used to regulate a time varying plant in the presence of disturbances with varying characteristics. This chapter presents the theory of adaptive Multi-Input Multi-Output (MIMO) predictive controllers. Three control schemes are developed. The first updates the system identification (system ID) and controller parameters every time step[2]. The second updates the system ID every time step, but only updates the controller parameters periodically i.e., controller parameters are updated after a number of time steps. This is known as multirate adaptive control[3]. The third control scheme uses the identification technique to directly determine the controller parameters without the need of explicit system identification. This is known as direct adaptive control[2].

Due to the recent increase in speed of digital signal processing (DSP) hardware, regulation of plate vibrations in the acoustic frequency range has become possible. However, the algorithms to accomplish this regulation task must have a small computation burden and have the ability to regulate a nonminimum-phase plant. Finite-horizon predictive controllers are more computationally efficient than Linear Quadratic Regulators (LQR) due to the fact that there is no Riccatti equation to solve[19]. The performance of predictive controllers has also been demonstrated in regulating plate vibrations[35].

An adaptive controller basically consists of an on-line system ID technique integrated with a control algorithm. The idea is to update the system ID parameters based on input and output data, use the updated system ID parameters to compute a new set of control parameters, and then compute the next control effort. Traditionally this process is repeated every time step[2]. However, due to the computational burden and fast sampling rate, this is not practical for broad-band control of modally-dense plate vibrations. In

order to meet the computational demands of adaptive control, both the DSP processor and the PC processor are utilized. One alternative is to use the DSP hardware to update the system ID and compute the control effort every time step based on existing control parameters. The controller parameters may then be updated periodically by the PC processor. This removes the computational burden of computing control parameters from the DSP processor and places it on the PC processor which allows for a large increase in bandwidth at the expense of slower adaptation. The adaptation rate in this case is limited by the speed of the host PC. If the host PC is fast enough to update the control parameters before the plant significantly changes with time, then the controller will track changes in the plant and provide regulation. Another alternative is to formulate the identification scheme such that the identified parameters are the control parameters. Since the control parameters are directly solved for, this decreases the computation burden. This technique is know as direct adaptive control and uses DSP hardware only.

It has been shown that when the system ID is performed in the presence of the disturbance, the Observer Markov Parameters (OMP) returned by the system ID technique incorporate information about the disturbance[6]. In the case of periodic disturbances, an exact map from the control input to sensor output may be obtained allowing for cancellation of the disturbance signal if the order of the OMP is sufficiently large[41,42]. In the case of stochastic disturbances, the OMP returned by the system ID technique contain the Kalman filter, which allows for optimal disturbance rejection[6]. So for both periodic and random disturbances, an optimal internal disturbance model is embedded into the controller computed from the OMP if the order of the OMP is sufficiently large.

In this chapter, Single-Input Single-Output (SISO) implementations on an acoustic plant are demonstrated using a PC and digital signal processing hardware. The performance of the different adaptive control schemes is demonstrated by plots of the system output autospectrum.

5.2 Real-time System Identification

The plant to be regulated may be represented by Eq. (3.1). The coefficient matrices, α_j *(j = 1,2, …,p)* of *mxm* and β_j *(j = 0,1,2,…,p)* of *mxr* are commonly referred to as Observer Markov Parameters (OMP)[6] or ARX parameters[1]. Eq. (3.1) may be used to predict the current system output based on the current system input and the past system inputs and outputs. β_0 is the direct transmission term.

It is the goal of the system ID technique to determine the OMP based on input and output data which may be done on line using closed-loop data if the input and output data is sufficiently frequency rich[2]. The RLS algorithm with conditional updating and forgetting factor[2] is shown below.

Algorithm 1:

$$\hat{\theta}'(k) = \begin{bmatrix} \alpha_1 & \alpha_2 & \cdots & \alpha_p & \beta_0 & \beta_1 & \cdots & \beta_p \end{bmatrix}$$

$$\varphi'(k) = \begin{bmatrix} y(k-1) & y(k-2) & \cdots & y(k-p) & u(k) & u(k-1) & \cdots & u(k-p) \end{bmatrix}$$

$$y'(k) = \begin{bmatrix} y_1(k) & y_2(k) & \cdots & y_m(k) \end{bmatrix}$$

$$If \quad \varphi'(k)P(k)\varphi(k) > 2(1-\lambda) \quad then$$

$$K(k) = P(k-1)\varphi(k)(\lambda + \varphi'(k)P(k-1)\varphi(k))^{-1}$$

$$P(k) = (I - K(k)\varphi'(k))P(k-1)/\lambda$$

$$\hat{\theta}(k) = \hat{\theta}(k-1) + K(k)(y'(k) - \varphi'(k)\hat{\theta}(k-1))$$

else do nothing

In *Algorithm 1*, $\hat{\theta}'(k)$ is a *mx(pm+pr+r)* matrix containing the OMP of Eq. (3.1) and $\varphi'(k)$ is a *1x(pm+pr+r)* vector containing the input and output data. The prime symbol denotes the matrix transpose and the hat symbol an estimate. $P(k)$ is a *(pm+pr+r)x(pm+pr+r)* covariance matrix and $K(k)$ is a *(pm+rp+r)xm* matrix containing the update gains at time step *k*. λ is the scalar forgetting factor and is chosen between *0* and *1*. *I* is a *(pm+rp+r)x(pm+rp+r)* identity matrix. For values of λ very close to one, the OMP updating is slow because old values require a long time to be forgotten. If λ is

chosen close to zero, updating is very rapid because old OMP are quickly forgotten[2]. The forgetting factor will cause the old values of the OPM to be forgotten in favor of the new values. In doing this, the system ID will track changes in the plant. However, since for an adaptive controller the new input and output data contain closed-loop information, the system ID has a tendency to drift off. To avoid this, conditional updating[2] is used where $\hat{\theta}'(k)$, $K(k)$, and $P(k)$ are updated only if there is a sufficient amount of system information in the vector $\varphi'(k)$ to warrant an update. After the system ID has converged to the OMP for the system and disturbances, the feedback controller cancels out the correlation in the system output data. Since the system output data no longer contains information, the system ID should no longer be updated in order to avoid drifting of the OMP. Conditional updating may be used in conjunction with RLS by using the following test condition as shown in *algorithm 1*.

$$\varphi'(k)P(k)\varphi(k) > 2(1-\lambda)$$

The estimated OMP are updated only if the above condition is true. This prevents the system ID from drifting off in the presence of closed-loop data.

Another system ID technique which may be used to determine the OMP is the projection algorithm[2]. This algorithm is much simpler than RLS, but converges slower. It is shown in *Algorithm 2.*

Algorithm 2:

$$\hat{\theta}(k) = \hat{\theta}(k-1) + \gamma\varphi(k)(1+\varphi'(k)\varphi(k))^{-1}(y'(k) - \varphi'(k)\hat{\theta}(k-1))$$

In *Algorithm 2,* the terms are as in *Algorithm 1* and γ is the learning rate chosen between 0 and 2. A value of γ close to 2 will cause the algorithm to learn faster, while values close to 0 will produce slower updating. In some cases, *Algorithm 2* may be chosen over *Algorithm 1* in order to decrease the computational burden if the slow convergence of the OMP can be tolerated. When the projection algorithm is used to perform system identification in a closed-loop system, the OMP will drift off because of the absence of conditional updating. In order to overcome this difficulty, a small amount of dither may be added to the control signal in order to insure that the OMP remains stable[3]. The addition of dither, (a small amount of band-limited white noise added to the control

signal), will slightly reduce the controllers ability to regulate. However, dither is necessary in some cases to prevent the OMP from drifting.

The choice of sampling rate and model order of any system identification routine is important. In general, a sampling rate which is 20% or 30% greater than the Nyquist frequency functions well[6]. If the sampling rate is chosen smaller than this, aliasing may occur[40]. If the sampling rate is chosen too fast, the system ID will return a poor model of the plant at low frequencies for a fixed order plant model. The system model order should be chosen large enough to account for all significant plant dynamics. In theory, a model order of 2 times the number of plate modes to be regulated should be chosen. However, in practice the plant model order is typically chosen to be around 5 or 10 times the number of modes[6]. This is because of disturbances in the system and the need for a very accurate system representation in order to achieve enhanced regulation.

5.3 Indirect Adaptive Predictive Control

The most intuitive way to design an adaptive controller is to update the system ID every time step, recalculate the control parameters based on the most recent system ID parameters, and use the new control parameters to calculate the new control effort[2]. In this way, the control system can track changes in the plant and disturbance characteristics every time step. A block diagram is shown in Fig. 5.1.

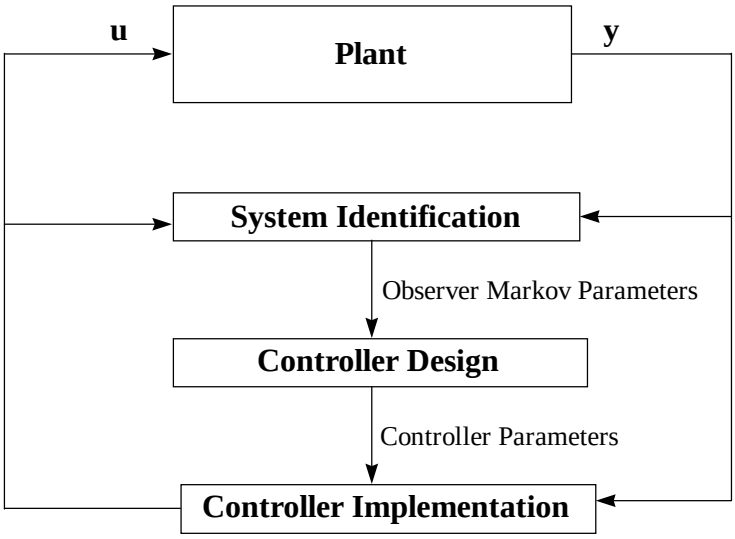

Figure 5.1 Block Diagram of Adaptive Control System.

The system shown in Fig. 5.1 performs all computations in one time step. This means that at the present time step the system ID, control parameter calculations, and control effort must be calculated in one time step. In practice, this is too great a computational burden for the DSP and PC to handle for the fast sampling rates needed to control plate vibrations over a several KHz bandwidth.

In order to reduce the computational burden, a multirate adaptive controller is proposed. In this scheme, the system ID is performed on the DSP hardware and updated every time step. However, the control parameters are only updated periodically by the PC. The control input is calculated on the DSP chip every time step. This control scheme is shown in Fig. 5.2.

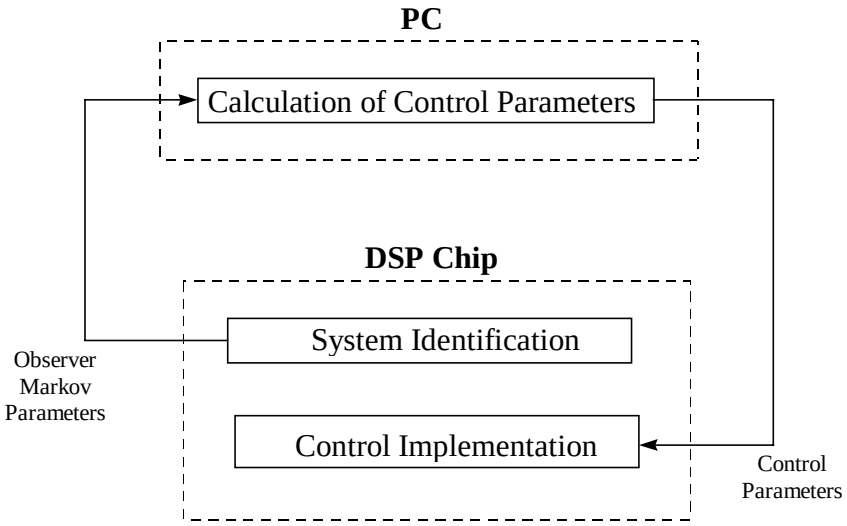

Figure 5.2 Block Diagram of Multirate Adaptive Control

The multirate adaptive controller shown in Fig. 5.2 computes the controller parameters on the PC. This presents a smaller computational burden for the DSP processor. The system ID and control implementation are done every time step. Periodically, the Observer Markov Parameters, (OMP) are passed from the DSP board to the PC. The PC then uses the OMP to compute the control parameters which are then sent back to the DSP board. This communication process between the PC and DSP board continues in a loop and the OMP are being updated at every time step. This results in an adaptive system which has a rate of adaptation dependent on the speed of the PC processor. However, since the closed-loop system does not adapt every time step, this limits the speed at which the controller can track changes in the plant and disturbance characteristics. The controller adapts at the same rate that the PC can perform the control parameter computations and communicate with the DSP board. The major computational burden which limits the bandwidth of the scheme shown in Fig. 5.2 is the system ID performed on the DSP chip.

5.4 Direct Adaptive Deadbeat Predictive Control

The computation of control parameters may be skipped if the system ID technique can be reformulated to estimate the control parameters directly[2]. In this formulation, both the system identification and the deadbeat controller design requirements are simultaneously satisfied. This formulation may be done by considering the multi-step output prediction shown in Eq. (5.1)[33].

$$y_p(k+q) = \bar{T}_c u_q(k) + T_0 u_p(k+q) + \bar{\beta}\ u_p(k-p) + \bar{A}\ y_p(k-p) \tag{5.1}$$

where

$$T_0 = T_c(qm+1{:}\ pm+qm, qr+1{:}\ qr+pr) = \begin{bmatrix} \beta_0 & 0 & \cdots & 0 \\ \beta_0^{(1)} & \beta_0 & \cdots & 0 \\ \vdots & \vdots & \ddots & \vdots \\ \beta_0^{(p-1)} & \beta_0^{(p-2)} & \cdots & \beta_0 \end{bmatrix} \qquad u_p(k+q) = \begin{bmatrix} u(k+q) \\ u(k+q+1) \\ \vdots \\ u(k+q+p-1) \end{bmatrix}$$

T_c is as defined in Eq. (4.7) and the remaining terms are defined in Eq. (4.14). In comparing Eq. (4.7) and Eq. (5.1), we see that Eq. (5.1) is simply rows $q+1$ to $p+q$ of Eq. (4.7). The formulation of Eq. (5.1) allows prediction of the plant response from time step $q+1$ up to time step $q+p$. It is desired to find a vector of future controls $u_p(k+q)$ which will make $y_p(k+q)$ a zero vector. Premultipling Eq. (5.1) by the pseudo-inverse of $\bar{T}_c$ and rearanging results in Eq. (5.2).

$$u_q(k) = T_c^{-1} y_p(k+q) - T_c^{-1} T_0 u_p(k+q) - T_c^{-1}\bar{\beta}\, u_p(k-p) - T_c^{-1}\bar{A}\, y_p(k-p) \tag{5.2}$$

Or in vector form,

$$u_q(k) = \begin{bmatrix} T_c^{-1} & -T_c^{-1}T_o & -T_c^{-1}\bar{\beta} & -T_c^{-1}\bar{A} \end{bmatrix} \begin{bmatrix} y_p(k+q) \\ u_p(k+q) \\ u_p(k-q) \\ y_p(k-q) \end{bmatrix}$$

The coefficients in Eq. (5.2) may be solved for by a system ID technique given the input and output time histories. In order to accomplish this, the data vector in Eq. (5.2) is shifted back by $p+q$ time steps in order to use only past data in the system identification technique. In this system ID formulation, the input data is the vector

$\begin{bmatrix} y_p(k+q) \\ u_p(k+q) \\ u_p(k-q) \\ y_p(k-q) \end{bmatrix}$ shifted by $p+q$ time steps in order to make the ID causal. The error in the ID

is given by $error = u_q(k)^{p+q} - \begin{bmatrix} \hat{T}_c^{-1} & -\hat{T}_c^{-1}\hat{T}_o & -\hat{T}_c^{-1}\hat{\bar{\beta}} & -\hat{T}_c^{-1}\hat{\bar{A}} \end{bmatrix} \begin{bmatrix} y_p(k+q) \\ u_p(k+q) \\ u_p(k-q) \\ y_p(k-q) \end{bmatrix}^{p+q}$. Here the hat symbol means the estimate and the superscript $p+q$ denotes a backwards shift in time by $p+q$ time steps. The output of the system identification technique will be the coefficient vector $\begin{bmatrix} \hat{T}_c^{-1} & -\hat{T}_c^{-1}\hat{T}_o & -\hat{T}_c^{-1}\hat{\bar{\beta}} & -\hat{T}_c^{-1}\hat{\bar{A}} \end{bmatrix}$. In comparing Eq. (5.2) with Eq. (4.15) and assuming that λ is zero, we see that the last two terms of Eq. (5.2) are the deadbeat control parameters. The computation of the control effort is shown in Eq. (5.3) using the parameters estimated by the system ID technique.

$$u_q(k) = \begin{bmatrix} -\hat{T}_c^{-1}\hat{\bar{\beta}} & -\hat{T}_c^{-1}\hat{\bar{A}} \end{bmatrix} \begin{bmatrix} u_p(k-p) \\ y_p(k-p) \end{bmatrix} \tag{5.3}$$

Therefore the vector form of Eq. (5.2) may be inserted into a system ID technique such as RLS in order to estimate the control parameters. The control produced by Eq. (5.3) is that of Eq. (4.15) with the control penalty set to zero and without the feedforward path. In practice, only the first *r* rows are solved for in the system ID technique since this is all that is needed to perform the control effort computation. This scheme allows for the direct computation of control parameters given the past input and output data and is updated every time step giving the direct adaptive DPC the ability to run on DSP hardware only.

5.5 Adaptive Implementations

This section presents the implementation of adaptive predictive control to regulate the vibrations of a rectangular plate. The test setup here is the same as described in section 3.3.1. The system to be regulated is shown in Fig. 3.1, the box experiment. For all

of the figures shown in this section, the vertical scales are not calibrated and are used only for open- and closed-loop comparisons.

Figure 5.3 is the autospectrum of the accelerometer signal obtained when the multirate adaptive controller, described in Fig. (5.2), was used to regulate the plant shown in Fig. 3.1. The accelerometer signal was measured by the B&K analyzer as shown in Fig 3.2.

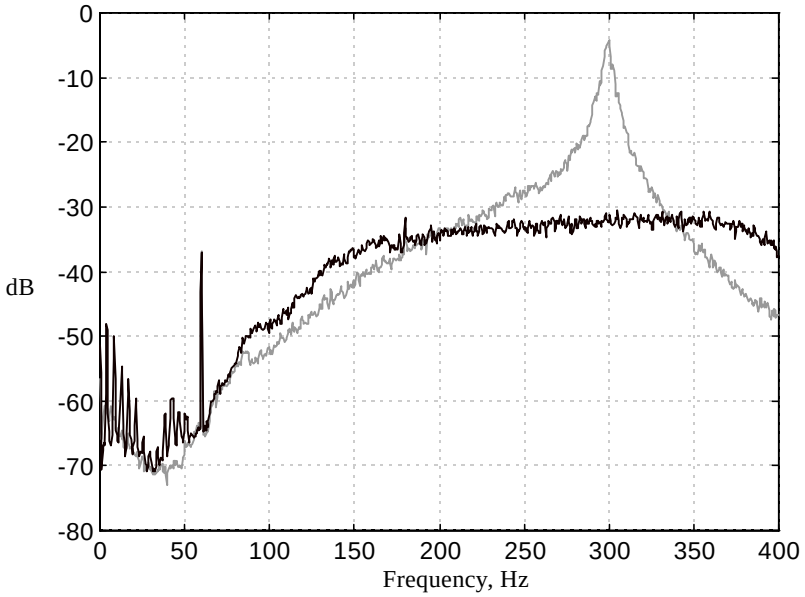

Figure 5.3 Plot of Multirate Adaptive Controller Using GPC

Figure 5.3 is the plot of the autospectrum of accelerometer signal. The total reduction was 13.37 dB. The open-loop is the gray line and closed-loop is the black line. Generalized Predictive Control (GPC) was used with a control penalty of 0.005. An 8^{th} order system model was used with a 1 kHz sampling rate and 400 Hz four pole filters were used to filter the control and accelerometer signals. The plot shown in Fig. 5.3 was generated using a multirate adaptive controller which ran on both the PC and the C-40 DSP chip. In the implementation, the system ID was updated every time step using Recursive Least Squares (RLS) with conditional updating[2], and the control calculations were done periodically on a i486 66 MHz PC using the GPC algorithm. The C-40 DSP chip was

used to implement the resulting controller coefficients and a new control effort was calculated every time step. As can be seen in Fig. 5.3, the first plate mode at 300 Hz was suppressed using this control technique.

Figure 5.4 shows the autospectrum of the accelerometer signal when the direct adaptive controller of Eq. (5.3) was used to regulate the first mode of the plate.

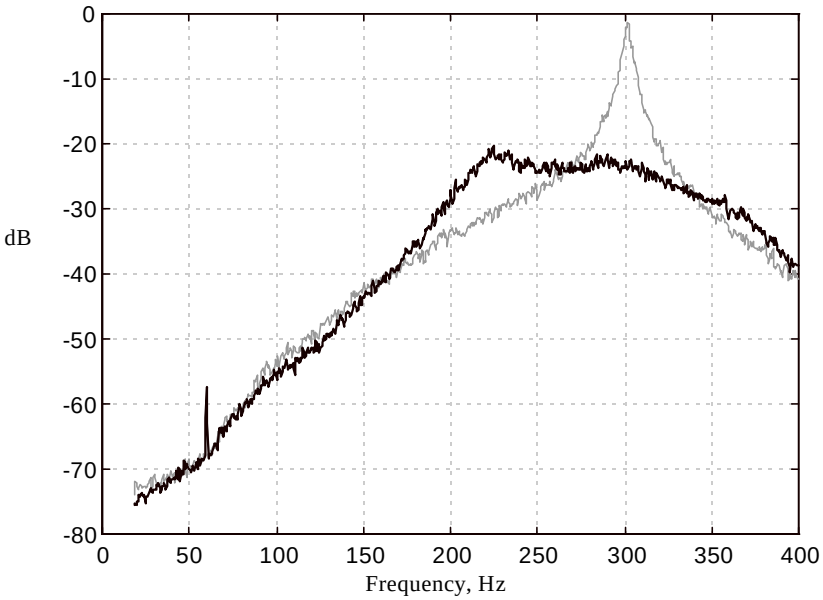

Figure 5.4 Plot of Direct Adaptive Controller Performance

Figure 5.4 is the plot of the autospectrum of the accelerometer signal. The total reduction was 8.85 dB. The open-loop is the gray line and closed-loop is the black line. Direct adaptive Deadbeat Predictive Control, (DPC) was used. A 4^{th} order system model was used and the control horizon was set to 6. A 1 KHz sampling rate was used and 400 Hz four pole filters were used to filter the control and accelerometer signals. The RLS forgetting factor was 0.99. In the direct adaptive controller, the PC is not used at all, i.e., all computations are performed on a single C-40 chip. Since all updates are done every clock cycle, the implementation here is truly real time. RLS with conditional updating was used to directly identify the control parameters based on input and output data. In comparing Fig. 5.3 with Fig. 5.4, we see that the multirate GPC algorithm performs

slightly better. This can be accounted for by considering that an 8th order model was used in Fig. 5.3 while a 4th order model was used in Fig. 5.4. The direct adaptive DPC algorithm was limited to a 4th order model because of the computational demand placed on the C-40 processor.

Figure 5.5 shows the autospectrum of the accelerometer signal for an increased bandwidth. This time the multirate adaptive DPC was used to regulate the plate vibrations.

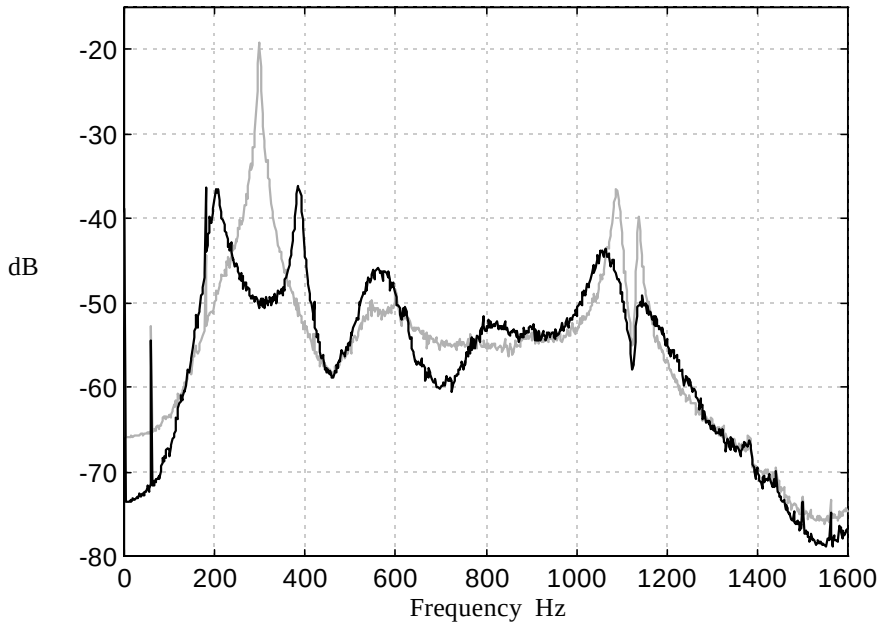

Figure 5.5 Increased Bandwidth DPC Multirate Controller

Figure 5.5 is the plot of autospectrum of accelerometer signal. The total reduction was 7.99 dB. Open-loop is the gray line and closed-loop is the black line. A 6th order system model was used and the control horizon was set to 8. A 2.5 kHz sampling rate was used. One kHz four pole filters were used. The results shown in Fig. 5.5 are not as good as those obtained for the single mode case of Fig. 5.3. The reason for this is the system order used is too low. In order to properly model the dynamics of the plate in this bandwidth, a larger system order should be chosen[6]. However, because RLS with conditional updating is performed every time step on the DSP chip, the system order is limited to a small value

which allows all system identification computations to be performed within a single time step.

The projection algorithm may be used to perform on-line system identification when regulation over a larger bandwidth is desired. In the projection algorithm, conditional updating can not be performed since there is no covariance matrix as there is in RLS. In order to prevent the system ID from drifting off in the presence of closed-loop data, a small amount of dither, (2-5% of the maximum control effort value), is added to the control signal. The dither is band-limited white noise and will insure that the closed-loop system remains persistently excited. The dither will add a small amount of broad-band noise to the plant output. However, this small sacrifice in performance will result in a controller which can track a time varying plant based on closed-loop data. Figure 5.6 shows the autospectrum of the accelerometer signal when the multirate adaptive controller is used in conjunction with the projection algorithm.

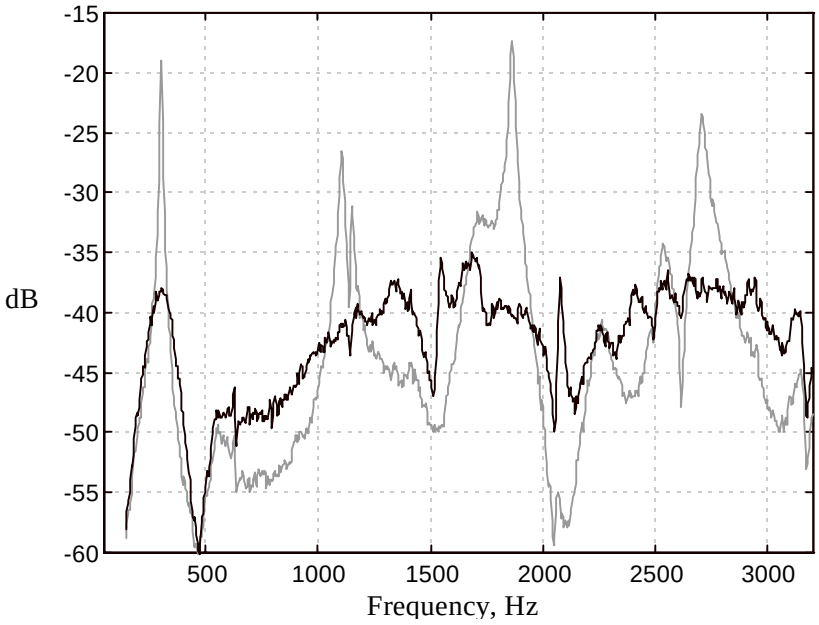

Figure 5.6 Multirate Adaptive Controller Using Projection Algorithm

Figure 5.6 is the plot of autospectrum of accelerometer signal. The total reduction was 6.35 dB. Open-loop is the gray line and closed-loop is the black line. GPC was used. A

40^{th} order system model was used and the control horizon and the prediction horizon were set to 40. A 8 KHz sampling rate was used and the control penalty was 0.001. The projection algorithm learning rate was 0.1 and 3.2 KHz seven pole elliptic filters were used as input and output filters.

5.6 Summary

Adaptive predictive control has been used in the regulation of plate vibrations. By combining the system ID technique with the controller design, an adaptive controller may be used to regulate an unknown plant. The adaptive controller possesses the ability to regulate both changes in the disturbance characteristics and changes in the plant. The theory and implementation of both the multirate adaptive controller and the direct adaptive controller have been demonstrated. In the case of the multirate adaptive controller, the system ID is performed every time step while the controller parameters are only updated periodically. Either Generalized Predictive Control (GPC), or Deadbeat Predictive Control (DPC), may be used in this technique. The multirate adaptive controller requires the use of both the DSP hardware and the PC. The direct adaptive controller does not require the use of the PC. In this formulation, the system ID is written to directly determine the controller parameters based on input and output data. Both the multirate adaptive controller and the direct adaptive controller may be used to regulate plate vibrations without an initial model of the system given that an estimate of the plant order is known. With the estimated plant order, the user may adjust the control horizon to obtain the desired DPC performance. If GPC is being used, the control horizon and the control penalty may be tuned to meet performance specifications.

The adaptive techniques used in the experiments demonstrate the ability to regulate an unknown plant in the presence of an unknown disturbance. Each technique has both advantages and disadvantages. The multirate adaptive controller using RLS and conditional updating has the advantages of being able to regulate the plant without the need of dither and the advantage of fast convergence. However, the bandwidth is limited because of the large computation burden placed on the DSP processor in performing the

RLS computations every time step. In order to improve this bandwidth limitation, the RLS algorithm may be replaced by the projection algorithm at the expense of slower convergence. In addition, another disadvantage in using the projection algorithm is the need for dither in the control system which introduces more noise in the system. However, this may be a small price to pay for the increased bandwidth gained. The multirate adaptive controller, whether it uses RLS or the projection algorithm, has to use both the DSP processor and the host PC. In order to reduce the amount of hardware needed to perform vibration control, the need for the host PC may be eliminated by using the direct adaptive controller. The direct adaptive controller does, however, have the most limited bandwidth because of the need to perform an identification which is larger than that required of the multirate adaptive controller.

For broadband regulation of modally-dense structures, the multirate adaptive controller using the projection algorithm offers the most promise. This is simply because of the algorithms considered in this chapter, it places the smallest computational burden on the DSP hardware which offers the largest regulation bandwidth.

Chapter 6

Block Adaptive Feedback Control

6.1 Introduction

As shown in Chapters 3 through 5, various techniques of adaptive predictive control have been successfully applied to regulate plate vibrations. These techniques performed the system identification every time step with periodic updates of the controller parameters. It has been demonstrated that adaptive feedback control can be used with current microprocessor technology to regulate plate vibrations over a portion of the acoustic frequency range. However, the adaptive feedback techniques presented so far require the use of recursive least squares which limits the bandwidth of the regulator, or dither must be added to the control effort of gradient descent algorithms which introduces additional noise into the system. If the level of dither can be made sufficiently small, dither provides one way to insure an accurate system identification in a closed-loop system. One way to increase the bandwidth of the controller is to remove the burden of updating the system identification every time step. Instead, the system identification is performed on blocks of input and output data and the controller parameters are updated based on the latest identification results. This scheme allows both system identification parameters and control parameters to be updated based on a block of data rather than every data point. This chapter presents the theory and application of block adaptive control. The system identification is performed using batch least squares[6]. Multi-input multi-output applications of vibration regulation are presented using a rectangular plate located between anechoic chambers. Acoustic far field power estimates are performed on both closed-loop and open-loop plate vibration data. In addition, it is shown that enhancements may be obtained by adding a feedforward path to the feedback controller. Results are presented for both broad-band disturbances and tonal disturbances.

Adaptive feedback control may be used to regulate vibrations of a slowly time-varying structure. Here the frequency range is broad resulting in a plant which is modally

dense and therefore of high order. In addition, since the regulation of most vibration modes calls for several actuators and sensors, the plant is MIMO[22]. In block adaptive control, both a PC processor is used as well as DSP hardware. The DSP processor is used to implement the controller and gather blocks of input and output data while the PC is used to compute the system identification and the controller coefficients. The computations that must be performed at every time step are the calculation of the next control outputs and the storage of the current inputs and outputs. The speed of the PC processor will determine the adaptation rate of the control system. In practice, the host PC may be replaced with one or more additional DSP chips which would create an adaptive control system operating with DSP hardware only. The resulting controller offers the ability to regulate a high-order MIMO plant over a broad frequency range provided that the plant is not varying in time too rapidly. This is to say that as long as the system identification and controller can be updated before the plant changes significantly, stability and regulation will be maintained.

In the adaptive regulation of plate vibrations, one must select a system identification technique as well as a control algorithm for the determination of control parameters. The system identification method chosen here is batch least squares based on the information matrix[8]. This method is well suited for block updates and is fast. The control method chosen is Generalized Predictive Control (GPC)[11]. The GPC offers a solution which closely approximates the Linear Quadratic Regulator[12] without the computational burden of solving a Riccati equation. Theoretical development and implementations are both done using finite-difference representations[1]. The reason for choosing GPC rather than DPC is due to the fact that a large system order is needed to provide enhanced plant regulation. The DPC algorithm necessitates predictions at least twice as far as the system order. The recursive computation presented in Eq. (4.5) results in an increase in error for an increase in prediction horizon due to the uncertainty in the OMP. The GPC algorithm may be used for shorter prediction horizons by adjusting the control penalty to avoid instabilities and actuator saturation.

6.2 System Identification for Block Adaptive Control

The objective of system identification is to determine the coefficients of a mathematical model used to represent the plant to be controlled. The plant to be regulated may be represented by the Auto-Regressive with eXogenous input model (ARX)[1] shown in Eq. (3.1) and presented here for convenience.

$$y(k) = \alpha_1 y(k-1) + \alpha_2 y(k-2) + \ldots + \alpha_p y(k-p) + \beta_0 u(k) + \beta_1 u(k-1) + \ldots + \beta_p u(k-p) \quad (6.1)$$

Equation (6.1) can be used to predict the current system output based on the current system input and the past system inputs and outputs. The quantity β_0 is the direct transmission term.

In block adaptive control the objective is to update the Observer Markov Parameters, (OMP, or ARX parameters), based on blocks of input and output data. Batch least squares[6] with a forgetting factor is chosen as the system identification technique. Writing Eq. (6.1) in vector form produces

$$y(k) = \bar{Y} v_p(k-1) \quad (6.2)$$

where

$$\bar{Y} = \begin{bmatrix} \alpha_1 & \alpha_2 & \ldots & \alpha_p & \beta_0 & \beta_1 & \beta_2 & \ldots & \beta_p \end{bmatrix}$$

$$v_p(k-1) = \begin{bmatrix} y(k-1) \\ \vdots \\ y(k-p) \\ u(k) \\ \vdots \\ u(k-p) \end{bmatrix}$$

Where $\bar{Y}$ is the vector containing the OMP. For different values of *k*, Eq. (6.2) may be used to form the matrix relationship

$$y = \bar{Y} V_p \quad (6.3)$$

where

$$y = \begin{bmatrix} y(k) & y(k+1) & \cdots & y(k+N-1) \end{bmatrix}$$

$$V_p = \begin{bmatrix} v_p(k-1) & v_p(k) & \cdots & v_p(k+N-2) \end{bmatrix}$$

Equation (6.3) may be used to formulate the batch least-squares solution for the OMP[6]

$$\hat{\bar{Y}}_p = yV_p^T\left[V_pV_p^T\right]^+ \tag{6.4}$$

Equation (6.4) involves the computation and inversion of a $(mp+rp+r)x(mp+rp+r)$ matrix where $^+$ means the pseudo inverse. The matrix y is of dimension $mx(N+1)$ and the matrix V_p is $(N+1)x\{(p+1)(r+m)\}$. The computation of the matrix $V_pV_p^T$ involves approximately $(N+1)(p+1)^2(r+m)^2$ multiplies and about the same number of adds. The inversion of $V_pV_p^T$ involves approximately $(p+1)^3(r+m)^3$ multiplies and adds. The computation of yV_p^T involves approximately $(N+1)(p+1)(r+m)$ multiplies and adds. Finally, the formation of $yV_p^T\left[V_pV_p^T\right]^+$ involves $(p+1)^2(r+m)^2$ multiplies and adds. So the total number of multiplications involved in the batch least squares solution is around $(N+1)(p+1)^2(r+m)^2+(p+1)^3(r+m)^3+(N+1)(p+1)(r+m)+(p+1)^2(r+m)^2$ with approximately the same number of adds. For large values of *p* and for large lengths of data *N* the computation of $V_pV_p^T$ becomes a burden because of the product $(N+1)(p+1)^2(r+m)^2$ which grows rapidly for large system orders and data lengths. This may be overcome by a recursive algorithm presented in Appendix B using the Information matrix[8]. A computation comparison is given in Appendix B.

When Eq. (6.4) is used in an adaptive controller, some sort of updating technique is needed to track changes in the plant. Consider Eq. (6.3) as representing the input and output relation for one block of data. If a second block of data is added on, the equation becomes

$$\left[y \quad y'\right] = (\bar{Y}+\Delta\bar{Y})\left[V_p \quad V_p'\right] \tag{6.5}$$

where y' is a second block of system outputs and V_p' is a second block of past inputs and outputs. There is a time difference between the start of the first data block and the start of the second data block. This time difference is greater than or equal to the amount of time taken to fill the data buffers. In terms of the data correlation matrixes, we have

$$yV_p^T + y'V_p'^T = (\bar{Y}+\Delta\bar{Y})(V_pV_p^T + V_p'V_p'^T) \tag{6.6}$$

Equation (6.6) is valid for two blocks of data and $\Delta\bar{Y}$ is the change in the OMP going from one data block to two data blocks. Recalling that $yV_p^T = \bar{Y}V_pV_p^T$, Eq. (6.6) may be rewritten as

$$y'V_p'^T - \bar{Y}V_p'V_p'^T = \Delta\bar{Y}(V_pV_p^T + V_p'V_p'^T) \tag{6.7}$$

Solving for $\Delta\bar{Y}$ produces an equation for the update of the OMP going from one block of data to two blocks of data,

$$\Delta\bar{Y} = (y'V_p'^T - \bar{Y}V_p'V_p'^T)(V_pV_p^T + V_p'V_p'^T)^+ \tag{6.8}$$

The block adaptive system identification equation for the OMP is given by

$$\bar{Y}' = \bar{Y} + \Delta\bar{Y} = \bar{Y} + (y'V_p'^T - \bar{Y}V_p'V_p'^T)(V_pV_p^T + V_p'V_p'^T)^+ \tag{6.9}$$

To track changes in the plant within a reasonable amount of time, a forgetting factor is introduced into Eq. (6.9) in order to forget old values of the data correlation matrix in favor of newer ones. This may be achieved by modifying Eq. (6.9) to become

$$\bar{Y}' = \bar{Y} + \Delta\bar{Y} = \bar{Y} + (y'V_p'^T - \bar{Y}V_p'V_p'^T)(\lambda V_pV_p^T + V_p'V_p'^T)^+ \tag{6.10}$$

where λ is the forgetting factor chosen between 0 and 1. Equation (6.10) may be used in the block adaptive controller to track changes in the plant to be regulated. If λ is set to zero, all past data is forgotten and the OMP is updated solely using new data. In practice, this is not done due to the lack of system information in the closed-loop data blocks. The amount of information in the closed-loop data blocks is limited by the fact that the controller removes the correlation between the control effort and the error sensors. In addition, the data blocks are usually chosen to be small in size in order to decrease the computational demand placed on the host PC during an update period. However, if the plant or the disturbance spectrum has changed enough to warrant an update, there is enough information in the data blocks to slightly alter the current OMP to reflect the changes in the plant or disturbance spectrum. Over a few block updates, the change will be realized and the most of the noise will be averaged out.

If an adaptive controller is allowed to continuously operate in the presence of closed-loop input and output data, the system identification runs a risk of drifting off the true identification parameters[3]. In order to avoid this, a conditional updating test is

introduced into the recursive algorithm in order to determine if the incoming input and output data set has enough correlation to warrant an update. The block adaptive controller may be modified to include conditional updating. Consider the matrix yV_p^T defined in Eq. (6.4). The elements of this matrix contain the amount of correlation between the control inputs and the plant outputs. When the feedback controller is properly regulating the plant, the elements of the yV_p^T matrix become very small. In fact, if the controller is canceling out all of the plant and disturbance dynamics and as the block length approaches infinity, there is no correlation between the control input and plant output so the elements of the yV_p^T matrix approach zero. In practice this ideal case is unattainable due to the finite size of the block lengths, the nonminimum-phase of the plant, and actuator saturation. The matrix yV_p^T may still, however, be used to provide a test condition for conditional updating. One way of achieving this is to simply sum the magnitude of each of the elements in the yV_p^T matrix and set a threshold for updating. If the value of the sum exceeds the threshold, then the blocks of data are used to update the identification parameter matrices. If the threshold is not exceeded, then the data blocks are discarded and the process repeated when a new set of data blocks is received. The threshold is tuned by trial and error to yield the desired level of regulation.

6.3 Block Adaptive Control

The block adaptive controller offers the ability to regulate a slowly time varying modally-dense plant over a large bandwidth. The rate at which the controller parameters are updated depends on the speed of the host PC processor, the order of the system, the number of inputs and outputs, and the block length. A diagram of the block adaptive controller is shown in Fig. 6.1.

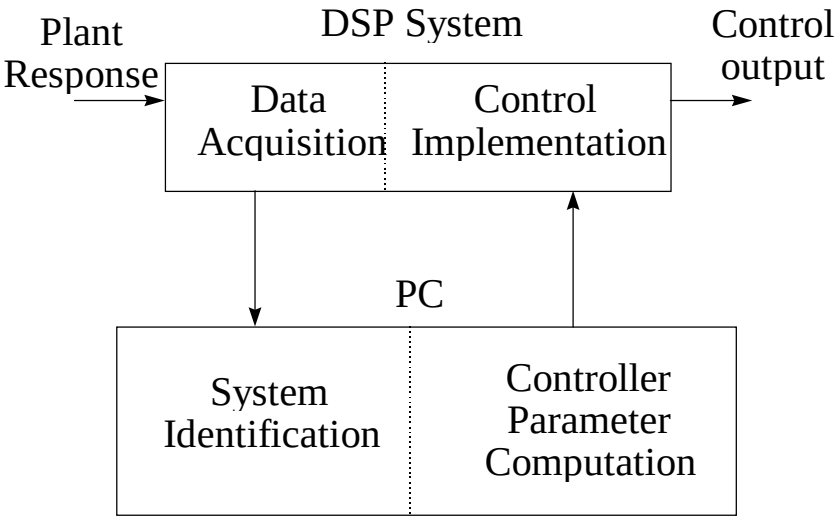

Figure 6.1 Diagram of Block Adaptive Controller

The DSP system gathers input and output data and implements the control parameters received from the host PC. It is the job of the host PC to perform the system identification based on the data received from the DSP system. Also, the host PC computes the control parameters to be returned to the DSP system. This places most of the computational burden on the host PC which allows for a substantial increase in bandwidth over other algorithms which use the DSP system for system identification. If the host PC processor is sufficiently fast, the rate of adaptation may be increased to the length of one data block. For high order MIMO applications, the amount of time taken for the host PC to update the control parameters is greater than the amount of time needed for the DSP system to gather the blocks of input and output data. For this reason, there is data skipped between input and output data blocks implying that the controller can not track a plant which is rapidly changing with time. However, most acoustic plants do not significantly change over a small length of time[38].

6.4 Experimental Results Using Block Adaptive Control

Several experiments were conducted to demonstrate the block adaptive controller. For all experiments in this chapter, GPC was used. These experiments involved an aluminum test plate. The plate was positioned between anechoic chambers. In one chamber, a large speaker was used as a disturbance source to excite the plate modes. The set up is shown in Fig. 6.2.

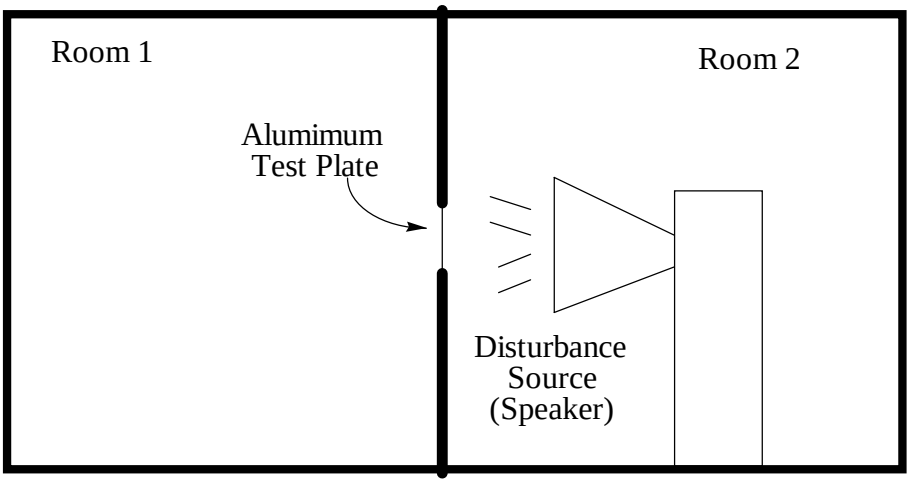

Figure 6.2 Diagram of Adaptive Controller Test Facility

The aluminum plate shown in Fig. 6.2 is rigidly held in place by many bolts on all four sides of the plate. This produces nearly clamped boundary conditions. A diagram of the plate is shown in Fig. 6.3.

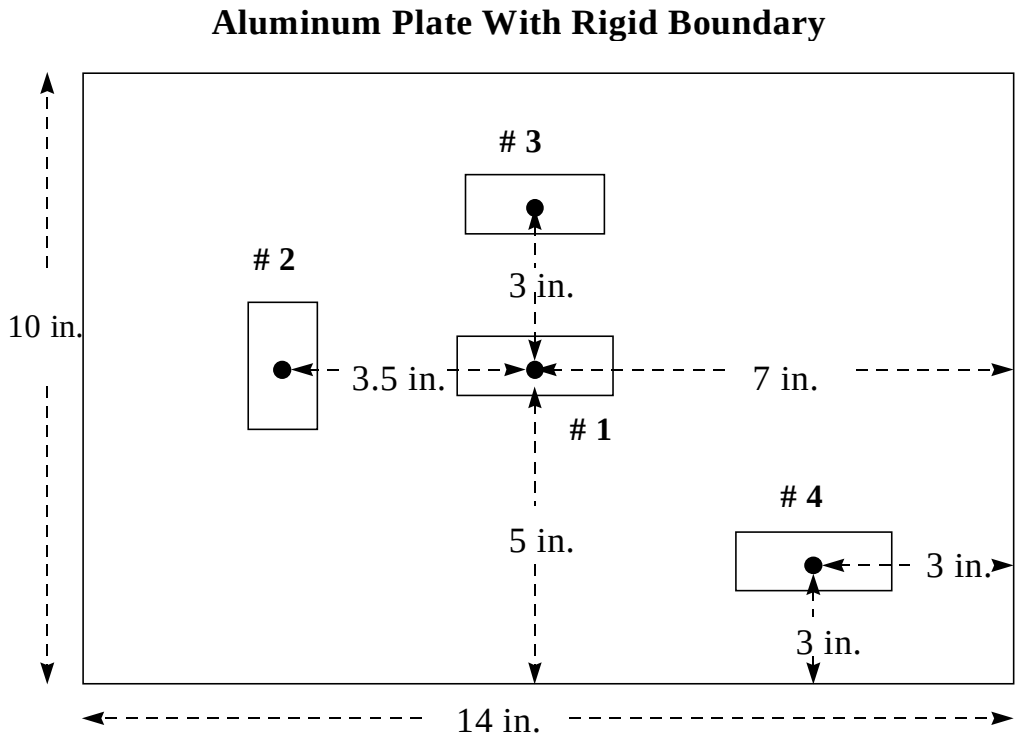

Figure 6.3 Test Plate with Sensors and Actuators

The aluminum plate shown in Fig. 6.3 is 0.040 inches thick. Mounted on the plate are piezo actuators # 1,2,3, and 4. The piezos are 2.25 inches by 1.25 inches and 0.010 inches thick. Mounted on the top of the piezos are accelerometers. The accelerometers are located at the centers of the piezos, although this is not necessary for the predictive control implementation[2]. The piezo and accelerometer locations were selected in order to observe and control both the even and odd plate modes[39]. In theory, any location selection could have been made and regulation achieved, although some locations will naturally yield better vibration regulation than other locations[22].

In order to give a physical interpretation of the plate resonance's, it is instructive to consider the natural vibration modes of the plate shown in Fig. 6.3. Table 6.1 list some of the plate modes found using different methods.

Table 6.1 Natural Frequencies of Test Plate

x = 0 horizontal center line, y = 0 vertical center line, see Figure 6.3	Leissa[43] Frequency, Hz	NASTRAN Frequency, Hz
Modes symmetric about both x = 0 and y = 0	109.78	110.37
	291.33	292.81
	495.33	497.82
Modes symmetric about x = 0 and asymmetric about y = 0	177.96	177.96
	446.89	449.18
	556.47	559.26
Modes asymmetric about x = 0 and symmetric about y = 0	262.96	264.32
	432.99	435.19
Modes asymmetric about x = 0 and asymmetric about y = 0	326.02	327.69
	583.32	586.33
Additional Higher Frequency Modes	-	646.55
	-	663.27
	-	779.99
	-	809.49
	-	810.20
	-	870.16

In Table 6.1 the second column was calculated by Leissa[43] and the third column was calculated by the software package NASTRAN. Table 6.1 shows the natural frequencies of the test plate. As can be seen, the NASTRAN results closely follow the results found by Leissa. The results from Leissa were obtained using a variation of the series method[43,44]. The results shown in the third column of table 6.1 were found by entering the appropriate physical characteristics of the test plate[45] into NASTRAN and obtaining the

natural frequencies of vibration. The frequencies determined in both cases were for the plate only without the piezos or accelerometers attached. When these frequencies are compared to the experimentally determined natural frequencies shown in the figures to follow, it is seen that the experimental frequencies are lower and in somewhat different locations than the computed frequencies. This is due for the most part to the mass loading which occurs when the piezos and accelerometers are attached to the test plate[39]. Also, it should be kept in mind that the actual plate does not have perfectly clamped boundary conditions as was assumed in the calculations.

Table 6.2 Experimental Natural Frequencies and Dampening

Frequency, Hz	Percent Dampening, %
92.150	0.687
154.614	2.721
266.914	0.497
294.195	0.449
393.468	0.347
414.970	0.319
451.752	1.016
513.243	0.346
550.361	0.178
609.400	0.538
611.434	0.200
756.997	0.183

Table 6.2 shows the natural frequencies and percent dampening based on the open-loop input and output data. The input was the disturbance signal driving the speaker and the output was the four accelerometer signals. A comparison of Table 6.2 with the open-loop plots of Figs. 6.4-6.7 shows that all significant plate modes are accounted for.

6.4.1 Non-Adaptive MIMO Control

Shown in Figs. 6.4-6.7 are the accelerometer signals to be regulated by the four-channel controller. For all figures, the gray line is the open-loop autospectrum of the acceleration in dB and the black line is the closed-loop acceleration in dB. The channel numbers correspond to the points shown in Fig. 6.3. The controller used in this case was a non-adaptive controller determined from a 75^{th} order system identification. The system identification technique used was the batch least squares method based on the information matrix[8] as described in Eq. (6.4). In order to perform the system identification, 5000 samples of input data and 5000 samples of output data for each of the four channels were used. The input data was four independent white noise sources band limited to 800 Hz. The output data was the four accelerometer signals low pass filtered at 800 Hz. The GPC[11] was used to determine the controller parameters based on the OMP returned from the system identification. In the GPC algorithm, both the prediction and control horizons were set to 75 which is the order of the finite-difference model (ARX model). A control penalty of 0.0004 was used and the sampling rate was 2.5 KHz. The plots shown in Figs. 6.4-6.7 were obtained with a B&K analyzer positioned as shown in Fig. 3.2. Fifty averages were used to determine the autospectrum of the accelerometer signals. A Hanning window was applied to the data with an overlap of 50%.

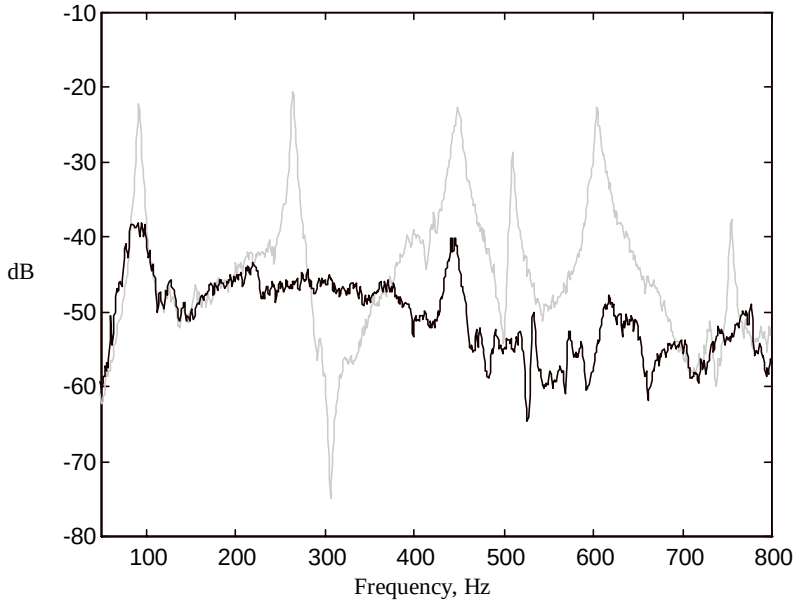

Figure 6.4 Plate Acceleration at Point #1 in dB

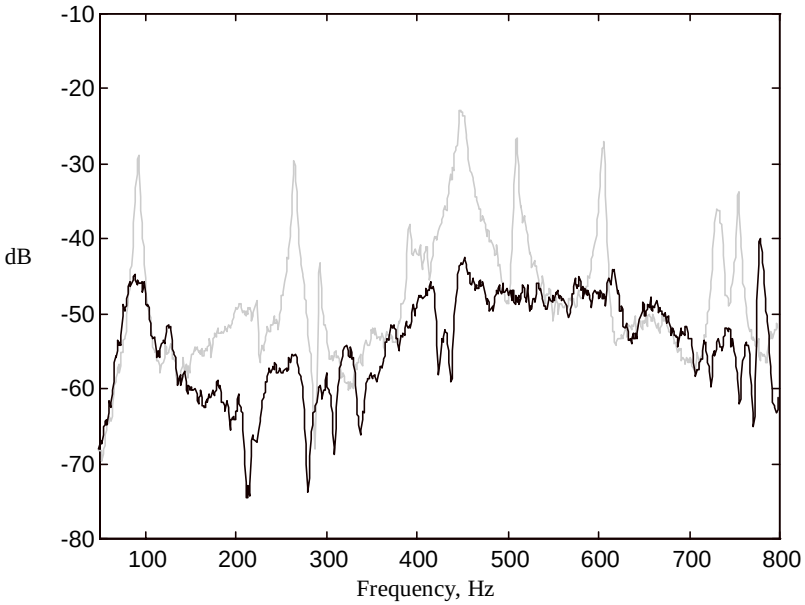

Figure 6.5 Plate Acceleration at Point #2 in dB

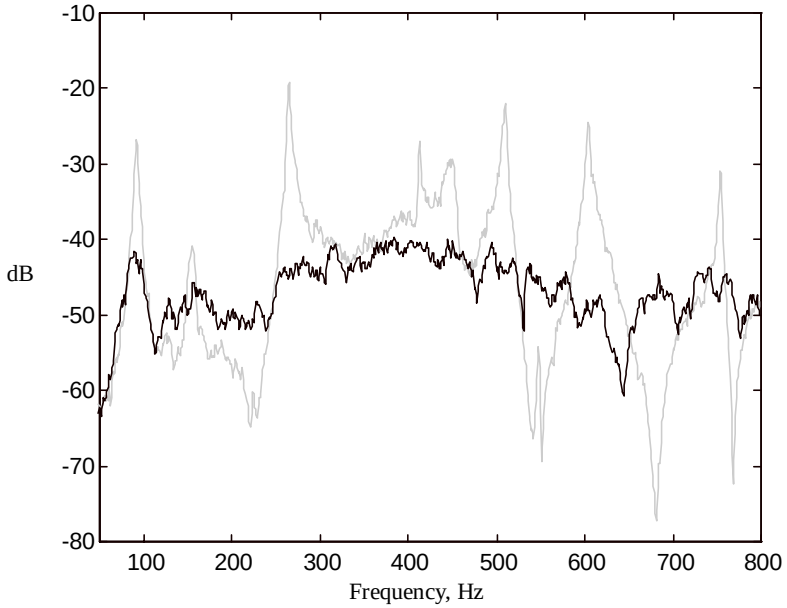

Figure 6.6 Plate Acceleration at Point #3 in dB

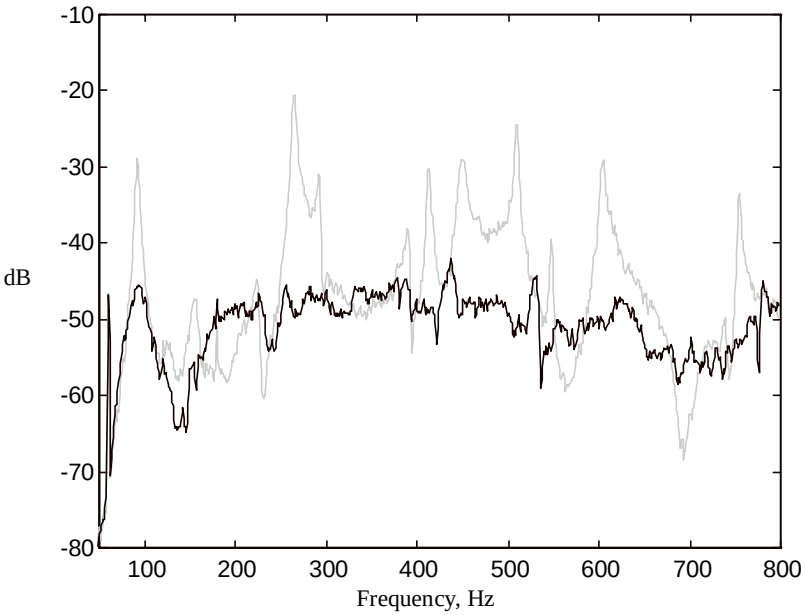

Figure 6.7 Plate Acceleration at Point #4 in dB

Table 6.3 summarizes the results presented in Figs. 6.4-6.7.

Table 6.3 Total Reductions, 4 Channel Non-adaptive Controller

	Total Reduction in Accelerometer Energy
Accelerometer Number	dB
1	12.24
2	11.97
3	9.23
4	11.87

In Figs. 6.4-6.7 the resonant peaks in the open-loop spectrum correspond to the natural frequencies of vibration of the plate. As can be seen in these figures, the predictive feedback controller regulates the modal response of the plate. The fundamental plate mode is around 90 Hz. It was found that this mode was difficult to regulate for two reasons. The first and most important is the problem of accurately modeling the plate at this low frequency. Because the sampling rate was set to 2.5 KHz and the finite-difference order to 75, the ID at 90 Hz is difficult to determine[6]. The second reason for reduced performance at 90 Hz is due to the fact that the piezo has a frequency dependent response. At low frequencies, the piezo looses actuation authority.

It is also of interest to examine the radiated sound power of the non-adaptive four channel controller and compare open- and closed-loop results. This is shown in Fig. 6.8-6.9.

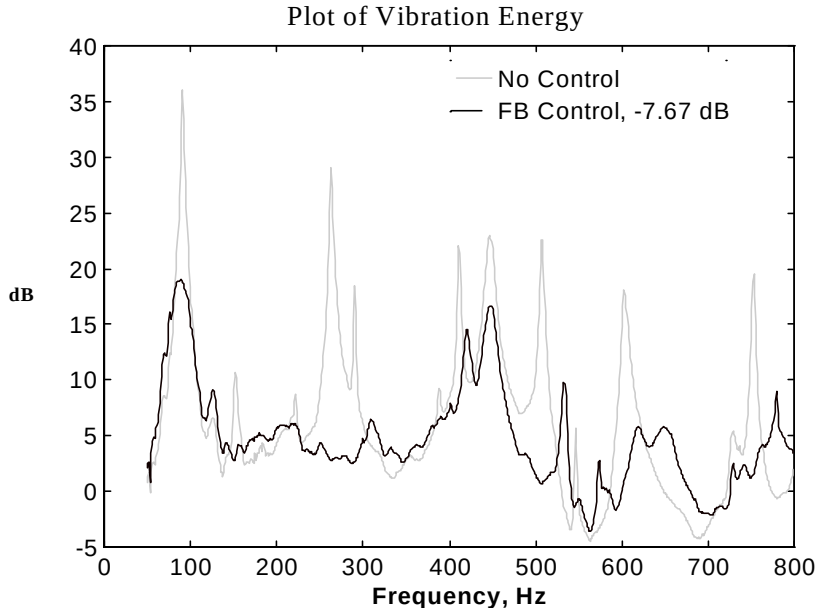

Figure 6.8 Plot of Vibration Energy

Figure 6.8 shows the plate vibration energy. The gray line is without control and the black line is with control. The total reduction in vibration energy is 7.67 dB. Figure 6.8 was obtained by scanning the plate with a laser and recording the velocity of 64 equally spaced points on the plate. Each of the 64 areas of the plate was treated as an independent vibrating mass. The total vibration energy at a fixed frequency *i* is given by summing the contribution from each patch for a given frequency[46].

$$E(\omega_i) = v(\omega_i)^H M v(\omega_i) \tag{6.11}$$

In Eq. (6.11), $E(\omega_i)$ is the total vibration energy at frequency ω_i and $v(\omega_i)$ is a vector of velocities for each point at frequency ω_i. *M* is a diagonal mass matrix and the super-script *H* is the Hermitian (conjugate transpose).

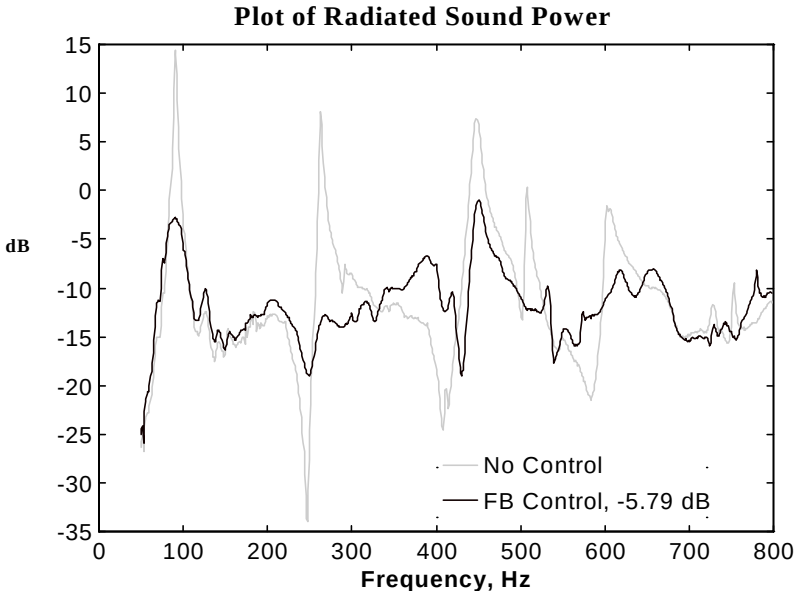

Figure 6.9 Plot of Radiated Sound Power

Figure 6.9 is a plot of the radiated sound power. The gray line is without control and the black line is with control. Total reduction in radiated sound power is 5.79 dB. Figure 6.9 was obtained using Eq. (6.12)[46].

$$W(\omega_i) = v(\omega_i)^H R(\omega_i) v(\omega_i) \tag{6.12}$$

Where

$$R(\omega_i) = \frac{\omega_i^2 \rho \; S^2}{4\pi \; c} \begin{bmatrix} 1 & \frac{\sin(k_i r_{12})}{k_i r_{12}} & \cdots & \frac{\sin(k_i r_{1N})}{k_i r_{1N}} \\ \frac{\sin(k_i r_{21})}{k_i r_{21}} & 1 & \cdots & \vdots \\ \vdots & \cdots & \ddots & \vdots \\ \frac{\sin(k_i r_{N1})}{k_i r_{N1}} & \cdots & \cdots & 1 \end{bmatrix}$$

Here, $W(\omega_i)$ is the power radiated at frequency i, ρ is the density of the medium, S is the area of the elemental radiator, $k_i = \omega_i/c$ where c is the speed of sound in the medium, and r_{hj} is the distance from element h to element j. Equation (6.12) may be used to compute the radiated sound power at a given frequency i. N is the total number of elemental areas and the off-diagonal terms are due to the interactions of the individual radiators. Equation (6.12) was solved with $i = 1,2,3,\ldots 800$ and $N = 64$ to produce Fig. (6.9).

6.4.2 Adaptive Feedback Control

The controller performance plots shown thus far were for the non-adaptive case. The GPC control scheme may also be used in an adaptive controller to regulate plate vibrations. Equation (6.10) was applied to regulate the vibrations of the plate shown in Fig. 6.3. The results are shown in Figs. 6.10-6.13. In these figures, the four-channel block adaptive controller adapted to the conditional updating threshold, and then stopped adapting. The algorithm used blocks of 4000 data points from each of the four input and output channels. The bandwidth to be regulated was from 0 to 800 Hz and a sampling rate of 2.5 KHz was used. The control penalty was 0.0002. For all channels, the finite-difference order was 50, and the control and prediction horizons were also set to 50. The accelerometer outputs and control inputs were filtered by four pole low-pass filters set to 800 Hz. The plots shown in Figs. 6.10-6.13 are the autospectrum of the accelerometer signals obtained with a B&K analyzer. The B&K analyzer performed 50 averages and used a Hanning window with 50% overlap. The system update period was 115.73 seconds. Once every 115.73 seconds, a new block of 4000 points from each input and output was uploaded to a Pentium 166 MHz PC and used to update the control parameters if the data was found to contain a level of correlation which exceeded the set threshold. The adaptation threshold is determined by summing the elements of the matrix $_{y}V_{p}^{T}$ as described in Section 6.2. Several runs were made and a set value was determined by trial and error. The threshold value was set low enough to allow the OMP to be updated if sufficient information exist in the current block of input and output data. The threshold value must also be set high enough to prevent the OMP from drifting off if the current blocks of data do not contain sufficient information. The gray lines are open-loop and the black lines are closed-loop.

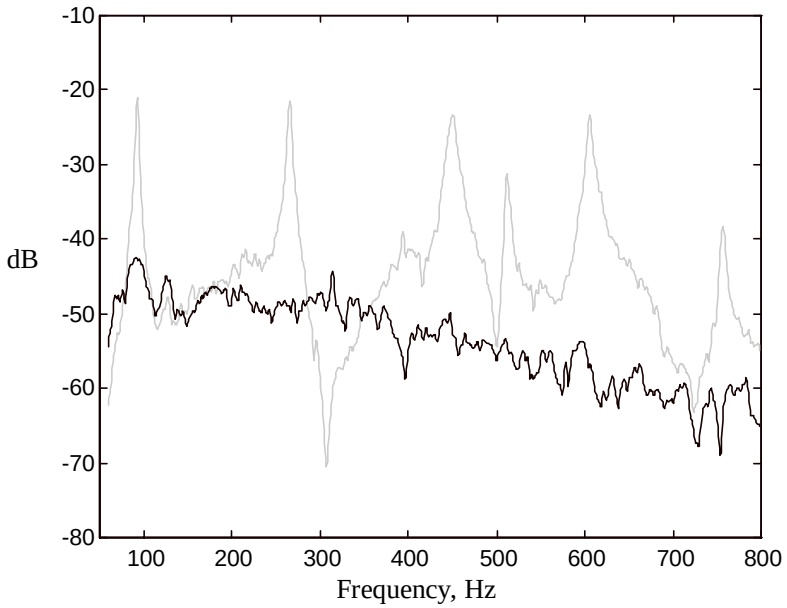

Figure 6.10 Plate Acceleration at Point #1 in dB

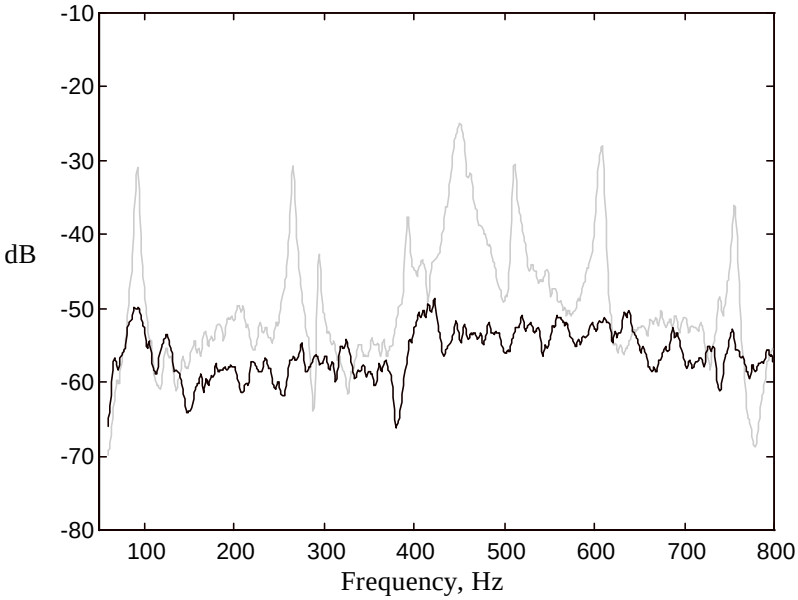

Figure 6.11 Plate Acceleration at Point #2 in dB

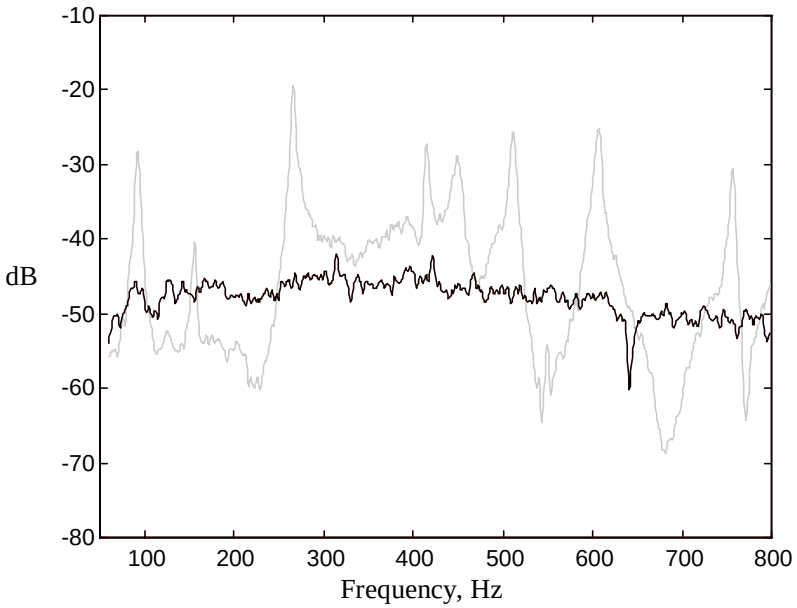

Figure 6.12 Plate Acceleration at Point #3 in dB

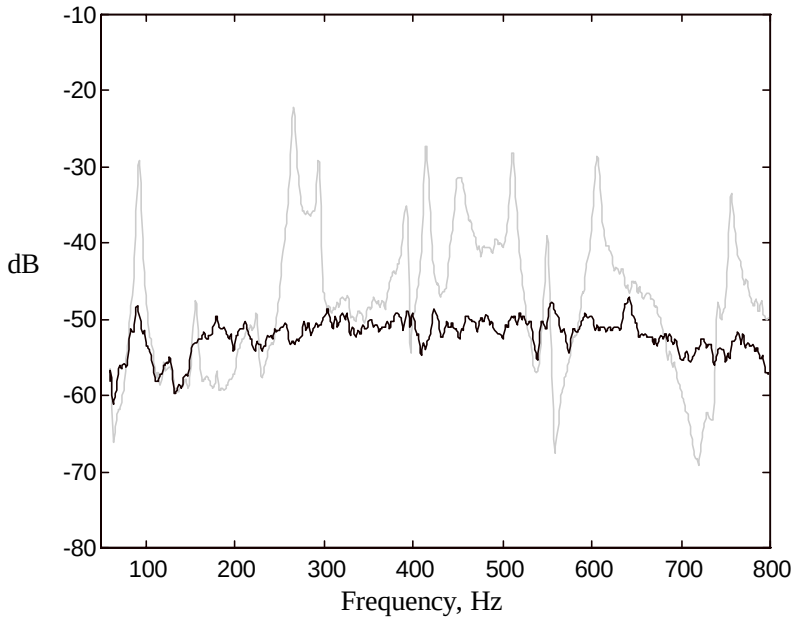

Figure 6.13 Plate Acceleration at Point #4 in dB

As can be seen in Figs. 6.10-6.13, the adaptive feedback controller performed slightly better than the non-adaptive controller. This occurred because in the adaptive case, the

controller was allowed to fine tune itself to the system to be regulated[2]. This is to say that the OMP are adjusted to yield the maximum level of regulation for the given system model order, horizons, and control penalty. The plant to be regulated in this case is time-invariant. The total reductions are summarized in Table 6.4.

Table 6.4 Total Reductions, 4 Channel Adaptive Controller

	Total Reduction in Accelerometer Energy
Accelerometer Number	dB
1	14.85
2	15.22
3	10.77
4	13.08

The figures shown thus far present the autospectrum of the open- and closed-loop accelerometer signals. However, the controller performance may also be demonstrated by plotting the magnitude of the Bode plot[16] of the closed-loop system. Here, the input of the system is the disturbance input and the output is the accelerometer signal. Figures 6.14-6.17 show the magnitude of the Bode plot for the four channel adaptive controller presented earlier. In these figures, the gray line is open-loop and the black line is closed-loop.

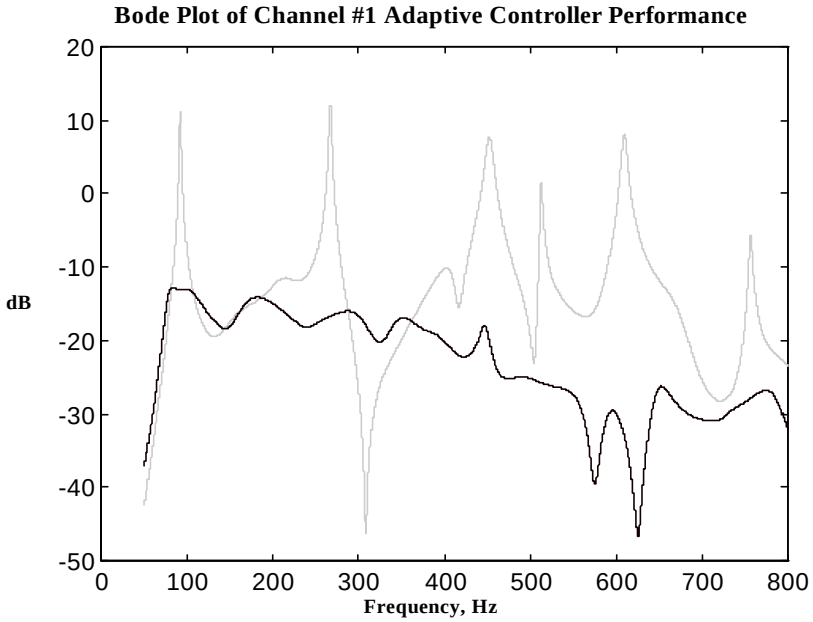

Figure 6.14 Bode Plot of Channel #1 Performance

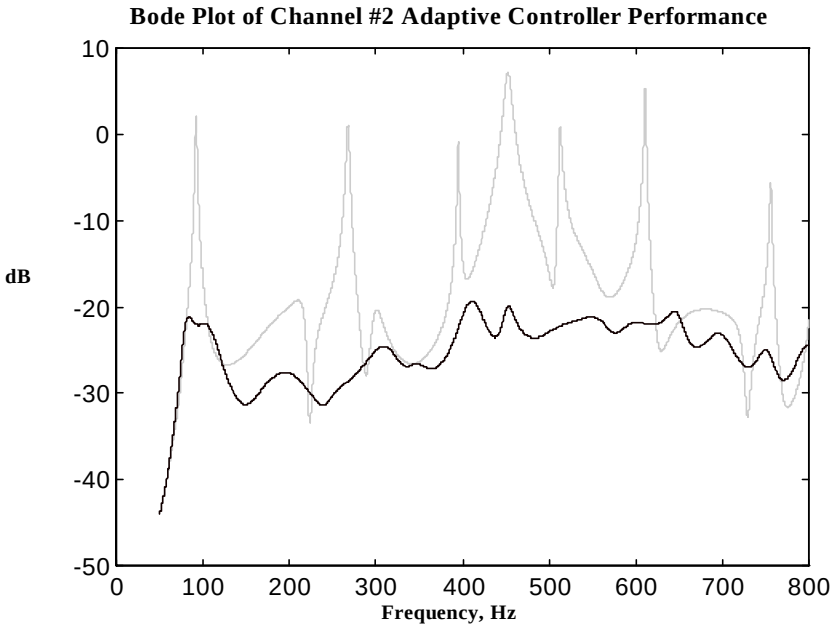

Figure 6.15 Bode Plot of Channel #2 Performance

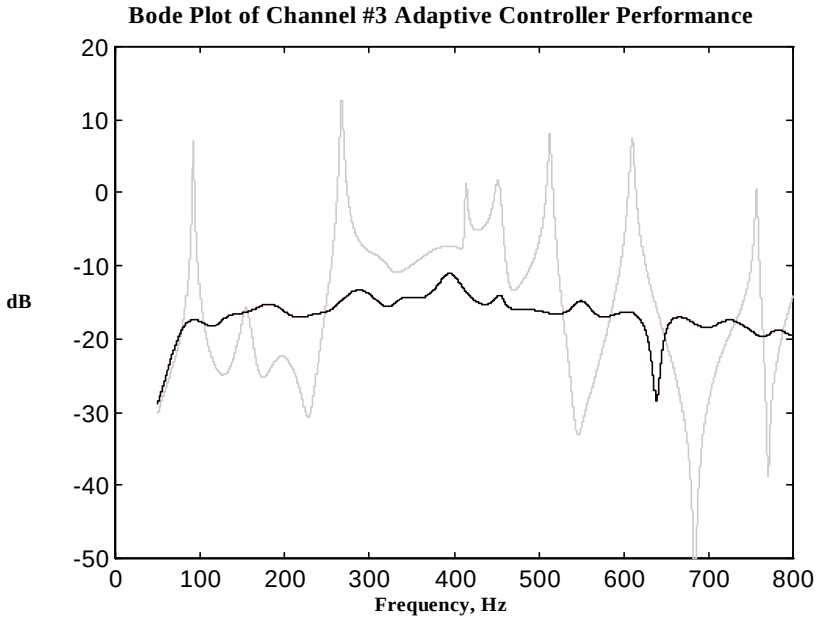

Figure 6.16 Bode Plot of Channel #3 Performance

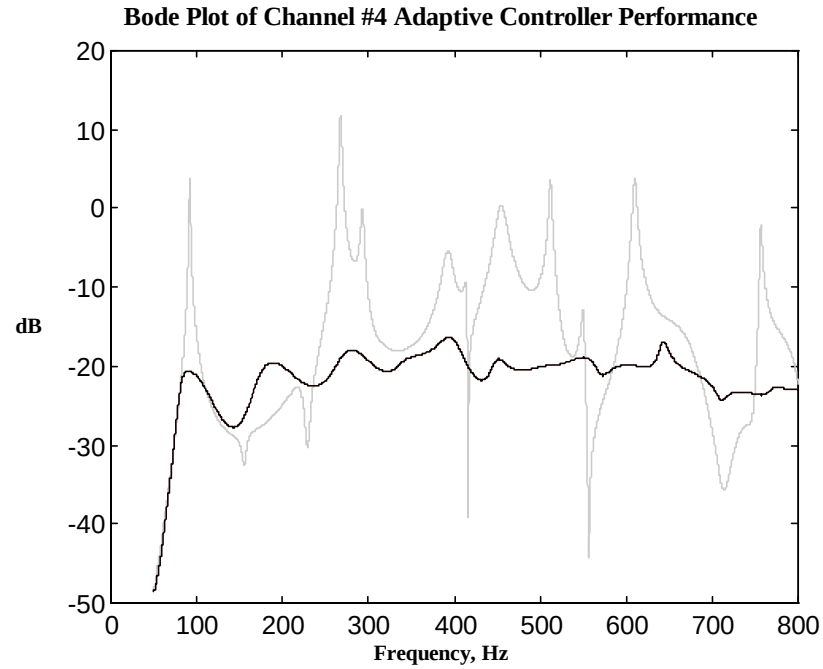

Figure 6.17 Bode Plot of Channel #4 Performance

The question naturally arises if it is necessary to have four channels to regulate the plate vibrations, or how well can the controller regulate if only one channel is used. It is

of interest to compare the performance of the four channel controller to that of a single channel controller. In the single channel controller implementation, only piezo #1 is used as a control actuator and accelerometer #1 is used as a sensor for feedback control. The other three accelerometers are used for performance evaluation only and are not used in the feedback control loop and therefore do not factor into the cost function, i.e. are not penalized. In this case piezos 2 through 4 are not used. The plots of the single channel controller are shown in Figs. 6.18-6.21. All settings for the single channel controller are the same as those of the four-channel controller shown in Figs. 6.10-6.13. Since there are far fewer parameters to update and identify in the Single-Input Single-Output (SISO) case, the controller had an update period of 6.32 seconds. Once every 6.32 seconds, a new block of 4000 points for the input and output was uploaded to the PC and used to update the control parameters if the data was found to contain a level of correlation which exceeded the set threshold. Shown below are the plots for all four accelerometer signals even though only the first channel is being used for control and therefore the only channel being directly regulated.

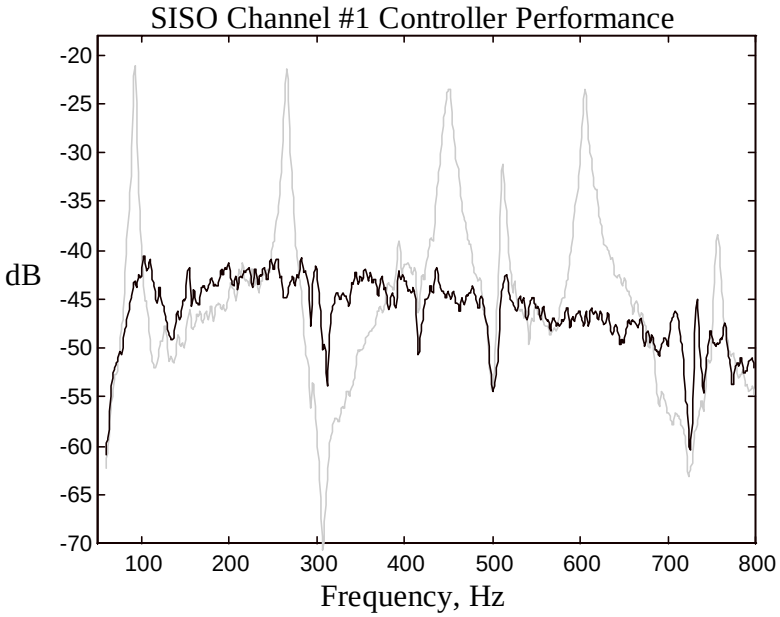

Figure 6.18 Acceleration at Point #1 in dB, Channel #1 Regulated

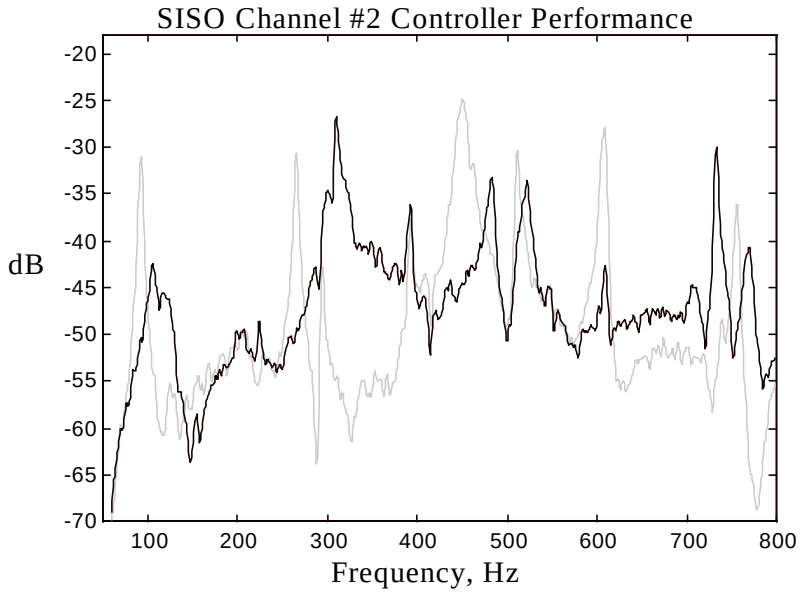

Figure 6.19 Acceleration at Point #2 in dB. Channel #1 Regulated

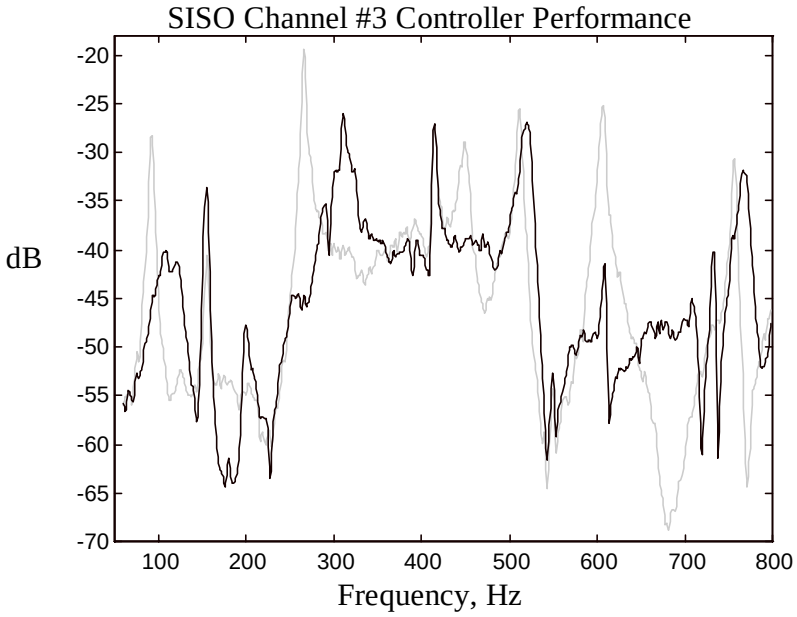

Figure 6.20 Acceleration at Point #3 in dB. Channel #1 Regulated

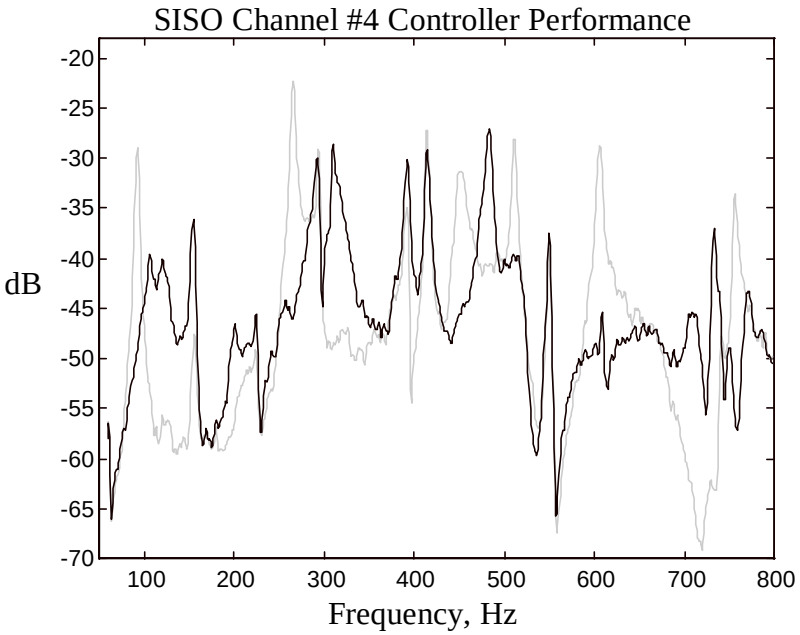

Figure 6.21 Acceleration at Point #4 in dB. Channel #1 Regulated

Table 6.5 summaries the results shown in Figs. 6.18-21.

Table 6.5 Total Reductions, Channel 1 Feedback Only

	Total Reduction in Accelerometer Energy
Accelerometer Number	dB
1	9.30
2 (no feedback)	2.09
3 (no feedback)	2.04
4 (no feedback)	1.86

Examining the above figures indicates that a large loss in plate vibration regulation is observed. This is due to the fact that some of the plate modes are neither observable nor controllable[38]. If a single actuator is to be used, it should be optimally placed to regulate the modes of interest. The optimal placement of sensors and actuators is an area of ongoing research. The plots shown in Figs. 6.18-6.21 are the autospectrum of

the accelerometer signals. The Bode plot for channel one is shown in Fig. 6.22 using the same controller as described by Figs. 6.18-6.21. Here, only channel one is regulated so it is the only channel shown. Compared with Fig. 6.14 we see that the regulation is not quite as good. This is because only one sensor and one actuator are used rather than four of each. In the SISO case we have reduced control authority due to fewer actuators and reduced system information to provide to the controller due to having only one sensor. Alternatively, if all four sensors were used as feedback sensors and only one actuator was used then the one actuator would try to minimize the overall variance of the four sensor signals. The ability to provide regulation of four sensor signals using only one actuator is limited by the fact that there will be modes which are observable but not controllable.

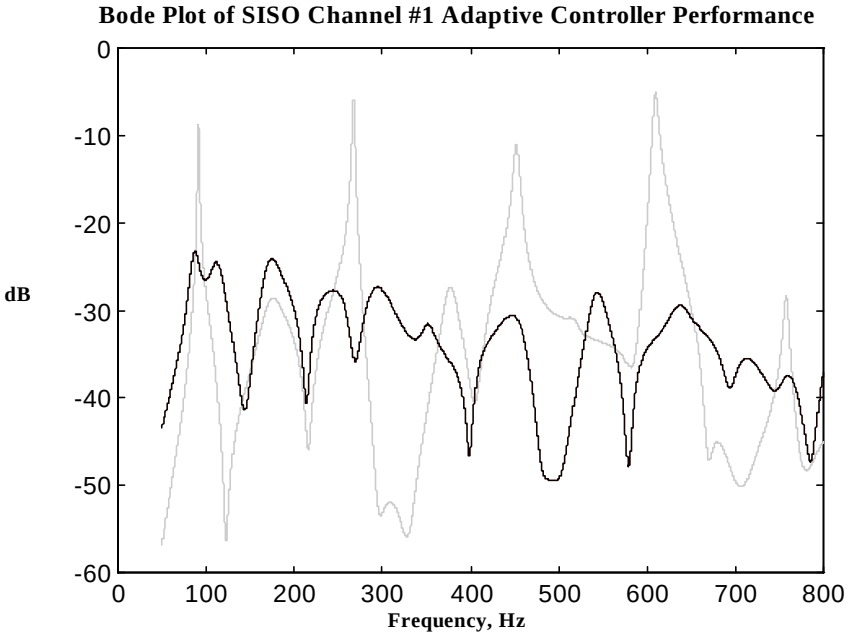

Figure 6.22 Bode Plot of Channel #1 Adaptive Controller Performance

The figures shown so far are for an 800 Hz bandwidth. However, the bandwidth may be increased as long as the hardware can support it. Shown in Fig. 6.23 is a SISO implementation of a 200^{th} order controller for channel one. Both the control horizon and the prediction horizon were set to the finite-difference order. The bandwidth here is 4 KHz. The accelerometer signal and the control effort were both filtered with four-pole

low-pass filters set to 4 KHz. The control penalty was set to 0.003 and a 10 KHz sampling rate was used. The adaptive controller updated the controller parameters every 2.3 min if the input and output data contained a sufficient level of correlation. The data block length was 8000 points. The reason for limiting the bandwidth to 4 KHz is due to the fact that the speaker which produced the disturbance did not respond to frequencies above 4 KHz, making it impossible to excite the plate at frequencies above 4KHz. As can be seen in Fig 6.23, the controller failed to regulate the 90 Hz mode. The problem here is one of system identification. Since the sample rate had to be set to 10 KHz to avoid aliasing, the number of OMP was too small to identify the 90 Hz mode at this fast sampling rate[6]. A total reduction of 6.04 dB was obtained.

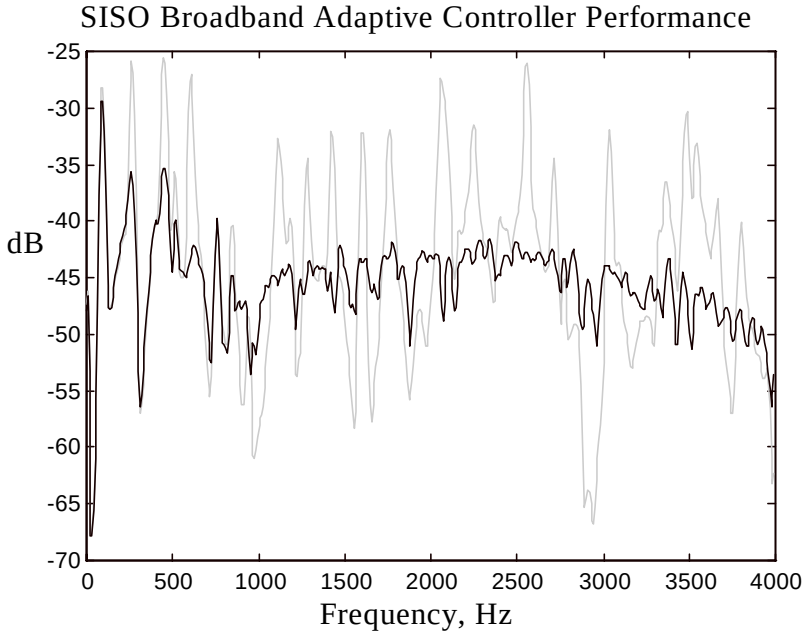

Figure 6.23 Broadband Acceleration at Point #1 in dB

6.4.3 Feedback/Feedforward Adaptive Control

The figures shown thus far were produced using feedback control only. However, if a coherent reference of the disturbance is obtainable, feedforward may be added to the feedback controller to enhance performance. In order to incorporate a feedforward path in the controller design, the feedforward path must be identified. This was accomplished by

measuring the disturbance signal driving the speaker of Fig. 6.2 and using this signal to estimate the ARMAX parameters as described in Chapter 4. For the experiments presented in this chapter, the disturbance single driving the speaker was used both to ID the disturbance path and as a reference for feedback/feedforward control. This resulted in an adaptive controller which updated both the control and feedforward paths based on blocks of disturbance input, control input, and output data. Figure 6.24 shows the performance of the feedback/feedforward block adaptive controller. In Fig. 6.24, the disturbance consists of band-limited white noise with a single tone disturbance added to the plate resonance at 460 Hz. The system was allowed to adapt by uploading a block of 4000 points from the input and output to the Pentium 166 MHz PC. The data was used to update the control parameters if the data was found to contain a level of correlation which exceeded the set threshold.

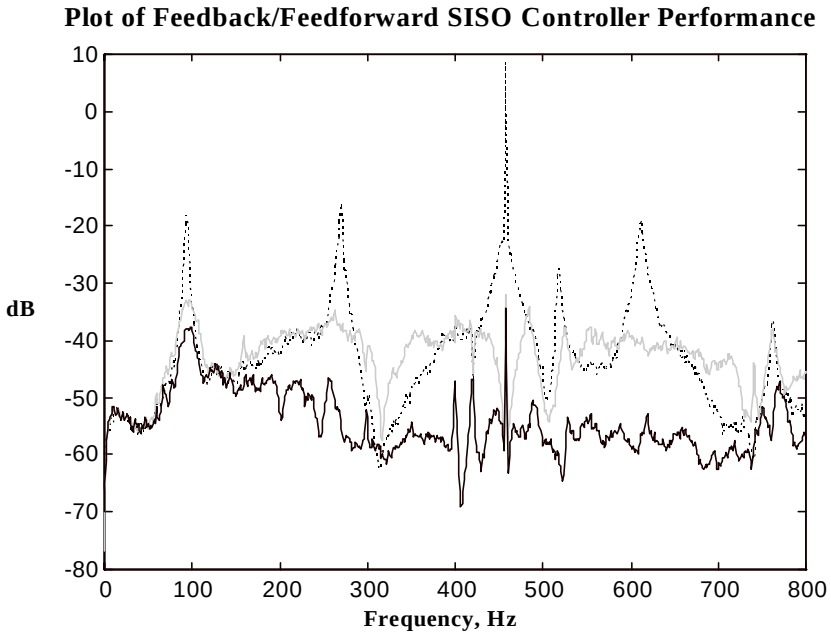

Figure 6.24 Feedback/feedforward SISO Controller Performance

In Fig. 6.24, the dotted line is open-loop, gray line is feedback only (22.11 dB reduction), and the black line is feedback/feedforward (31.46 dB reduction). The finite-difference

order was 50 with prediction horizon and control horizon set to 50. The sample rate was 2.5 KHz with a control penalty of 0.002.

As described in chapter 4, the feedback/feedforward regulation at a single tone can be improved by the addition of an AR noise predictor. From Fig. 6.24, adding feedforward to the feedback controller did enhance broadband regulation, however only a few dB were taken off the 460 Hz tone. Figure 6.25 shows the enhancements obtained by adding a 6^{th} order AR noise predictor to the feedforward path. Although the controller is adaptive as in Fig. 6.24, the AR noise predictor was found off line and is fixed for this experiment. As can be seen, about a 5 dB gain in regulation at 460 Hz is obtained beyond that of using only feedback/feedforward.

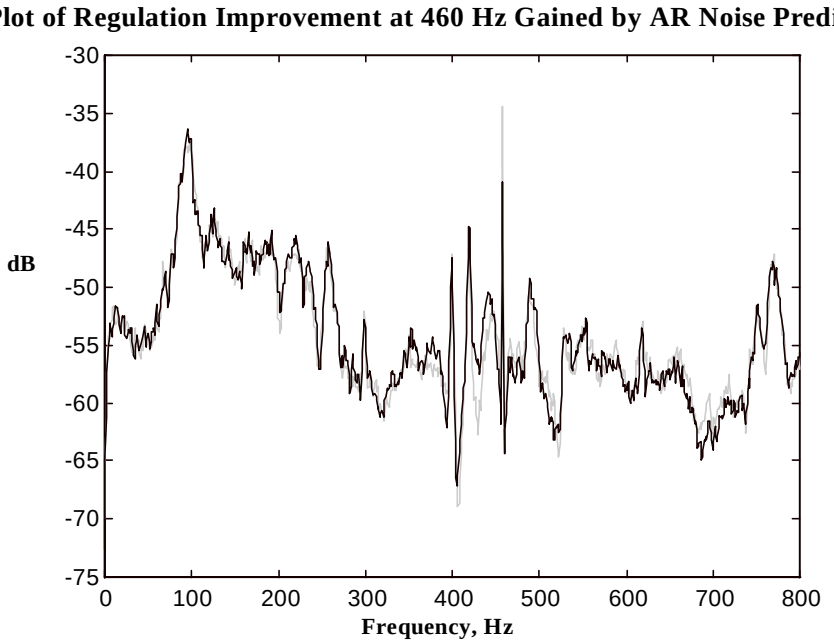

Figure 6.25 Improvement Using Noise Predictor

In Fig. 6.25 the tone disturbance was still not driven to the noise floor. The reduction in this plot is 0.06 dB. This may be attributed to a combination of uncertainties in the tone and plant model and lack of actuator authority. In addition, the AR noise predictor will predict future disturbance values based on past measured disturbance values. Since the

past disturbance values are a combination of broadband noise and the tone, it is not surprising that predicted future disturbance values are only approximate because they are based on a noisy reference.

The feedback/feedforward controller may also be used to regulate a tone only. In this case, a coherent reference of the broadband disturbance signal is unavailable, however a reference of the tonal disturbance signal is available. In this experiment, the feedback/feedforward controller is adaptive although the AR noise predictor is fixed. For this case, the harmonic disturbance only is used in the feedforward path. As can be seen in Fig. 6.26, an additional 5 dB is gained at 460 Hz by using feedforward with a 6^{th} order AR noise model.

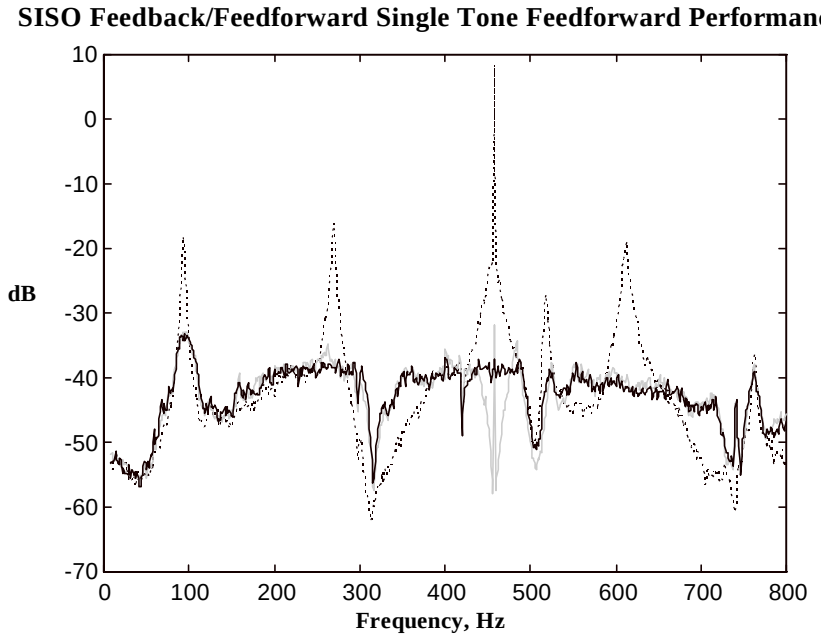

Figure 6.26 Single Tone Feedback/Feedforward With AR Noise Predictor

In Fig. 6.26 the tone was driven into the noise floor. This is because the feedforward reference signal used to predict future disturbance values at 460 Hz was pure, i.e., not contaminated with the broadband disturbance as in the reference single of Fig. 6.25.

The feedback/feedforward regulation plots shown so far were for broadband disturbances with a single tone at a plate resonance. The question naturally arises if the disturbance tone must be near a resonance frequency of the plate for the controller to reject it. As can be seen from the open-loop plot for channel one in Fig. 6.4, there is an anti-resonance at 320 Hz. To test the anti-resonance response, the disturbance was broadband with a 320 Hz tone added. The tone was increased in intensity until a significant part of the disturbance seen in the sensor was the 320 Hz tone. Here the controller is adaptive with a fixed 6^{th} order AR noise predictor and all other settings were the same as in Fig. 6.26. Figure 6.27 shows the open-loop response and the feedback/feedforward controller performance. The total reduction is 8.09 dB.

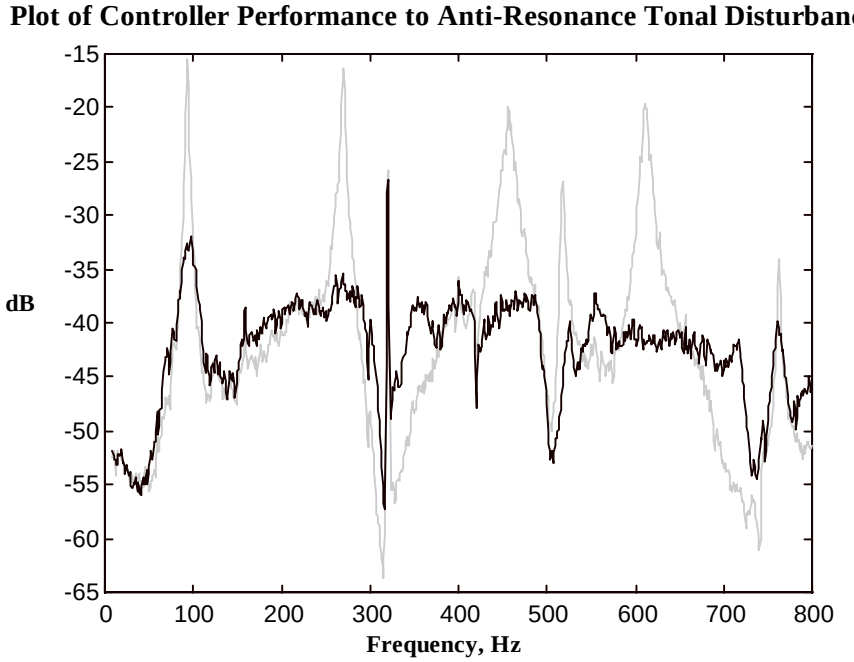

Figure 6.27 Feedback/Feedforward with Anti-resonance Tonal Disturbance

As can be seen in Fig. 6.27, the regulator failed to reject the 320 Hz tone even with feedforward and the AR noise predictor. The problem here is actuator authority coupled together with closed-loop instability. It is very difficult for the piezo to drive the plate at an anti-resonance due to the fact that there is a voltage limitation on the piezo. In order to increase the control effort being applied to the plate, the control penalty must be

reduced. This reduction in control penalty will eventually lead to instabilities due to non-linearities. Reducing the control penalty will drive up the voltage making the piezo non-linear. Also, the electronics providing the filtering and amplification will eventually clip the control signal once the maximum operating voltage is exceeded.

There are only a few places within the frequency range of interest where the controller lacks the authority needed to perform some regulation. Shown in Fig. 6.28 is the controller performance plot for an off-resonance tonal disturbance with broadband noise. The purpose of this plot is to demonstrate the regulators ability to reject off resonance tones which are not at an anti-resonance.

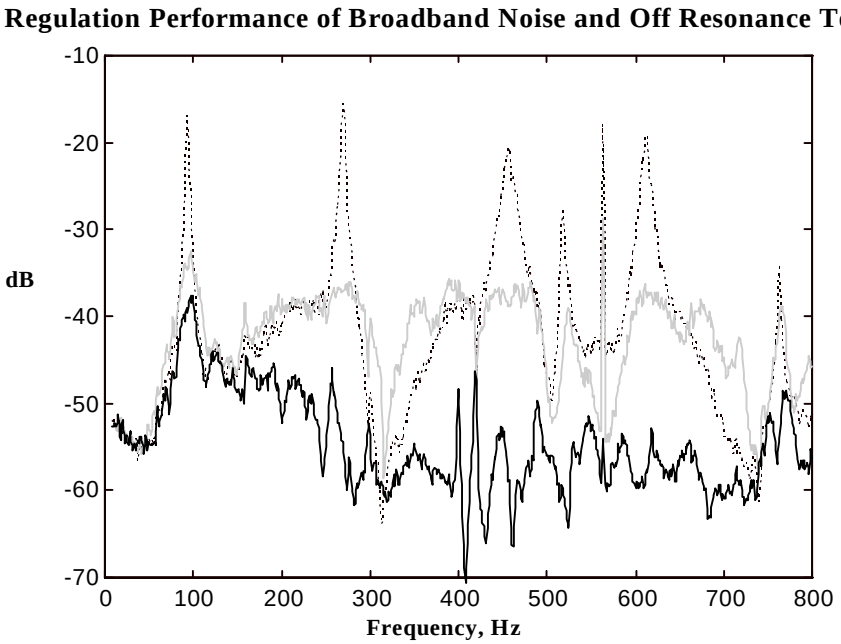

Figure 6.28 Feedback/Feedforward With Off Resonance Tonal Disturbance

Figure 6.28 shows the autospectrum of the accelerometer signal for open-loop (dotted line), feedback only (gray line, 8.41 dB reduction), and feedback/feedforward with AR noise model (black line, 18.57 dB reduction). The disturbance is broadband noise plus a single tone at 560 Hz. Both the broadband noise and the 560 Hz tone are used in the feedforward path. Both the feedback and the feedback/feedforward controllers here are

adaptive with a fixed AR noise predictor in the case of the latter. The blocks of input and output data were used to update the control parameters if there was a level of correlation which exceeded the threshold of adaptation. This threshold was determined by summing the elements of the matrix $_yV_p^T$ as described in Section 6.2. Several trails were made to determined a threshold value which provided both adequate OMP updates while avoiding drifting.

In some cases, the broadband disturbance is unavailable for feedforward, but the tone is available. The plot shown in Fig. 6.29 demonstrates the ability of the controller to cancel the off resonance tonal disturbance and the enhanced regulation gained by incorporating the AR noise model. Figure 6.29 shows the adaptive feedback/feedforward controller performance using single tone feedforward (gray line, 8.65 dB reduction), and single tone feedforward with fixed AR noise model (black line, 8.79 dB reduction). The open-loop is the dotted line. All settings are the same as those of Fig. 6.28.

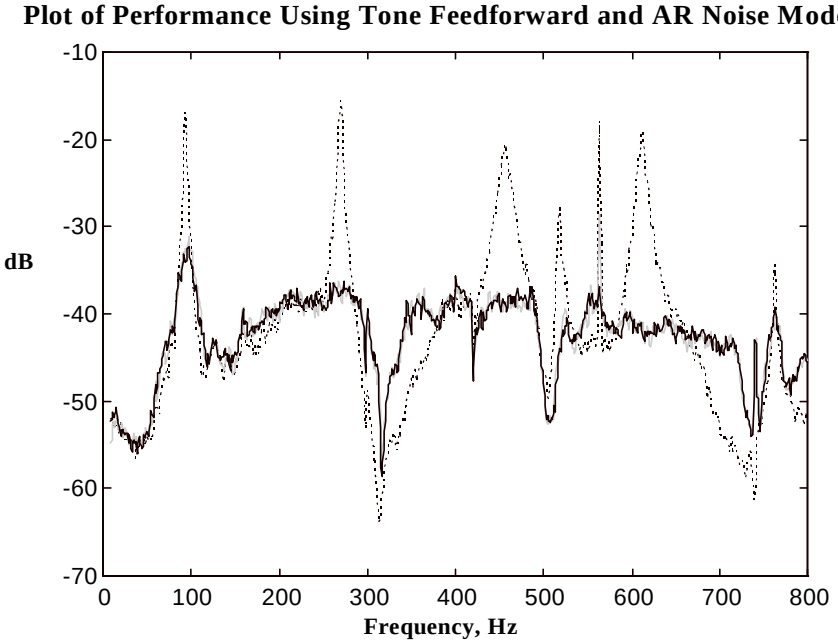

Figure 6.29 Feedback/Feedforward With Off Resonance Tone and AR Model

Single tone regulation may be obtained using the Multi-Input Multi-Output (MIMO) feedback controller. In addition, broad-band regulation may be improved by incorporating feedforward if the broad-band disturbance signal is available. The disturbance in the feedback case is band-limited white noise plus a single tone at 400 Hz. Shown in Figs. 6.30-6.33 are the plots of the accelerometer autospectrum. Three plots are shown for each of the four channels. The gray line is the open-loop response to the broad-band noise plus tonal disturbance, the dashed line is the regulation performance of the feedback controller with the disturbance being tonal plus broadband noise, and the black line is the feedback/feedforward controller regulation of broadband disturbance only. For both adaptive controllers, the finite-difference order was 50 and the prediction and control horizons were also 50. The sample rate was 2.5 KHz and the control penalty was 0.0005. Four pole filters set at 800 Hz were used to filter the accelerometer signals and the control efforts. The controllers were allowed to adapt until the data correlation fell below the set threshold of adaptation. For all plots, 50 averages were taken with a B&K analyzer. A Hanning window was used with an overlap of 50%.

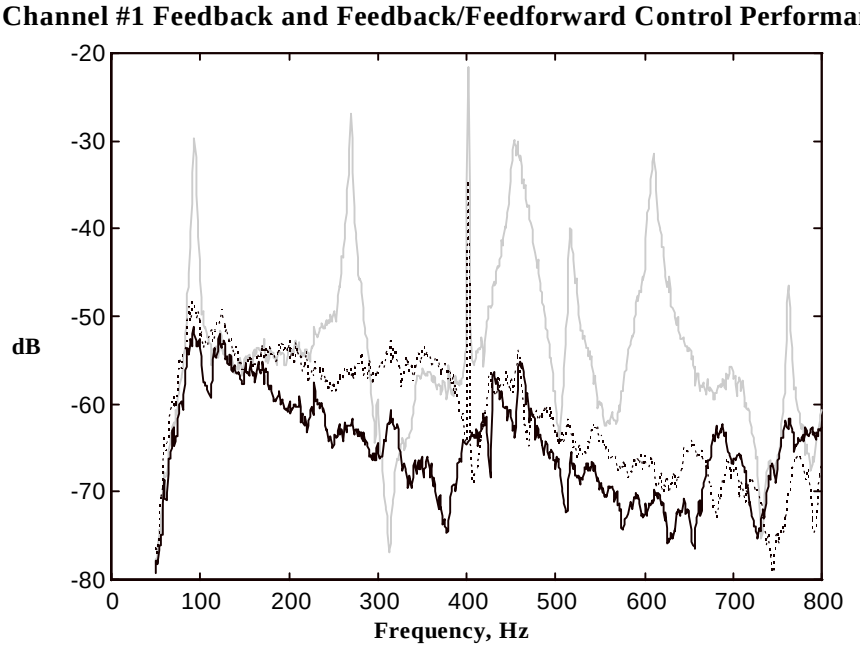

Figure 6.30 Channel #1 MIMO With Tonal Disturbance

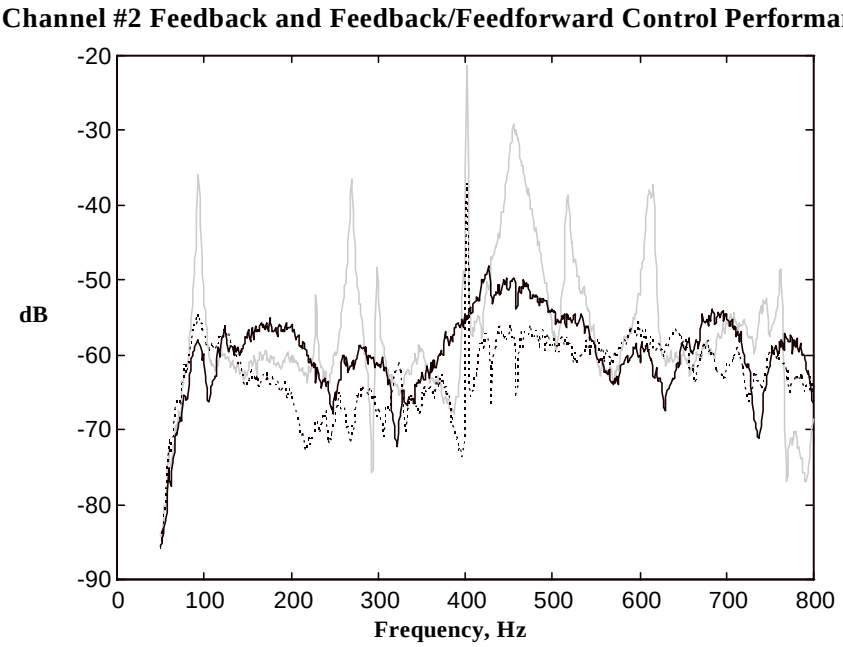

Figure 6.31 Channel #2 MIMO With Tonal Disturbance

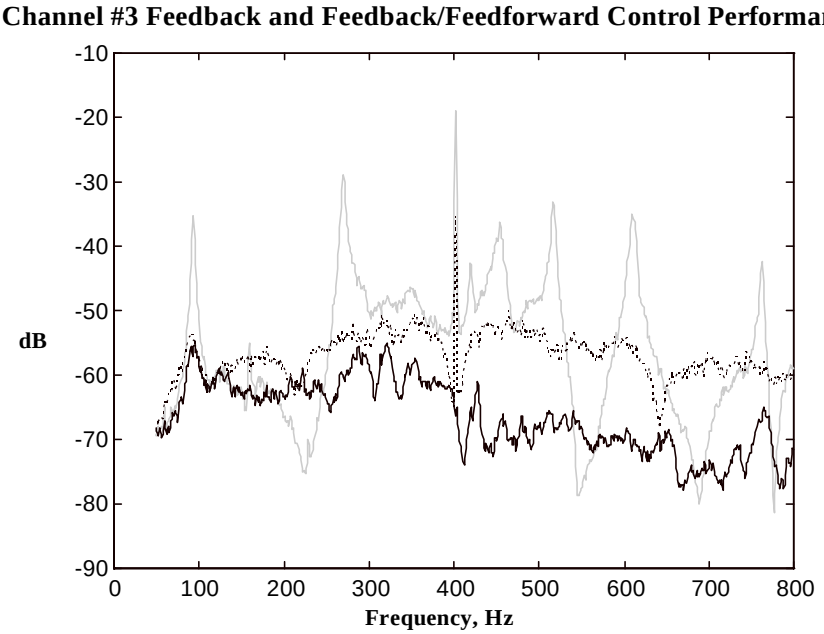

Figure 6.32 Channel #3 MIMO With Tonal Disturbance

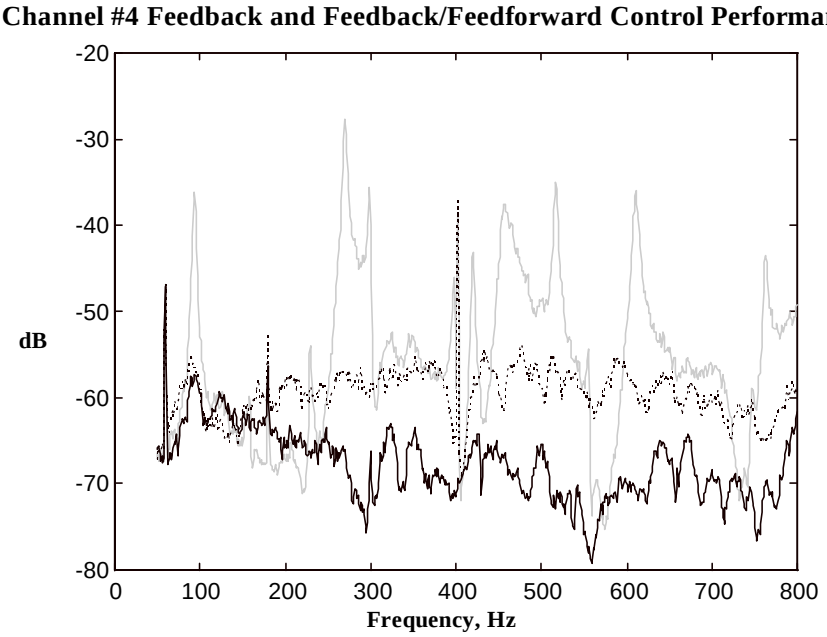

Figure 6.33 Channel #4 MIMO With Tonal Disturbance

To summarize the results shown in Figs. 6.30-6.33, Table 6.5 lists the total dB attenuation obtained by the controller for the case of feedback control of broadband disturbance plus the 400 Hz tone and the case of feedback/feedforward control of broadband noise only. The dB reduction is comparing the open-loop response to the closed-loop response. The values were obtained by averaging the accelerometer signal energy across the bandwidth for the open- and closed-loop cases and then taking the difference.

Table 6.6 Total Reductions, Feedback and Feedforward/Feedback Control

Channel Number	Total Reduction Using Feedback Control (Broadband Plus Tone) dB	Total Reduction Using Feedback/Feedforward Control (Broadband Disturbance Only) dB
1	13.6	17.6
2	16.3	11.5
3	12.8	17.3
4	12.4	19

6.4.4 Non-Collocated Adaptive Control

The plots shown so far are for physically collocated sensors and actuators. Collocation is not necessary for predictive feedback control to provide vibration regulation. For the experiments in this section, only feedback control will be investigated. Figure 6.34 illustrates a non-collocated setup of the piezos and accelerometers.

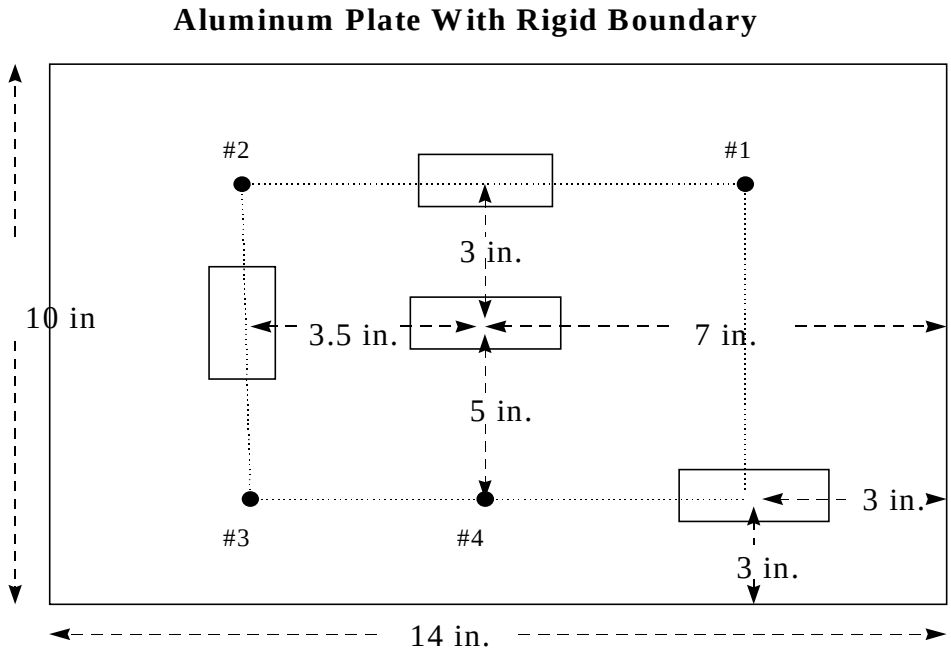

Figure 6.34 Diagram of Non-Collocated Sensors and Actuators

Shown in Figs. 6.35-6.38 are the autocorrelation of the accelerometer signals for channels one through four for the given arrangement shown in Fig. 6.34. In this adaptive control implementation, the finite-difference order was set to 50. Both the control and prediction horizons were also set to 50. The sampling rate was 2.5 KHz and a control penalty of 0.0005 was used. As usual for the block adaptive controller, blocks of input and output data were gathered by the DSP system and sent up to the host PC. If the data contained a sufficient amount of correlation, it was used to update the control parameters. If there was an insufficient level of correlation, no control update was performed. As can be seen in these figures, broadband regulation of plate vibrations may be obtained using predictive control with non-collocated sensors and actuators.

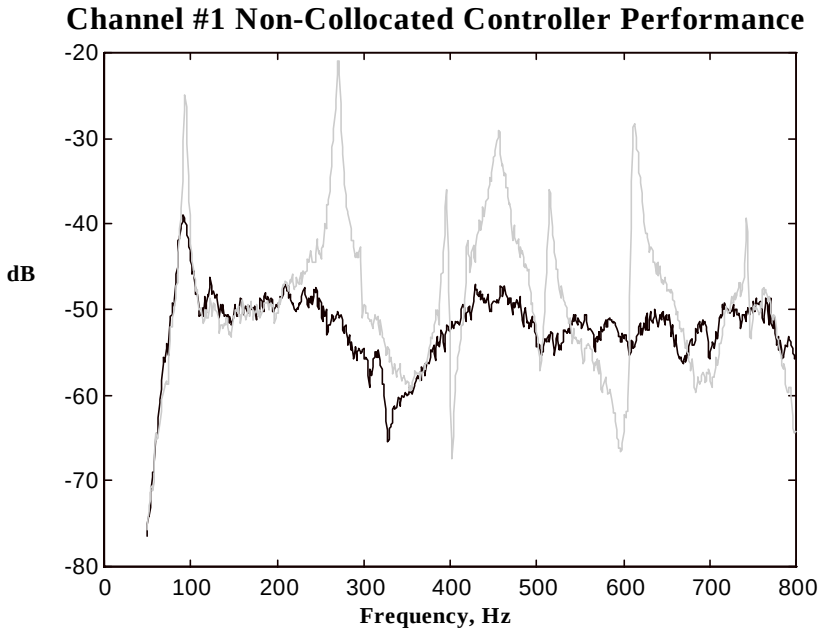

Figure 6.35 Channel #1 Feedback for Non-Collocated Sensors and Actuators

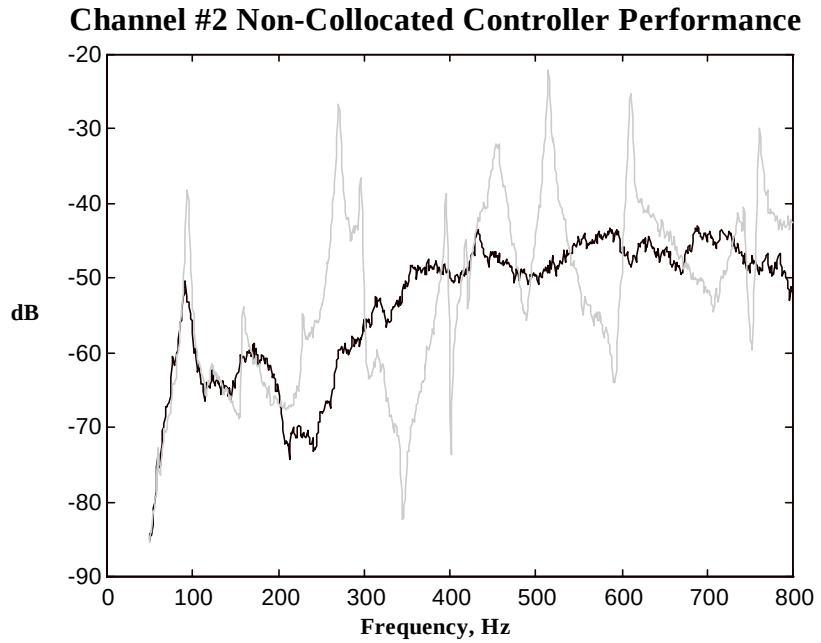

Figure 6.36 Channel #2 Feedback for Non-Collocated Sensors and Actuators

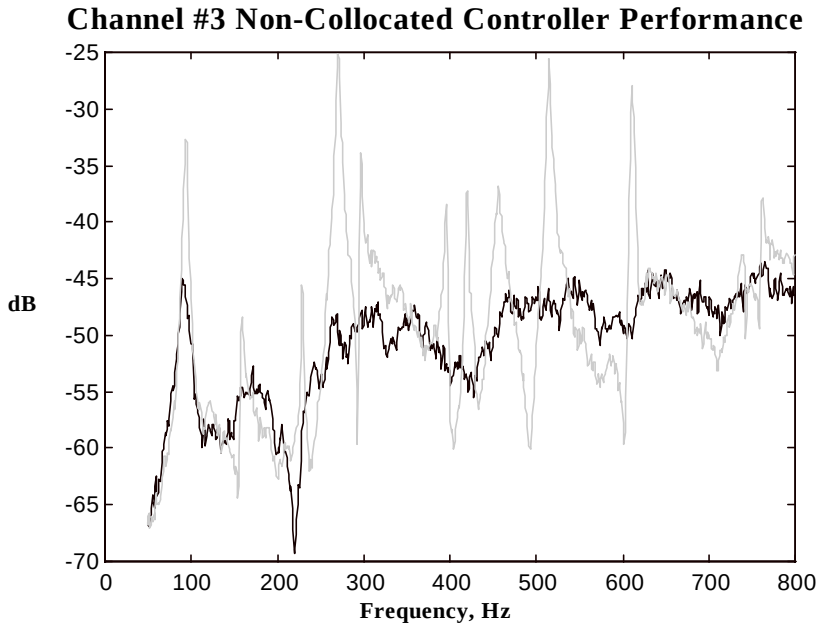

Figure 6.37 Channel #3 Feedback for Non-Collocated Sensors and Actuators

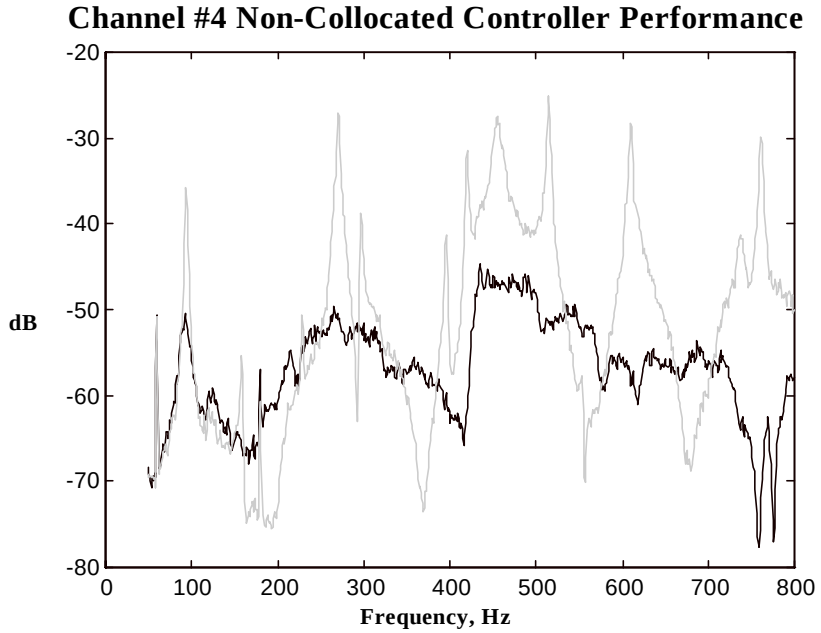

Figure 6.38 Channel #4 Feedback for Non-Collocated Sensors and Actuators

To summarize the results shown in Figs. 6.35-6.38, the total reduction in accelerometer signal energy is shown in Table 6.7 for each accelerometer.

Table 6.7 Total Reduction Using Non-Collocated Sensors and Actuators

Accelerometer Number	Total Reduction in Accelerometer Signal Energy dB
1	11.3
2	9.1
3	7.2
4	13.4

6.5 Experimental Results Using Time Varying Plate

The block adaptive controller may be used to regulate a time varying plate. In this experiment, the rectangular plate shown in Fig. 6.3 is mounted in a frame with a cavity behind it as shown in Fig. 6.39. The cavity is air tight and connected to a vacuum pump.

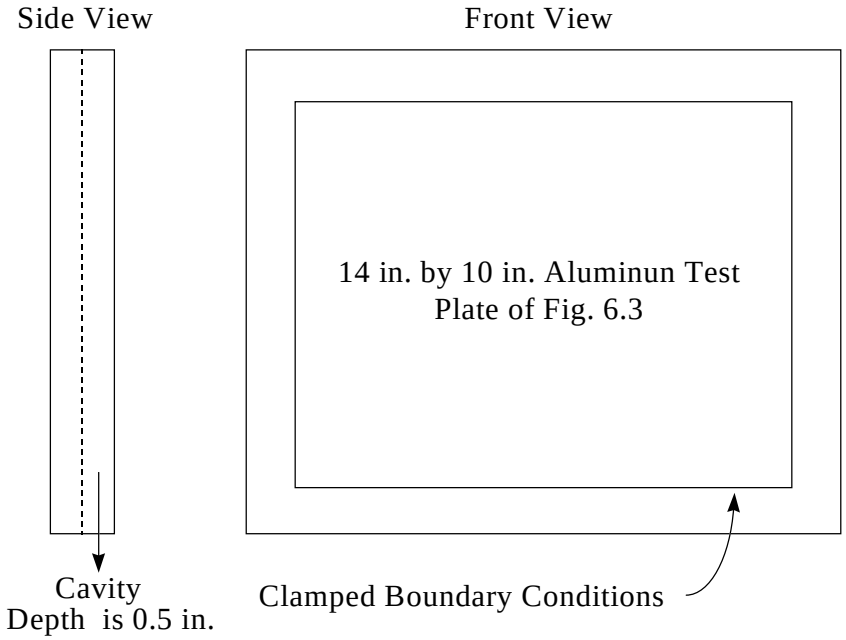

Figure 6.39 Test Plate With Time Varying Pressure Differential

The structure shown in Fig. 6.39 was placed before a large speaker which served as a disturbance source. The speaker was driven with white noise band-limited to 800 Hz. The noise from the speaker was used to excite the plate modes within this frequency range and the accelerometers shown in Fig. 6.3 were used as error sensors. Both piezos and accelerometers were arranged as shown in Fig. 6.3. At the beginning of the test, a vacuum pump was used to lower the pressure on one side of the plate relative to the other, causing a pressure differential between the plate sides. The vacuum was then slowly released while the controller was running. Sometimes the controller was able to track the changes in the plate and provide some regulation while remaining stable. At other times, however, the controller failed to remain stable. It is believed that the controller went unstable due to poor adaptation in the presence of closed loop data and the fact that there is no setting for the control penalty which will yield both a stable controller and a satisfactory level of regulation throughout the entire range of plant variation. It was found that the plant took approximately 25 to 30 minutes to go from full pressurization to around 0.01 of full pressurization.

An example of stable performance for the SISO controller is shown in Fig. 6.40-6.41 . Here, piezo #1 and accelerometer #1 are being used. The results shown where obtained using the block adaptive controller with conditional updating as described in Section 6.3. Several runs were performed before deciding where to set the threshold for conditional updating, the control penalty, and the horizons. A 30^{th} order system was used with a prediction horizon of 60 and a control horizon of 30. The control penalty was set to 0.01 and a 2.5 KHz sampling rate was used. The control and accelerometer signal was filtered with 3 pole filters set to 800 Hz. An additional four pole filter set to 800 Hz was used to filter the accelerometer signal which aided in stability. The block adaptive controller results shown in Fig. 6.40-6.41 used block lengths of 3000 and a forgetting factor of 0.97. When the controller was run, it was found to perform updates around every 2 seconds.

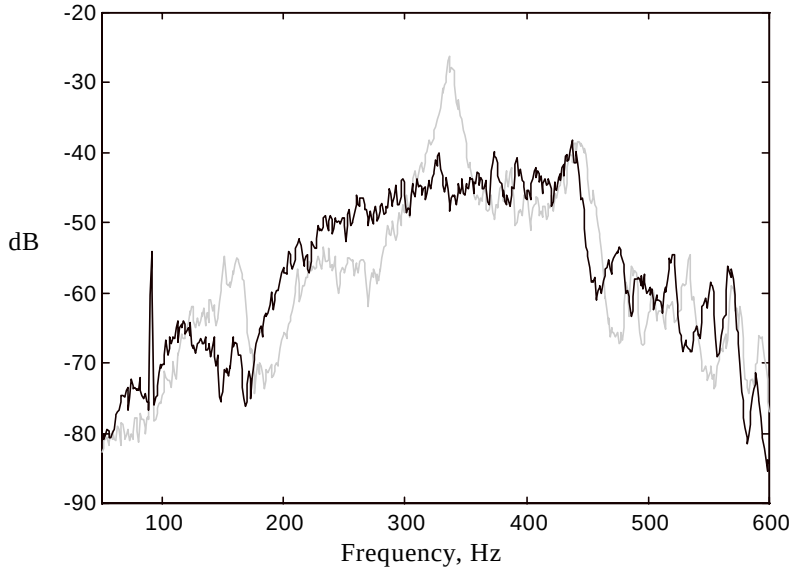

Figure 6.40 Controller With Large Pressure Differential (Starting)

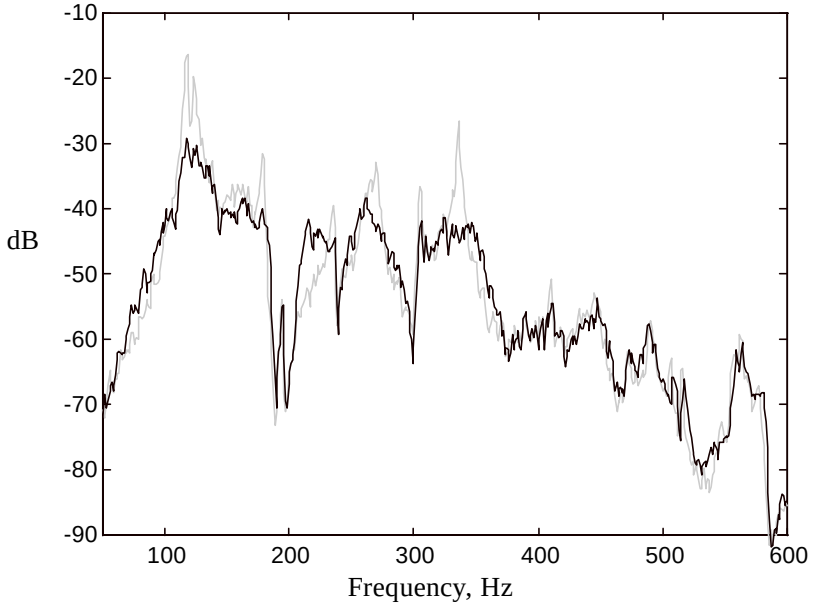

Figure 6.41 Controller With No Pressure Differential (Finishing)

Figures 6.40-6.41 show the beginning and end of the test. As can be seen, the controller was able to regulate the plate vibrations around these pressure levels. It should be noted, however, that the controller went unstable several times around the middle of the test.

Most of the time the controller was able to regain stability on its own and continue. There were, however, a few times when the controller had to be restarted. By properly adjusting the adaptation threshold and control penalty a stable controller was realized. However, it was found to have very poor regulation, i.e., only a few dB were taken off the top of the resonant peaks.

One of the main reasons for the instabilities of the block adaptive controller resulted from the inability to find a conditional updating threshold which provided both the ability to track changes in the plant and at the same time discard updates which would only cause the controller to drift off. It is not clear, and may not be possible, to chose a threshold which will cause both the controller to adjust to changes in the plant and at the same time not drift off in the presence of closed-loop data.

In order to remove the requirement of setting a conditional updating threshold, a small amount of dither was added to the control signal. The control voltage range was ± 10V and the dither level was ± 0.5V. In this control scheme, the system identification is updated every time a new block of input and output data is received. Here again, the controller is SISO using piezo and accelerometer pair #1. As can be seen in the autospectrum of the accelerometer signal plots shown in Fig. 6.42-6.46, the exclusion of conditional updating and the use of dither removed the instability problems encountered with the controller using conditional updating. For each of the plots shown in Fig. 6.42-6.46, the gray plot is without control and the black plot is with control. The open- and closed-loop plots do not represent exactly the same instance in time, and therefore they are not at the same pressure differential. The plots were, however, taken as close as possible to the same pressure differential.

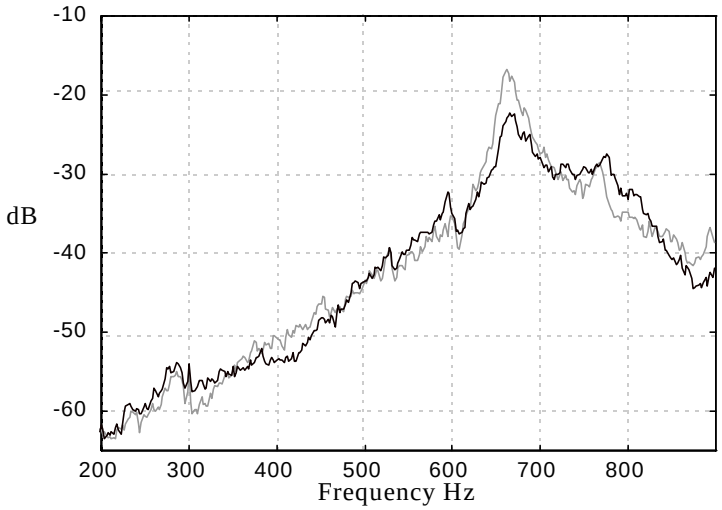

Figure 6.42 Plot # 1 Gray Open-loop, Black Closed-Loop

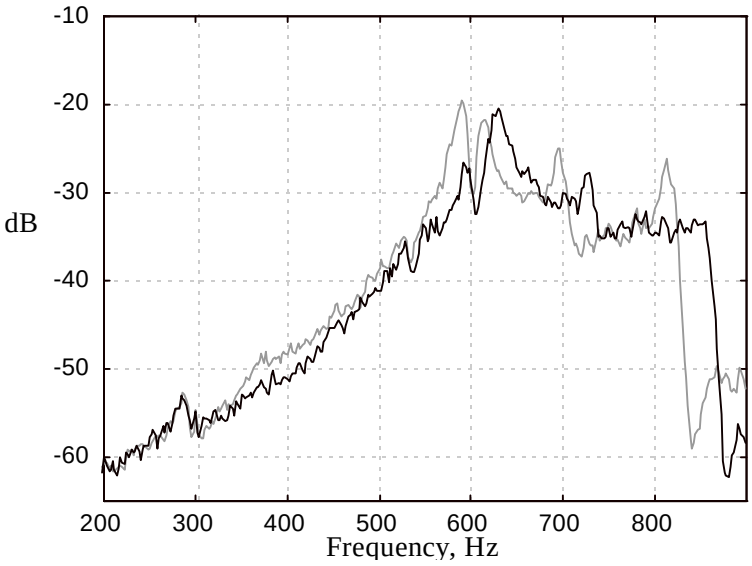

Figure 6.43 Plot # 2 Gray Open-loop, Black Closed-Loop

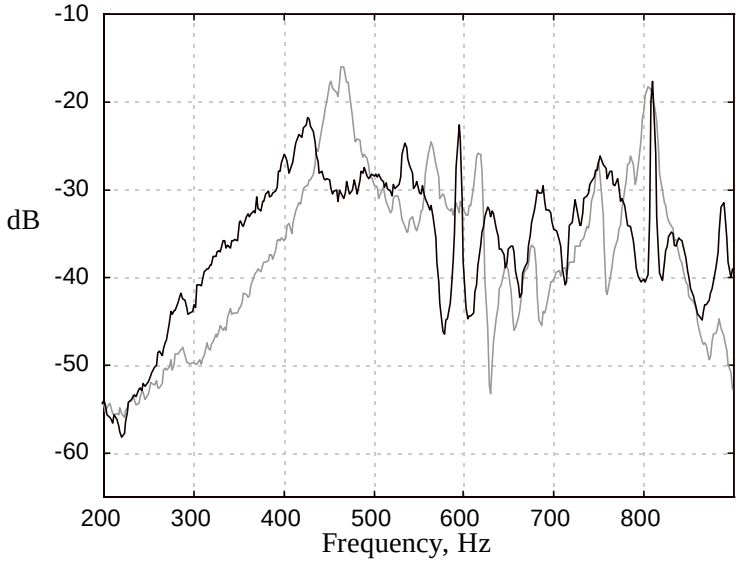

Figure 6.44 Plot # 3 Gray Open-loop, Black Closed-Loop

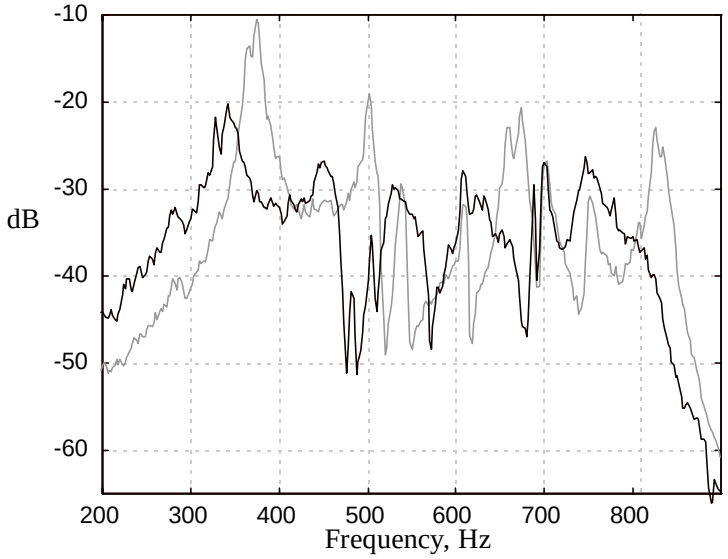

Figure 6.45 Plot # 4 Gray Open-loop, Black Closed-Loop

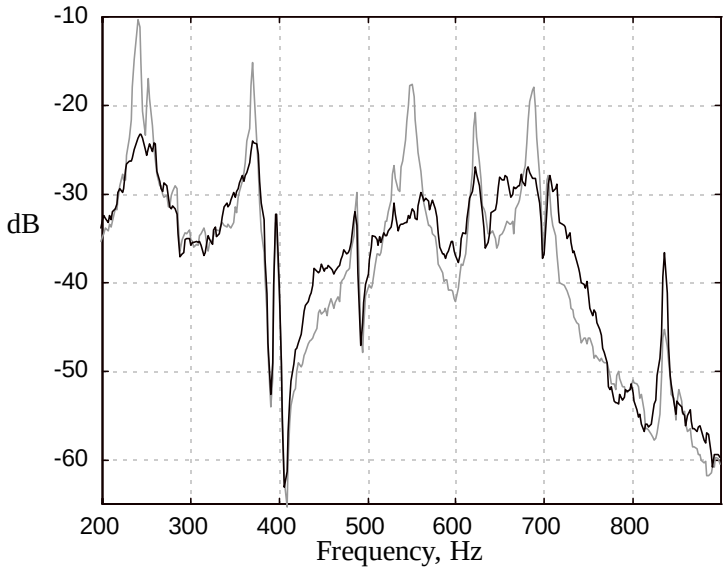

Figure 6.46 Plot # 5 Gray Open-loop, Black Closed-Loop

Figures 6.42-6.46 show five plots of the autospectrum of the accelerometer signal at five different times during the controllers test. The SISO controller was tested with piezo #1, the center piezo, as the control actuator and the accelerometer collocated. The block adaptive controller without conditional updating and with dither was used as the control scheme. GPC was used with the system order chosen as 50^{th}. The control horizon was set to 20 and the prediction horizon was set to 30. A control penalty of 0.05 was used throughout regulation and the sample rate was 2.5 KHz. Both the control signal and the accelerometer signal were filtered with 7 pole elliptic filters set at 800 Hz. Several tests were run before stable settings could be found.

The block adaptive controller with dither offers the ability to provide some regulation for a time varying plant. As can be seen by comparing plots 1 and 5 of Fig. 6.42-6.46, the plant changes dramatically from full pressure differential to none. Even though the system identification technique can track these changes in a closed-loop setting by the use of dither, the prediction horizon, control horizon, and control penalty remain fixed throughout the test. Because of this, they must be set to insure stability at all

times throughout the changes in the plant. For the test results shown in Fig 6.42-6.46, the prediction horizon and control horizon were first set and several different levels of pressure were applied to the plant. For each of these initial runs, a different control penalty was found which offered both a stable controller while providing the greatest level of disturbance rejection. After the initial runs, the largest control penalty of the group was chosen and used throughout the test. The result was a stable controller, however, the controller was found to provide poor regulation performance at times during the test. This can be attributed to the fact that the control penalty was set needlessly high for portions of the test in order to ensure stability in other portions. Table 6.4 below summarizes the results obtained from running the pressurized plate test. The plot numbers correspond to Fig. 6.42-6.46 shown above.

Table 6.8 Total Reductions Using Block Adaptive Controller and Dither

Pressure Differential $x10^3$ mm Hg	No Control (integrated spectra) dB	Control (integrated spectra) dB	Reduction dB
0.6553 (Plot # 1)	-9.4	-6.8	2.6
0.5572	-8.8	-8.0	0.8
0.4840 (Plot #2)	-7.0	-5.6	1.4
0.4363	-6.1	-4.4	1.7
0.3785	-7.2	-4.6	2.6
0.3503	-6.1	-3.1	3.0
0.3220 (Plot # 3)	-7.9	-2.6	5.3
0.2843	-7.3	-3.5	4.0
0.2440 (Plot # 4)	-6.6	-4.1	2.5
0.1574	-7.0	-5.0	2.0
0.09431	-6.8	-4.3	2.5
0.0008 (Plot # 5)	-8.2	-3.1	5.1

The results presented in Table 6.8 show that some regulation of a time varying plate may be obtained using the block adaptive controller with dither. However, in comparing these results with those presented earlier in this chapter it can be seen that the ability to regulate has been reduced due to the necessity of setting the control penalty too high in order to maintain a stable solution throughout the plants variations.

6.6 Conclusions

This section is a summary of the work presented in Chapter 6 and suggests possible applications of the control algorithms. Advantages and disadvantages of the block adaptive controller are identified.

6.6.1 Summary

This chapter presents an algorithm for block adaptive regulation of plate vibrations and demonstrates the performance of the block adaptive controller using a rectangular plate. The block adaptive controller has been shown to regulate plate vibrations over a large bandwidth in the presence of both band-limited white noise and tonal disturbances. Also, as seen in Fig. 6.9, by regulating the plate vibrations the block adaptive controller can be used regulate the acoustic radiation from a vibrating structure. The block adaptive controller consists of a fast batch least squares algorithm for system identification updates coupled with the Generalized Predictive Controller for control parameter calculations. This control scheme has been shown to provide vibration regulation for both single-input single-output systems and multi-input multi-output systems.

When applied to a time varying plate, the block adaptive controller with conditional updating failed to provide stable regulation. It is believed that this failure is due to two reasons. The first is the inability to set a conditional updating threshold which will allow for system updates and at the same time prevent drifting of the system identification in the presence of closed loop data. For the case of the time invariant plant, a threshold could be found which would allow for both. For the case of the time-varying plant, a single threshold could not be found which would hold true throughout the variations of the plant. The second reason for the inability of the block adaptive controller to provide a consistently stable and acceptable solution is the fact that a constant control penalty will not work well for all conditions of the plant tested. In order to produce a solution which will remain stable throughout the plant variations, the control penalty must be set to a value which will provide stability anywhere within the plant variation. This means choosing the largest value from among the control penalty values needed to provide stability throughout the plant variations. For these reasons, the conditional updating portion of the algorithm was abandoned in favor of adding dither to the control effort.

By adding a small amount of dither to the control signal, it was found that the controller could track changes in the plant and provide some regulation. The level of regulation was limited by the fact that the largest control penalty must be chosen to provide stability throughout the dynamic range of the plant. However, the addition of dither did eliminate the problem of the system identification drifting off.

6.6.2 Suggested Applications

The block adaptive controller with conditional updating was found to be unable to regulate a time varying plant. However, as shown in Section 6.4 this controller proved to be a consistently stable regulator for a time-invariant plant. The advantage of using this adaptive technique rather than the non-adaptive controller may be seen by comparing Figs. 6.4-6.7 with Figs. 6.10-6.13. As can be seen, the adaptive controller was able to tune itself to produce superior regulation due to its ability to fine tune itself. In addition, even though the block adaptive controller with conditional updating can not regulate a time varying plant, it was found that regulation of a time invariant plant with a time varying disturbance was possible as long as the authority of the actuator was not exceeded. This fact was established by varying the frequency of a tonal disturbance and observing the adaptive controller update its control parameters to incorporate the new internal noise model. Once the updating was complete, the correlation of the input and output data fell below the conditional updating threshold and the adaptation stopped until the disturbance spectrum varied again. In this manner a disturbance with a time varying spectrum could be regulated as long as the plant remained fixed, the actuator had sufficient authority, and the order of the system identification model was sufficiently large.

The regulation of time varying plants using the block adaptive controller calls for the use of dither rather than conditional updating. As shown in Section 6.5, this controller offers a stable control solution with some degree of regulation. Alternatively, it is believed that the multirate adaptive control techniques of Chapter 5 may provide regulation of a time varying plant. However, these techniques are still limited by the fact

that a fixed control penalty must be chosen and held throughout the variation of the plant which means that they are faced with the same limitation as the block adaptive controller with dither presented in Section 6.5. Alternatively, an additional sensor could be employed to measure some physical quantity such as pressure and this information used to adjust the control penalty accordingly. Also, the multirate adaptive controllers have a smaller possible bandwidth than the block adaptive controller due to the fact that the DSP system has the additional burden of performing the system identification.

Therefore, it is concluded that for broadband regulation of a modally-dense, time-invariant plant, the block adaptive controller with conditional updating be chosen. If the plant is time varying then the conditional updating is dropped and dither is used. Of the controllers examined in this thesis, the block adaptive controller offers the greatest possibility for MIMO broadband regulation using current microprocessor technology. This conclusion is based primarily on bandwidth considerations since the block adaptive controller places the smallest computational demand on the DSP hardware.

Appendix A

Application of Predictive Control Using Active Foam

Predictive control techniques have been shown to provide regulation of plate vibrations over a wide bandwidth using piezo actuators. However, regulation may be obtained using other forms of transducers. This appendix presents the results obtained when Generalized Predictive Controller (GPC)[11] was used to regulate the acoustic power radiating from a vibrating plate using active foam. All experiments presented in this appendix used adaptive control with conditional updating. Figure A.1 shows the plant to be regulated by active foam.

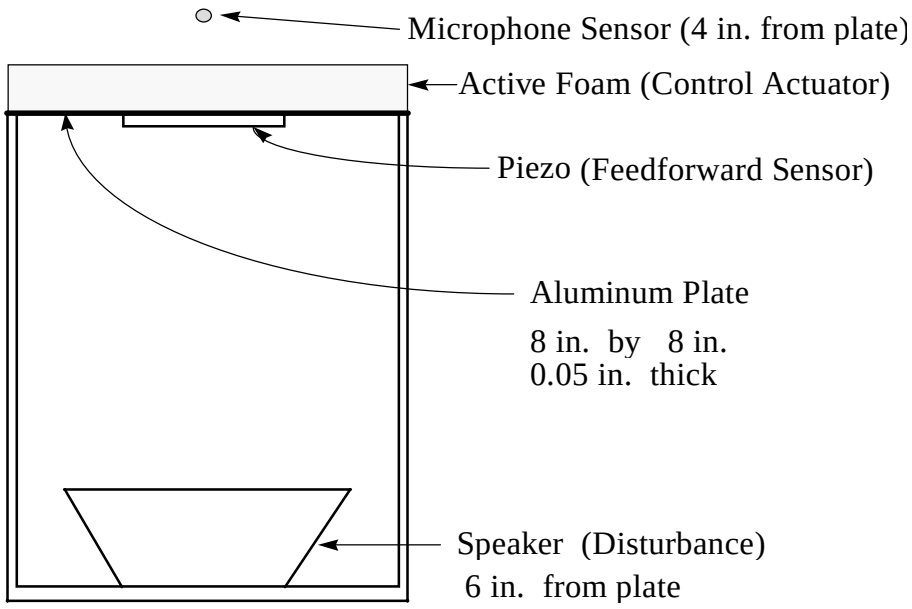

Figure A.1 Diagram of Plant to be Regulated by Active Foam

The plant shown in Fig. A.1 consist of a plexi-glass box with an aluminum plate at the top and a speaker at the bottom of the box as a disturbance source. The active foam covers the top of the box and serves to reduce the noise radiated by the vibrating plate both passively and actively. The piezo mounted on the bottom of the plate may be used as

a feedforward source to help regulate the plant. A microphone is mounted at the top of the structure as an error sensor for feedback control.

Two pieces of active foam were tried out. The first piece consisted of one active element located in the center of the foam. A diagram is shown in Fig. A.2.

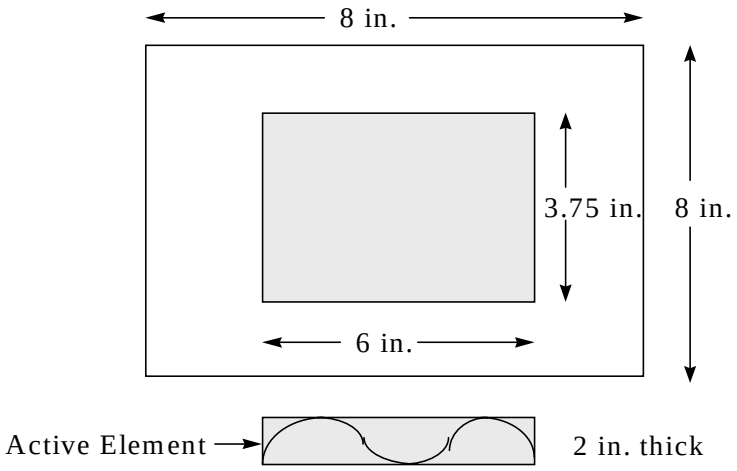

Figure A.2 Diagram of Active Foam #1

In Fig. A.2 the shaded area in the middle of the foam contains the active element. The remainder of the foam is only passive. Shown in the bottom of the figure is a side view of the active element which consists of regular foam with piezoelectric polymer PVDF (polyvinylidene fluoride) embedded in it and shaped similar to a sine wave. The foam is able to act as a passive absorber because the air molecules in the interstices of this porous material, (polyurethane foam), oscillate at the same frequency as the disturbance. This oscillation causes frictional losses. Also, the changes in flow direction and expansions and contractions of the flow throughout irregular pores result in a loss of momentum in the direction of wave propagation. Both of these phenomena result in the foam acting as a passive absorber. As an active device, the PVDF element driven by the control signal is constructed to behave in a linear sense. It is cylindrically curved to couple in-plane strain associated with piezoelectric effect with out-of-plane motion needed to radiate sound

from the foam surface. The result is a control actuator which adaptively modifies the acoustic impedance of the vibrating surface. The goal of the active foam is to modify the acoustic radiation impedance seen by the structure in order to yield a net decrease in the far-field sound power radiated by the vibrating surface. More information on active foam may be found in Ref. [48].

The second piece of active foam contains four active elements. These four elements are electrically connected to be driven together as one. A diagram of foam #2 is shown in fig. A.3.

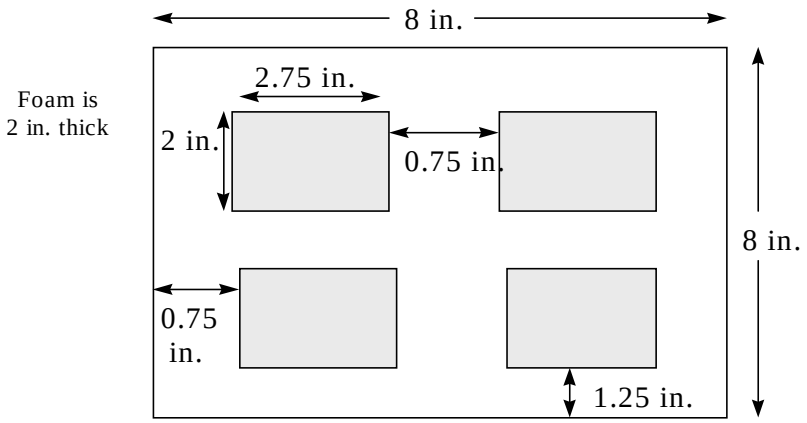

Figure A.3 Diagram of Active Foam #2

In Fig. A.3 the four active elements are surrounded by wooden supports separating the active foam elements from the passive foam. The four elements are connected in parallel so they all receive the same control signal. As in foam #1, the active material is sine wave shaped in all four active elements. Unfortunately, neither foam #1 nor #2 was found to be able to respond to frequencies below 500 Hz. Since the first plant mode is at 300 Hz, the disturbance was high pass filtered so as not to excite this mode. The second plant mode was found to be around 1 KHz, so the high pass filter was set to 800 Hz.

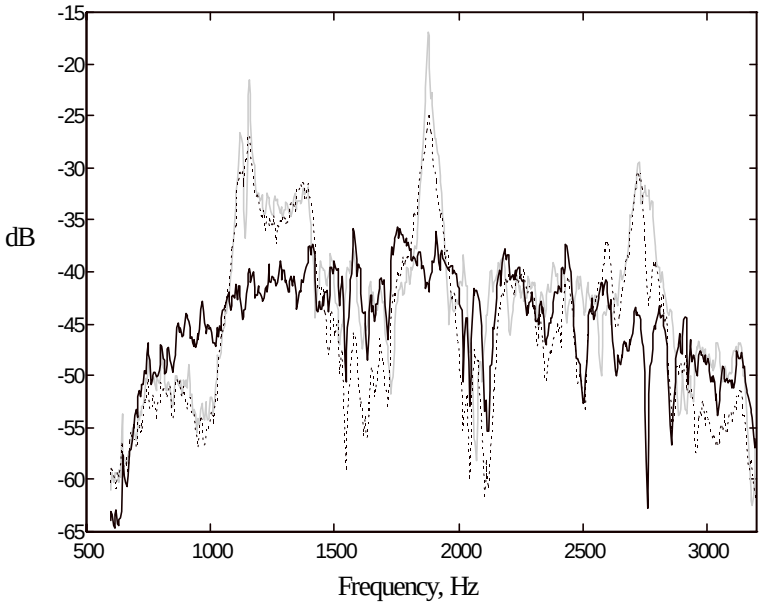

Figure A.4 GPC Feedback Using Foam #1

Figure A.4 is a plot of the autospectrum of the microphone signal using active foam #1 and feedback control. For the dotted line the foam was used as a passive attenuator and the solid black line is with the foam as a feedback actuator. GPC was used with a sampling rate of 10 KHz and control penalty of 0.00005. The system order was 30 and both prediction horizon and control horizon were set to 30. The control signal and microphone signal were low pass filtered by four pole filters set to 3.2 KHz. A high pass filter was set to 800 Hz and was used to filter the microphone signal and the disturbance. As can be seen in Fig. A.4, the addition of feedback control using the active foam as a control actuator greatly improved the ability of the foam to reduce the acoustic energy received by the microphone.

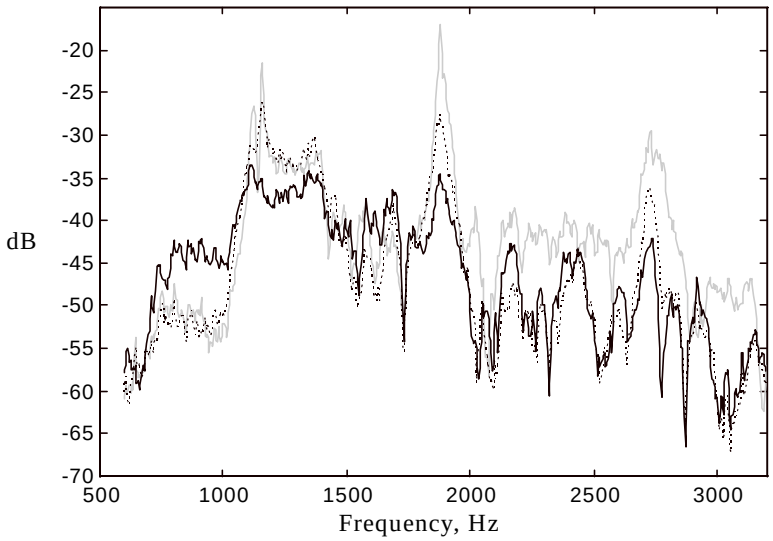

Figure A.5 GPC Feedback Using Foam #2

Figure A.5 shows the performance of foam #2. It is a plot of the autospectrum of the microphone signal using active foam and feedback control, black line, foam only as passive attenuator, dotted line, and without foam, gray line. GPC was used with a sampling rate of 10 KHz and control penalty of 0.00005. The system order was 30 and both prediction horizon and control horizon were set to 30. The control signal and microphone signal were low pass filtered by four pole filters set to 3.2 KHz. A high pass filter was set to 800 Hz and was used to filter the microphone signal and disturbance signal.

Figures A.4 and A.5 demonstrate that there is a large improvement in regulation when feedback control is used in conjunction with the active foam rather than using the foam as a passive atenuator only. Foam #1 was found to provide the best regulation as can be seen in by comparing Fig. A.4 with Fig. A.5. For this reason, foam #1 was chosen to be used in further testing.

If a coherent reference is available, feedforward may be added to the feedback controller to improve regulation this is shown in Fig. A.6.

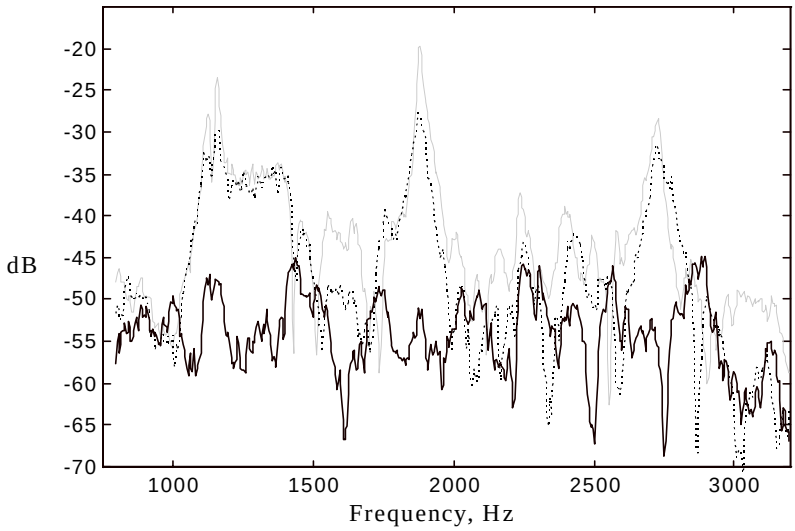

Figure A.6 Feedback/Feedforward Control Using Foam #1

Plot of autospectrum of microphone signal using active foam and feedback/feedforward control, black line, foam only as passive attenuator, doted line, and without foam, gray line. The feedforward signal was taken from the electrical signal driving the disturbance speaker. GPC was used with a sampling rate of 10 KHz and control penalty of 0.0001. The system order was 50 and both prediction horizon and control horizon were set to 50. The control signal and microphone signal were low pass filtered by four pole filters set to 3.2 KHz. A high pass filter was set to 800 Hz and was used to filter the microphone signal.

The feedforward signal for Fig. A.6 was the disturbance driving the speaker. In reality, such a signal is rarely obtainable for feedforward control. However, a feedforward signal may be obtained by placing a sensor on the plate and using it as a feedforward reference. The piezo shown in Fig. A.1 may be used to provide such a signal.

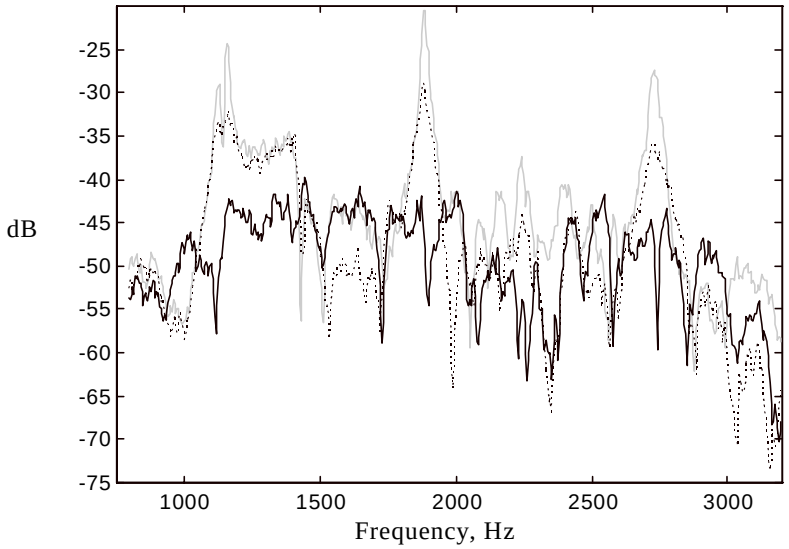

Figure A.7 Feedback/Feedforward Using an External Reference

Figure A.7 is a plot of the autospectrum of the microphone signal using active foam and feedback/feedforward control, black line, foam only as passive attenuator, dotted line, and without foam, gray line. The feedforward signal was taken from the piezo. GPC was used with a sampling rate of 10 KHz and control penalty of 0.002. The system order was 30 and both prediction horizon and control horizon were set to 30. The control signal and microphone signal were low pass filtered by four pole filters set to 3.2 KHz. A high pass filter was set to 800 Hz and was used to filter the microphone signal.

By comparing Fig. A.4 with Fig. A.6, an improvement in regulation using the piezo as a feedforward signal versus feedback only can be noticed. However, as seen by comparing Fig. A.6 with Fig. A.7, the best regulation is obtained by having access to the disturbance signal driving the speaker, even though this set up is not obtainable in most practical situations.

The experiments presented in this section demonstrate the use of feedback control for the regulation of broadband disturbances. The plots shown suggest that active noise control is achieved at the sensor location. However, global noise control is not

investigated. In order to evaluate the performance of the regulator as an active noise control method, an array of microphones is needed to plot the far field radiation. This was not done in these experiments due to the fact that the focus is on feedback control techniques.

Appendix B

Fast Computation of the Information Matrix

This appendix contains an outline for the fast computation of the information matrix. All material is taken from Ref. [8].

The entries of the correlation matrix R_{yu} may be computed recursively after determining the first *m* rows and the first *m* columns of the product $Y_p(k)U_p^T(k)$. Based on these first values, the remaining matrix entries may be found with very few additional computations. Consider the matrixes $Y_p(k)$ and $U_p^T(k)$ shown in Eq. (B.1).

$$Y_p(k)=\begin{bmatrix} y(k) & y(k+1) & \cdots & y(k+N-1) \\ y(k+1) & y(k+2) & \cdots & y(k+N) \\ \vdots & \vdots & \ddots & \vdots \\ y(k+p-1) & y(k+p) & \cdots & y(k+p+N-2) \end{bmatrix} \tag{B.1}$$

$$U_p^T(k)=\begin{bmatrix} u^T(k) & u^T(k+1) & \cdots & u^T(k+N-1) \\ u^T(k+1) & u^T(k+2) & \cdots & u^T(k+N) \\ \vdots & \vdots & \ddots & \vdots \\ u^T(k+p-1) & u^T(k+p) & \cdots & u^T(k+p+N-2) \end{bmatrix}$$

In Eq. (B.1), *u* is the system input and *y* is the output response to *u*. The symbol ^{T} is the matrix transpose. The matrixes of Eq. (B.1) may be used to determine the correlation matrixes R_{uu}, R_{yu}, and R_{yy}. The computation of R_{yu} will be considered, the others follow in like manner. The product $Y_p(k)U_p^T(k)$ is shown below in Eq. (B.2).

$$Y_p(k)U_p^T(k)=\begin{bmatrix} \sum_{\tau=k}^{k+N-1} y(\tau)u^T(\tau) & \sum_{\tau=k}^{k+N-1} y(\tau)u^T(\tau+1) & \sum_{\tau=k}^{k+N-1} y(\tau)u^T(\tau+2) & \cdots \\ \sum_{\tau=k+1}^{k+N} y(\tau)u^T(\tau-1) & \sum_{\tau=k+1}^{k+N} y(\tau)u^T(\tau) & \sum_{\tau=k+1}^{k+N} y(\tau)u^T(\tau+1) & \cdots \\ \sum_{\tau=k+2}^{k+N+1} y(\tau)u^T(\tau-2) & \sum_{\tau=k+2}^{k+N+1} y(\tau)u^T(\tau-1) & \sum_{\tau=k+2}^{k+N+1} y(\tau)u^T(\tau) & \cdots \\ \vdots & \vdots & \vdots & \ddots \end{bmatrix} \tag{B.2}$$

By examining Eq. (B.2), it is seen that all diagonal and subdiagonal *mxr* submatrices are basically the same except for the limits of summation. This motivates the following recursive relationship for the main diagonal *mxr* matrixes.

$$\sum_{\tau=k+i+1}^{k+N+i} y(\tau)u^T(\tau) = \sum_{\tau=k+i}^{k+N+i-1} y(\tau)u^T(\tau) + y(k+N+i)u^T(k+N+i) - y(k+i)u^T(k+i) \quad \text{(B.3)}$$

Equation (B.3) may be used to fill in the diagonal of the matrix R_{yu} once the first diagonal *mxr* matrix is found. The other *mxr* diagonal submatrices may be filled in based on the previous one until the diagonal is complete, i.e., for $i = 0,1,2,\ldots,p-1$. Likewise all subdiagonals may be found by a recursive relationship based on the first entry. The first upper off-diagonal submatrices may be found by Eq. (B.4) once the second mxr submatrix of the first row of *mxr* submatrices in R_{yu} is found.

$$\sum_{\tau=k+i+1}^{k+N+i} y(\tau)u^T(\tau+1) = \sum_{\tau=k+i}^{k+N+i-1} y(\tau)u^T(\tau+1) + y(k+N+i)u^T(k+N+i+1) - y(k+i)u^T(k+i+1) \quad \text{(B.4)}$$

for $i = 0,1,2,\ldots,p-2$.

Also, the second upper off-diagonal *mxr* submatrices may be found by Eq. (B.5).

$$\sum_{\tau=k+i+1}^{k+N+i} y(\tau)u^T(\tau+2) = \sum_{\tau=k+i}^{k+N+i-1} y(\tau+1)u^T(\tau+2) + y(k+N+i)u^T(k+N+i+2) - y(k+i)u^T(k+i+2) \quad \text{(B.5)}$$

for $i = 0,1,2,\ldots,p-3$.

From Eq. (B.4) and (B.5), it is seen that the remaining upper off-diagonals up to the (p-1) upper off-diagonal may be found in a similar fashion as soon as the first row of *mxr* submatrices are found. Equation (B.6) shows the recursive relationship for the first lower off-diagonal *mxr* submatrices.

$$\sum_{\tau=k+i+1}^{k+N+i} y(\tau)u^T(\tau+1) = \sum_{\tau=k+i}^{k+N+i-1} y(\tau)u^T(\tau+1) + y(k+N+i)u^T(k+N+i-1) - y(k+i)u^T(k+i-1) \quad \text{(B.6)}$$

for $i = 1,2,\ldots,p-1$.

The second lower off-diagonal *mxr* submatrices may be found recursively from Eq. (B.7).

$$\sum_{\tau=k+i+1}^{k+N+i} y(\tau)u^T(\tau-2) = \sum_{\tau=k+i}^{k+N+i-1} y(\tau)u^T(\tau-2) + y(k+N+i)u^T(k+N+i-2) - y(k+i)u^T(k+i-2) \quad \text{(B.7)}$$

for $i = 2,3,\ldots,p-1$.

The other lower off-diagonal submatrices follow in like manner. From this, we see that all lower off-diagonal *mxr* submatrices may be recursively obtained once the first column of *mxr* submatrices are found.

The computation of both $Y_p(k)Y_p^T(k)$ and $U_p(k)U_p^T(k)$ follow the above recursive procedure as well. It should be noted that both these matrices are symmetric, so only the upper or lower half need be done. More details on the efficient computation of the information matrix may be found in Ref. [8].

The system model may be written as shown in Eq. (B.8).

$$\alpha \; Y_p(k) = \beta \; U_p(k) \tag{B.8}$$

We may define correlation matrixes as shown in Eq. (B.9).

$$R_{yy} = \frac{1}{N} Y_p(k) Y_p{}'(k) \qquad R_{yu} = \frac{1}{N} Y_p(k) U_p{}'(k) \qquad R_{uu} = \frac{1}{N} U_p(k) U_p{}'(k) \tag{B.9}$$

Post multiplying Eq. (B.8) by $U_p(k)$ produces Eq. (B.10).

$$\alpha \; R_{yu} = \beta \; R_{uu} \tag{B.10}$$

Post multiplying Eq. (B.8) by $Y_p(k)$ produces Eq. (B.11).

$$\alpha \; R_{yy} = \beta \; R_{yu}{}' \tag{B.11}$$

Equations (B.10) and (B.11) may be combined into the matrix relationship shown in Eq. (B.12).

$$\begin{bmatrix} -\alpha & \beta \end{bmatrix} \begin{bmatrix} R_{yy} & R_{yu} \\ R_{yu}{}' & R_{uu} \end{bmatrix} = 0_{mx\{(p+1)(m+r)\}} \tag{B.12}$$

In compact notation, Eq. (B.12) becomes

$$\theta \; R = 0 \tag{B.13}$$

where

$$\theta = \begin{bmatrix} -\alpha & \beta \end{bmatrix} \qquad \text{and} \qquad R = \begin{bmatrix} R_{yy} & R_{yu} \\ R_{yu}{}' & R_{uu} \end{bmatrix}$$

In Eq. (B.13), R is a $\{(r+m)(p+1)x(r+m)(p+1)\}$ matrix known as the data correlation matrix. By extracting the first m rows of R, Eq. (B.13) may be rewritten as shown in Eq. (B.14).

$$\theta \; R\{(m+1):(r+m)(p+1),:\} - R\{1:m,:\} = 0 \tag{B.14}$$

where

$$\theta = \begin{bmatrix} -\alpha_1 & -\alpha_2 & \dots & -\alpha_p & \beta_0 & \beta_1 & \dots & \beta_p \end{bmatrix}$$

The OMP may be solved for as shown on Eq. (B.15).

$$\theta = R\{1{:}m,:\}\left[R\{(m+1){:}(r+m)(p+1),:\}\right]^{+} \tag{B.15}$$

In compact notation, Eq. (B.15) becomes

$$\theta = R_m \tilde{R}^{+}$$

where

$$R_m = R\{1{:}m,:\} \qquad \text{and} \qquad \tilde{R} = R\{(m+1){:}(r+m)(p+1),:\}$$

and $^{+}$ means the pseudo inverse. In order to make $\tilde{R}$ a square matrix, the first *m* columns may be deleted. Equation (B.15) involves fewer computations than does the solution given by Eq. (6.4). To see this, consider that it takes approximately $r^3(N-1)(2p+1)+p^2r^3$ multiplies and around the same number of adds to form R_{uu}. Likewise $rm^2(N-1)(2p+1)+p^2m^2r$ multiplies are needed to form R_{yu} and $m^3(N-1)(2p+1)+p^2m^3$ multiplies to form R_{yy}. A similar number of adds are needed for each. In addition, the matrix inversion requires approximately $(p+1)^3(r+m)^3$ multiplies and also $(p+1)^2(r+m)^2 m$ multiplies are needed to form the final matrix product. Adding these together, the approximate total number of multiplies required is given by $\{(N-1)(2p+1)+p^2\}\{r^3+m^3+m^2r\}+(p+1)^2(m+r)^2m+(p+1)^3(r+m)^3$. Here, there is no product between terms involving *N* and terms involving *p*. So then for large order systems and data blocks, the system identification technique presented in this section in more computationally efficient than the batch least squares described in Eq. (6.4).

Appendix C

Frequency Shaped Predictive Control

C.1 Control Derivation

In this appendix, a modification to Generalized Predictive Control (GPC) is presented which offers the ability to frequency shape the level of regulation. The adaptive case is not addressed here and the derivation and implementations are limited to SISO, although the extension to the MIMO case is straightforward.

Consider the derivation of GPC shown in section 3.2.1. The cost function may be written in vector form.

$$J = y^T y + u^T \lambda\, u \tag{C.1}$$

In Eq. (C.1), u is a vector of future control inputs and y is a vector of future plant outputs. It is desired to redefine the cost function in order to penalize the control effort as a function on frequency. This may be done by introducing a filtered control effort into the cost function. The control effort filter may be designed in the frequency domain to produce a large magnitude response in areas of the frequency spectrum were little control is desired while producing a small magnitude response in areas where the most regulation is desired. Consider the filtered control effort.

$$u_f(k) = N(z^{-1})u_f(k) + M(z^{-1})u(k) \tag{C.2}$$

Here, $u_f(k)$ is a filtered version of the control effort $u(k)$ and the polynomials $N(z^{-1})$ and $M(z^{-1})$ may be chosen to produce the desired controller performance. As in section 3.2.1, recall that $y = Gu + f$. Making this substitution and replacing u with u_f in the control penalty term we have that

$$J = (Gu + f)^T (Gu + f) + u_f^T \lambda\, u_f\ . \tag{C.3}$$

Equation (C.3) involves a vector of future control values u yet to be determined and future filtered control values u_f. The vector of future filtered control values may be written as the sum of past control values and past filtered control values plus future

control values just as *y* was written into past and future components. Doing this results in Eq. (C.4).

$$u_f = Hu + g \tag{C.4}$$

Here, u_f is the vector of future filtered controls, H is the pulse response of the control filter, and the vector g is a combination of past control inputs and past filtered control values. Substituting Eq. (C.4) into Eq. (C.3) one obtains Eq. (C.5).

$$J = (Gu + f)^T (Gu + f) + (Hu + g)^T \lambda\ (Hu + g) \tag{C.5}$$

Minimizing Eq. (C.5) with respect to u results in Eq. (C.6).

$$u = -(G^T G + H^T \lambda\ H)^+ (G^T f + H^+ \lambda\ g) \tag{C.6}$$

The control defined in Eq. (C.6) may be used to tailor the amount of regulation in the frequency domain based on the filter design of Eq. (C.2). This is one approach to shaping the level of regulation, however, other definitions of the cost function may be employed to produce similar results. One method may be to rewrite the cost function in terms of a filtered output y_f in place of y.

C.2 Experimental Results

The feedback control of Eq. (C.6) may be used to regulate parts of the frequency spectrum of the plant output while not regulating other parts. In this experiment, channel one of the plate described in Fig. 6.3 is the plant to be regulated. The control loop is described in Fig. 3.2 and the experimental setup in Fig. 6.2. The plate was excited with white noise band limited to 800 Hz. For all experiments described in this section, the control effort was first filtered by a 3 pole Butterworth with 3 dB cutoff frequency set to 754 Hz. The control effort was then further filtered by a 7 pole elliptic filter with cutoff frequency of 800 Hz. The accelerometer signal was filtered by a 4 pole Butterworth with a cutoff frequency of 800 Hz followed by a 3 pole Butterworth with cutoff frequency of 754 Hz. A sample rate of 2 KHz was used in all experiments. A single block of 20000 input samples and 20000 output samples was used to perform the system identification. No adaptation was used in these experiments. The samples were used to form the

information matrix as described in Appendix B. Based on the information matrix, the 100^{th} order OMP were determined for the single-input signal-output experiments performed in this section. In all experiments the GPC algorithm was used with both prediction and control horizons set to 200 and a control penalty of 0.001. The plots shown in this section were obtained with a B&K analyzer. For all plots, 100 averages were taken and a Hanning window with 50% overlap was used.

Shown in Fig. C.1 is the autospectrum of the accelerometer signal when no control weighting filter was used. The black line is closed-loop and the gray line is open-loop. As can be seen, all frequencies within the 800 Hz bandwidth were regulated.

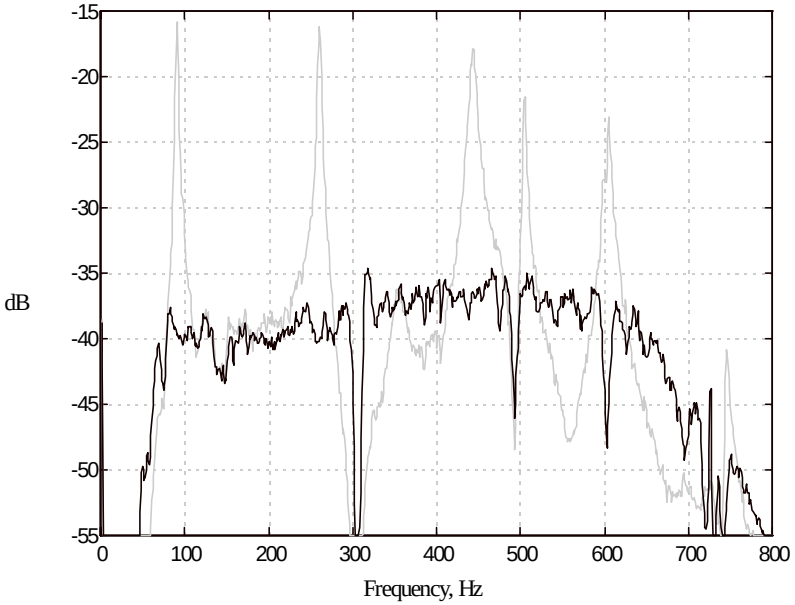

Figure C.1 Plot of acceleration with no control weighting filter

Figure C.2 is the plot of the accelerometer signal when the control weighting filter of Fig. C.4 was used as described in Eq. (C.6). The control weighting filter was designed in MATLAB using *yulewalker*. The black line is with control and the gray line is without control. In this implementation, the frequencies around the neighborhoods of 260 Hz and 505 Hz were regulated while little regulation was performed elsewhere. The black line of Fig. C.3 is a plot of the control effort which is applied to the piezo to perform regulation.

As can be seen, most of the control effort is concentrated around the frequencies of interest. The gray line is a plot of the control spectrum when no control weighting function is used. This control effort was used to obtain the results shown in Fig. C.1 and is presented here for comparison.

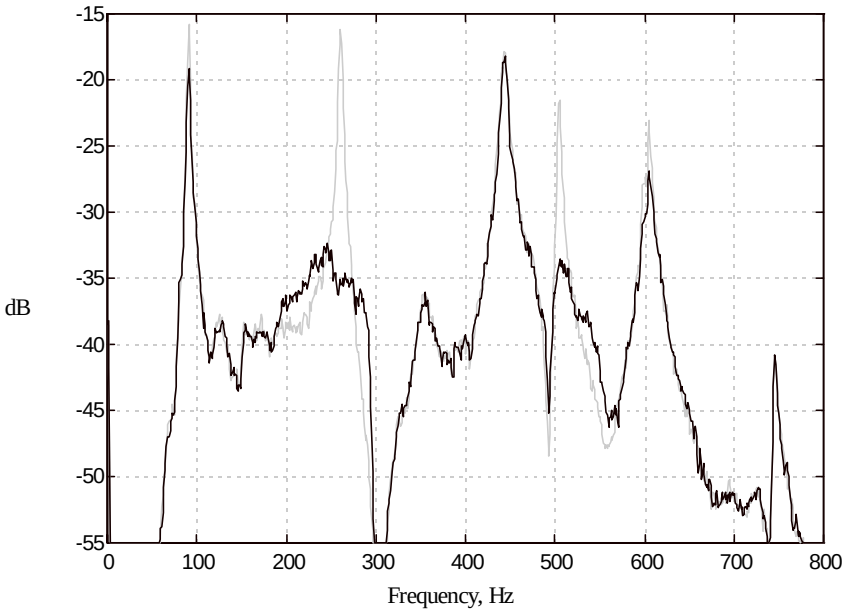

Figure C.2 Plot of acceleration when filter #1 was applied

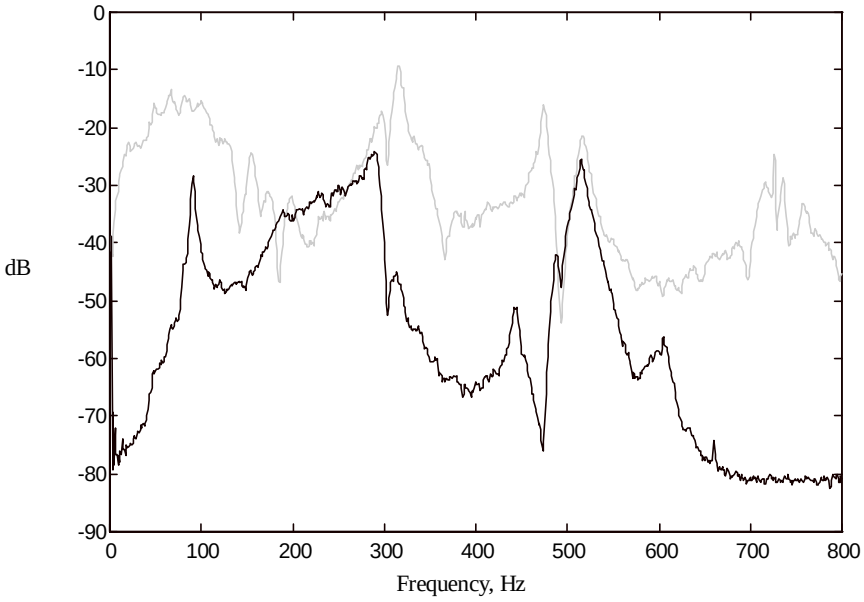

Figure C.3 Control effort when filter #1 was applied

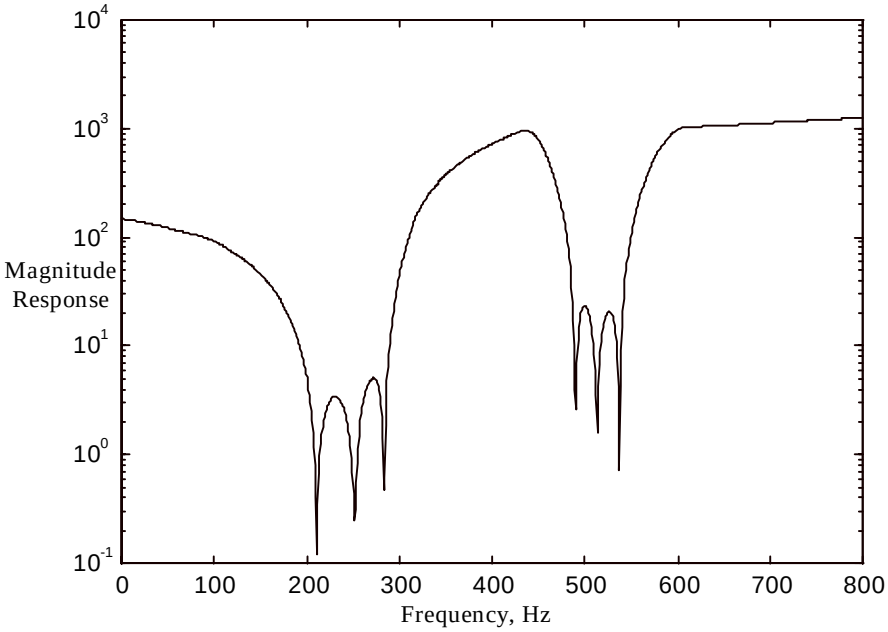

Figure C.4 Frequency magnitude response of control filter #1

The plots shown thus far were obtained using the filter of Fig. C.4. However, the control weighting filter may be redesigned to regulate the resonance's which were

unregulated by the filter C.4 while allowing the others which were regulated to be unregulated. This demonstrates the versatility of the frequency weighted controller. Shown in Fig. C.5 is the autospectrum of the accelerometer signal when the control weighting function on Fig. C.7 was used. This function was designed in MATLAB using *yulewalker()*.

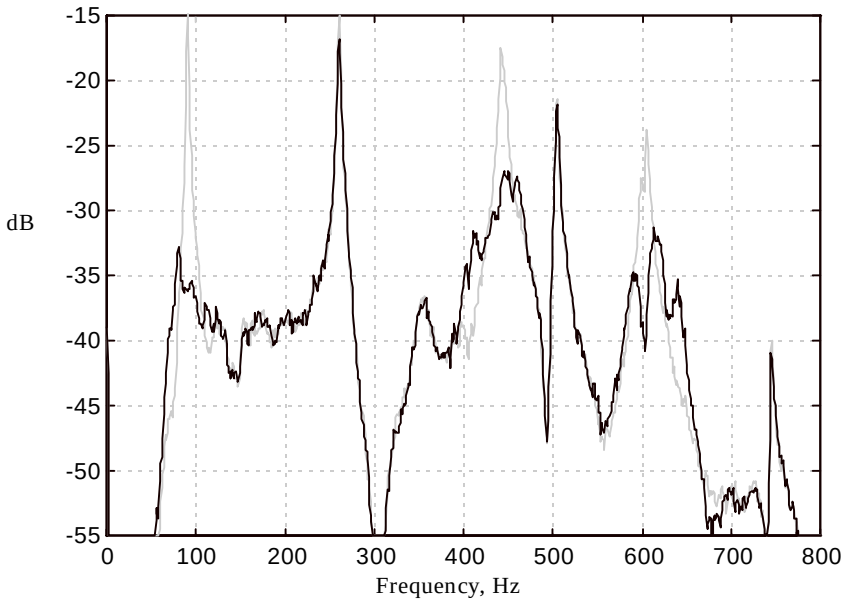

Figure C.5 Plot of acceleration when filter #2 was used

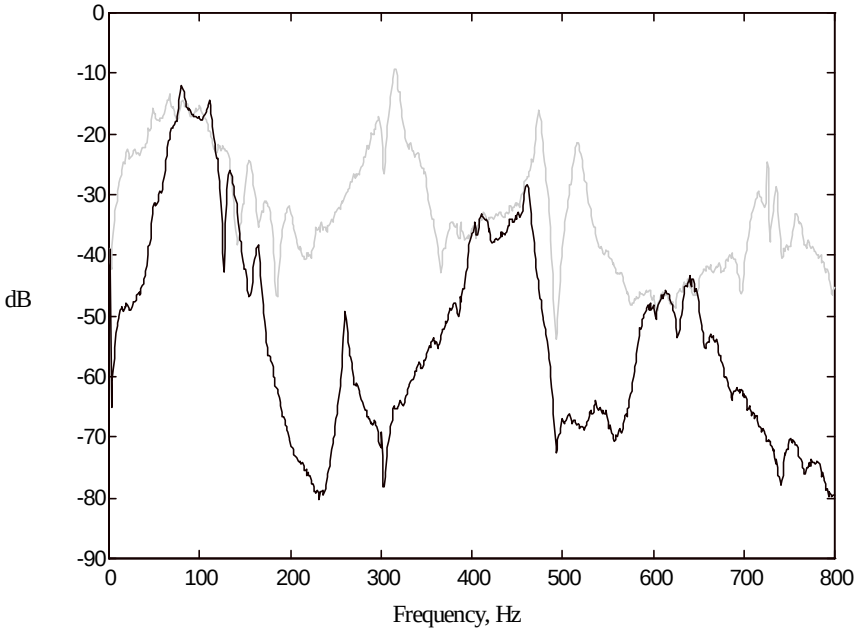

Figure C.6 Plot of control effort when filter #2 was used

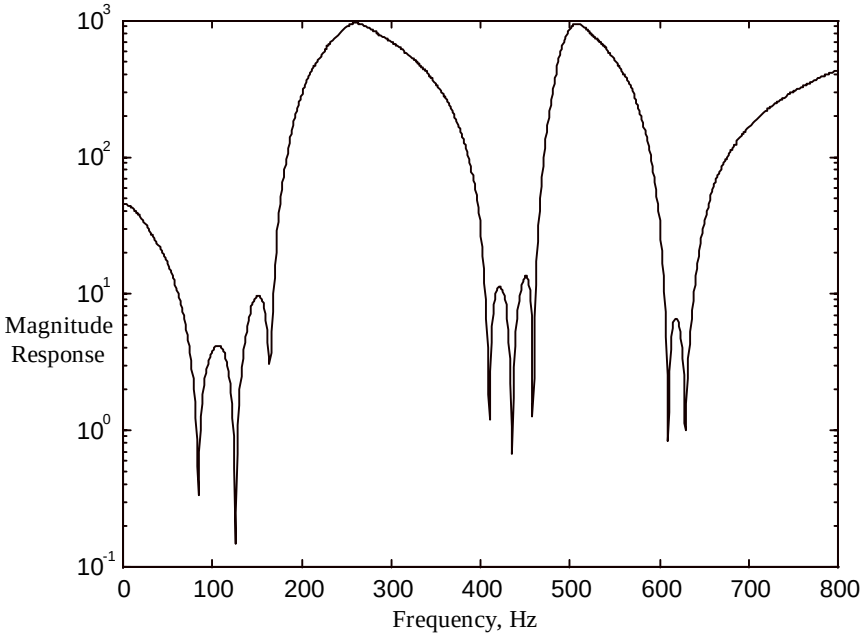

Figure C.7 Frequency magnitude response of control filter #2

As can be seen in Fig. C.5, the frequencies around 90 Hz, 442 Hz and 604 Hz were regulated while little regulation was performed elsewhere. The black line in Fig. C.6 is the control effort and the gray line is the control effort with no frequency weighting filter applied.

The controllers presented in this appendix demonstrate that predictive control may be applied to regulate only specified sections of the frequency spectrum. In addition, the amount of regulation may be specified as a function of frequency across the bandwidth of interest given actuator authority limits are not exceeded. With the ability to specify regulation as a function of frequency, the introduction of acoustic filters into the feedback control scheme is possible. The acoustic filters may be used in the controller design to cancel plate vibrations according to the amount of energy coupled into the acoustic field. This will produce a controller which seeks to minimize acoustic intensity rather than plate vibrations, resulting in a control scheme tailored for active noise control.

References

1. Ljung, L., System Identification, Theory for the User, Prentice Hall, 1987.

2. Astrum, K.J., and Witenmark, B., Adaptive Control, Addison-Wesley Publishing Company, 1995.

3. Chalam, V.V., Adaptive Control Systems, Marcel Dekker, Inc., 1987.

4. Goodwin, G.C. and Sin, K.S., Adaptive Filtering, Prediction, and Control, Prentice-Hall, 1984.

5. Haykin, S., Adaptive Filter Theory, Prentice-Hall, 1996.

6. Juang, J.-N., Applied System Identification, Prentice-Hall, 1994.

7. Juang, J.-N., "Unification of Several System Realization Algorithms", Journal of Guidance, Control, and Dynamics, Vol. 20, Num. 1, January-February, 1997, Pages 67-73.

8. Juang, J.-N., "System Realization Using Information Matrix", Journal of Guidance, Control, and Dynamics, Vol. 20, No.3, May-June 1997.

9. Phan, M., Horta, L.G., Juange, J.-N., and Longman, R.W., "Improvement of Observer/Kalman Filter Identification (OKID) by Residual Whitening," Journal of Vibrations and Acoustics, Vol. 117, April 1995, pp. 232-239.

10. Juang, J.-N., "State-Space System Realization With Input- and Output-Data Correlation", NASA Technical Paper 3622, April 1997.

11. Clarke, D.W., Mohtadi, C., and Tuffs, P.S., "Generalized Predictive Control - Part I. The Basic Algorithm," Automatica, Vol. 23, No. 2, pp. 137-148, 1987.

12. Clarke, D.W., Mohtadi, C., and Tuffs, P.S., "Generalized Predictive Control - Part II. Extensions and Interpretations," Automatica, Vol. 23, No. 2, pp. 149-160, 1987.

13. Kouvaritakis, B., Rossiter, J.A., and Chang, A.O.T., "Stable Generalized Predictive Control: an algorithm with guaranteed stability", University of Oxford, Department of Engineering Science, Parks Road, Oxford.

14. Phan, M.G., and Juang, J.-N., "Predictive Feedback Controllers for Stabilization of Linear Multivariable Systems," Journal of Guidance, Control, and Dynamics, To appear.

15. Juang, J.-N., and Phan, M. Q., "Deadbeat Predictive Controllers," AIAA 35th Aerospace Sciences Meeting, AIAA paper number 97-0455, Reno, January 1997.

16. Kuo, B.C., Digital Control Systems, Saunders College Publishing, 1992.

17. Dorato, P., Abdallah, C., and Cerone, V., Linear-Quadratic Control, An Introduction, Prentice-Hall, 1995.

18. Baumann, W.T., Saunders, and W.R., Rodertshaw, H.H., "Active suppression of acoustic radiation from impulsively excited structures", J. Acoust. Soc, Am., Vol. 90, pp. 3202-3208, 1991.

19. Mosca, E., Optimal, Predictive, and adaptive Control, Prentice-Hall, 1995.

20. Favier, G., Dubois, D., "A review of k-Step-ahead Predictors", Automatica, Vol. 26,. No. 1, pp.75-84, 1990.

21. Phan, M., Juang, J.-N., and Hyland, D.C., "On Neural Networks in Identification and Control of Dynamic Systems", NASA Technical Memorandum 107702, 1993.

22. Meirovitch, Leonard, Dynamics and Control of Structures, John Wiley & Sons, 1990.

23. Shoureshi, R., "Active Noise Control: A Marriage of Acoustics and Control", Proceedings of the American Control Conference, Baltimore, Maryland, pp. 3444-2448, 1994.

24. Vipperman, J.S., Burdisso, R.A., and Fuller, C.R., "Active Control of Broadband Structural Vibration Using the LMS Adaptive Algorithm", Journal of Sound and Vibration, 166(2), pp. 283-299, April 1992.

25. Clarke, D.W., "Self-tuning Control of Nonminimum-phase Systems", Automatica, Vol. 20, No. 5, pp. 501-517, 1984.

26. Baumann, W.T., "An Adaptive Feedback Approach to Structural Vibration Suppression", Dep. Of Elec. Engr., VA Tech, Blacksburg, VA, 24061, USA.

27. Borgan, W. L., and Han, S.-D., "Parameteric Study of Adaptive Generalized Predictive Controllers", J. Guidance, Vol. 16, Num. 2, pp. 405-407, 1992.

28. Clarke, D.W., "Adaptive Generalized Predictive Control", Department of Engineering Science, Parks Road, Oxford OX1 3PJ, UK

29. Clarke, D. W., Mosca, E., and Scattolini, R., "Robustness of an Adaptive Controller", IEEE ransactions on Automatic Control, Vol. 39, Num. 5, pp. 1052-1056, May 1994.

30. Lin, W., Wang, Y., and Yong, J., Unified adaptive control of nonminimum-phase systems, Part 1. Weighted control effort and pole placement for stochastic systems", Int. J. Control, Vol. 50, No. 3, pp., 917-935, 1989.

31. Wang, W., Henriksen, H., "Direct Adaptive Generalized Predictive Control", Proceedings of the American Control Conference, Chicago, U.S.A., pp. 2402-2406, 1992.

32. Wang, W., "A Direct Adaptive Generalized Predictive Control Algorithm for MIMO Systems", Int. J. Control, Vol. 60, No. 6, pp. 1371-1381, 1994.

33. Juang, J.-N., and Phan, M., "Recursive Deadbeat Predictive Control", 1997 American Control Conference, I-97115A, Albuquerque Convention Center, New Mexico, June 4-6, 1997.

34. Eure, K.W. and Juang, J.-N., "Adaptive Predictive Feedback Control of Plate Vibrations", To be released as NASA Technical Memorandum.

35. Eure, K.W., and Juang, J.-N., "Broadband Noise Control Using Predictive Techniques," NASA Technical Memorandum 110320, January 1997.

36. Eure, K.W., Juang, J.-N., and Silcox, R., "Block Adaptive Feedback Control of Plate Vibrations", To be released as NASA Technical Memorandum.

37. Ellite, S.J., Sutton, T.J., Rafaely, B., and Johnson, M., "Design of Feedback Controllers using a Feedforward Approach", Active 95, Newport Beach, CA, USA, 1995.

38. Fuller, C. R., Elliott, S. J., & Nelson, P. A., Active Control of Vibration, 1995.

39. Fahy, F., Sound and Structural Vibration, Academic Press, 1985.

40. Oppenheim, A.V., Schafer, R.W., Discrete-Time Signal Processing, Prentice-Hall, 1989.

41. Juang, J.-N., and Eure, K.W., "Predictive Feedback and Feedforward Control for Systems with Unknown Disturbances", Patent pending, TM112864.

42. Goodzeit, N.E., and Phan, M.Q., "System and Periodic Disturbance Identification for Feedforward-Feedback Control of Flexible Spacecraft", AIAA 97-0682, 35th Aerospace Science Meeting & Exhibit, Reno, NV, Jan. 6-10, 1997.

43. Leissa, A.W., "Vibration of Plates", NASA SP-160, 1969.

44. Thomas, William T., Theory of Vibration with Applications, Prentice Hall, 1988.

45. Kinsler, L.E., Frey, A.R., Coppens, A.B., and Sanders, J.V., Fundamentals of Acoustics, Wiley, 1982.

46. Elliott, S.J, and Johnson, M.E., “Radiation modes and the active control of sound power”, J. Acoust. Soc. Am., Vol. 94, pp. 2194-2204, 1993.

47. Kwakernaak, H. and Sivan, R., Linear Optimal Control Systems, Wiley-Interscience, NewYork, 1972.

48. Gentry, C.A., Guigou, C., Fuller, C.R., “Smart foam for applications in passive-active noise radiation control”, J. Acoust. Soc. Am., 101 (4), pp. 1771-1778, April, 1997.

Vita

Kenneth W. Eure

Education:

B.S.E.E.	Old Dominion University	August 1990
M.S.E.E.	Virginia Tech	December 1991
Ph.D. E.E	Virginia Tech	May 1998

Work Experience:

Norfolk Naval Shipyard	Electronics Technician	Sept. 1983 - Jan. 1988
Naval Surface Warfare Center	Electronics Engineer	Jan. 1992 - Sept. 1994
NASA Langley	Engineer	Sept. 1994 - present